SMART CONTROLLED RELEASE MEMBRANES

Domenico Pirone

UNIVERSITAT ROVIRA i VIRGILI

Smart controlled release membranes

DOMENICO PIRONE

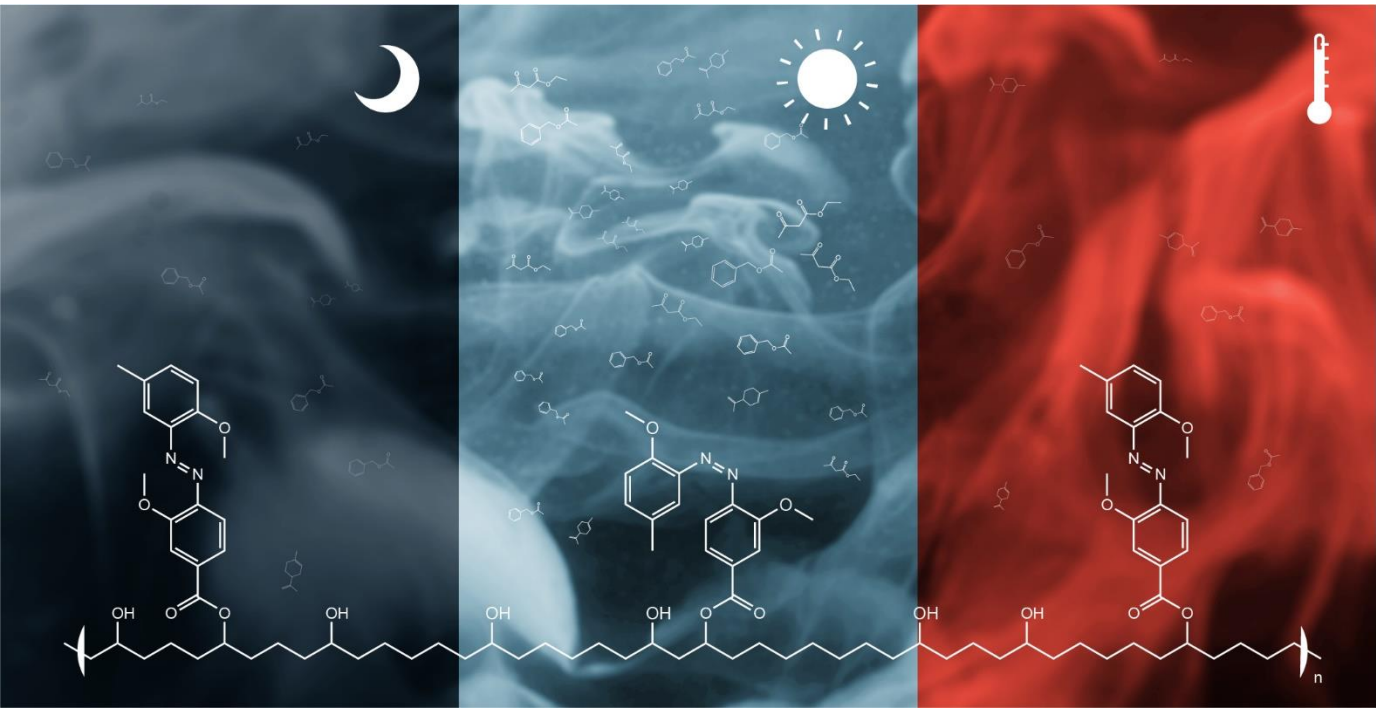

DOCTORAL THESIS

2020

Smart controlled release membranes

by

Domenico Pirone

Doctoral Thesis

Supervisors:

Marta Giamberini

Ricard Garcia-Valls

Regine Labeque

Emily Boswell

Universitat Rovira i Virgili

Tarragona

2020

UNIVERSITAT ROVIRA I VIRGILI

Department d'Enginyeria Química
Campus Sescelades,
Avda. Països Catalans, 26
43007 Tarragona
Tel: 977 55 97 87
Fax: 977 55 96 21

Marta Giamberini and Ricard Garcia-Valls, Associate Professors at the University Rovira i Virgili, Department of Chemical Engineering. Regine Labeque, R&D Research Fellow at Procter & Gamble company and Emily Boswell, Principal Engineer at The Procter & Gamble company.

We state that the present study, entitled "Smart controlled release membranes", presented by Domenico Pirone for the award of the degree of Doctor, has been carried out under our supervision at the Chemical Engineering Department at the University Rovira i Virgili, and that it fulfils all the requirements to be eligible for the Doctor International Mention.

Tarragona, February 2020

Supervisors of the doctoral thesis:

Dr. Marta Giamberini

Dr. Ricard Garcia-Valls

Dr. Regine Labeque
5th February 2020

Dr. Emily Boswell
5th February 2020

“A scientist in his laboratory is not a mere technician: he is also a child confronting natural phenomena that impress him as though they were fairy tales.”

Marie Curie

Table of Contents

Acknowledgments

Firstly, I would like to thank my supervisors Dr. Marta Giamberini Dr. Ricard Garcia-Valls, Dr. Regine Labeque and Dr. Emily Boswell for giving me the wonderful opportunity to join this program under their supervision, for their constant support, for their knowledge, great patiance and guidance.

I also want to thank all the members of the MEMTEC group for sharing their expertize with me: Dr. José Antonio Reina, Dr. Tània Gumí, Dr. Bartosz Tylkowski, Josefa Lázaro, Ania, Adrianna, Monika, Rita, Mario, Gianmarco and Jie. Thank you Pepa for your help in the lab and in all the administrative things that without you would have been much more complicated.

A special thanks to all the people working in Eurecat and in the Servei de Recursos Científics i Tècnics of Tarragona: Josep M. Montornés, Montse Carrasco, Benedetta Palucci, Mercè Moncusí Mercadé, Mariana Stefanova Stankova, Rita Marimon Picó and Ramon Guerrero Grueso. You have collaborated to increase the scentific value of this work. Your expertize and knowledge helped me in the thoughest moment of this research.

My stay in Tarragona would not be so fantastic without special people I met on my way. Thanks to Dailyn, Adrian, Xavi, Kris, Claudio, Francesco, Lorenza, Chiara, Mario, Rubén, Isaac for the good times spent together.

Next, I would like to thank all the people involved in the SMARTMEM program for their professional advice and their support

and all the TPT department of Procter & Gamble, in Brussels:, Florence Courchay, Susana Fernandez Prieto, Miguel Brandt, Alberto Martinez, Raul Rodrigo Gomez, Johan Smets and Fabienne De Decker.

For the amazing time spent together I want to thank all the special people that I had the chance to know in Brussels: Luca, Silvia, Charlene, Keo, Xavi, Inês, Alessandro, Peppe, Livio, Gianmarco P., Fabiana, Licia, Mattia, Giusy and Ulderico.

To the guys who accompanied me from the beginning to the end of this wonderful adventure I would like to give all my acknowledgments. Those with whom I have shared my whole life for the past 3 years and who have become my second family: Gianmarco, Rita and Mario.

Finally, I have to thank my family for the unconditional support, understanding, help and love I have always received. This would not be possible without you.

Domenico Pirone

Summary

During these century many studies were focused around the smart materials as promising way to boost and arise the performances of devices used in our daily life. As matter of interest, these polymers are being used in application like drug delivery, diagnostics, biotechnology, sensors, actuators and optical systems, as well as coatings, textiles and consumers goods. Scientists are creating system that could be more and more versatile and "smart", depending on the conditions of the environments in which they are placed.

The aim of this PhD project is to improve, the performance of the Air Care devices for small environments and cars, produced by Procter & Gamble company. In the specific, these are passive devices that work in a continuous manner evaporating fragrances from a porous membrane. This membrane represent the core of the product and it allows the diffusion of the volatile materials with poor selectivity, while avoiding leakage of the liquid mixture with higher fragrance delivery rate per unit area.

However, there are several possibilities of improving the performances of this membrane. For instance, in conditions of prolonged higher temperature, like in a hot parked car or household condition, too much fragrance can evaporate, affecting the longevity of scent experience to the consumer; another problem lies in the lack of control on the rate at which the top notes (more volatile part of the perfume) and the bottom notes (less volatile part of the perfume) evaporate from the membrane, which gives rise to an altered perception of the perfume, since the top notes come out much faster than the bottom ones. To get a better perfume spectrum balance, enabling the perfume to be delivered to the consumer according to the desired design, it would be preferred a membrane that could be tuned to set the rate of evaporation, depending on the volatility of the perfume components.

A possible solution to some of these problems could lie in membrane coating with new and properly functionalized polymers, which could act as a selective "gate", allowing or preventing the release of the volatile material under certain stimuli. As a matter of fact, the reversible changes of polarity and

conformation imparted to a photochromic polymer system by photoirradiation can be applied to controlling mass transfer through membranes. For instance, it has been reported that azo-benzene based systems can successfully act as light-triggered membrane. At a molecular level, *E-Z* isomerization leads to a substantial change in geometric conformation and size. On the other hand, it is also known that the interaction of some polymer groups with the dipole of *Z* azobenzene form can lead to a change in the wettability and swelling degree of a membrane, thus modifying its permeability to low molar mass compounds. From the letterature is well known that azobenzenes are very receptive to inclusion in different types of materials. This brilliant property of azobenzenes makes them useful in the preparation of different photoresponsive membranes. Moreover, the wavelength which induces the opening of the membrane, and subsequent release, could be adjusted by properly design the structure of the azo-bearing moiety. Darkness and/or temperature increase would drive the azobenzene units back to the more stable *E* configuration, thus inhibiting release. Moreover, since the so functionalized polymer is more polar when in its *Z* form, the “open” membrane would favor the release of hydrophilic fragrances over the hydrophobic ones, thus contributing to some flattening of the top and bottom notes.

In conclusion, the objective of this PhD project is to improve the performance of Air Care devices developing a membrane that can release the perfume raw materials charged inside the resevoir without being extremely affected by temperature fluctuations of the external environment, thus, being significantly less temperature sensitive than the current membrane used in nowadays products. In order to do this the main polyolefin/silica membrane will be coated with a polymer modified with novel azobenzene moieties.

This system could be triggered by light to act as an intelligent gate for the perfume diffusion, improving both selectivity and releasing control of the perfume raw materials in the home/car environment. In addition, by a proper design of the functionalizing unit, temperature could act as an additional external stimulus, able to conveniently trigger (i.e. reduce) membrane permeability through thermal back-isomerization.

Sommario:

Durante questo secolo, gli smart materials (materiali intelligenti) sono stati oggetto di numerosi studi come modo promettente per aumentare sempre più le prestazioni dei dispositivi utilizzati nella nostra vita quotidiana. Per motivi d'interesse, questi polimeri sono utilizzati in applicazioni come drug carriers, nella diagnostica, nella biotecnologia, come sensori, attuatori e sistemi ottici, nonché rivestimenti, prodotti tessili e beni di consumo. Al giorno d'oggi, la comunitá scientifica é focalizzata nella creazione di sistemi sempre più versatili e "intelligenti" che possano adattare le proprie caratteristiche a seconda delle condizioni ambientali in cui sono collocati.

Lo scopo di questo progetto di dottorato è migliorare le prestazioni dei dispositivi per Air Care per piccoli ambienti e automobili, prodotti dalla società Procter & Gamble. Nello specifico, si tratta di dispositivi che funzionano in modo continuo permettendo alle fragranze di evaporare permeando attraverso una membrana porosa costituita da poliolefina/silice. Questa membrana rappresenta il nucleo del prodotto e consente la diffusione dei profumi con scarsa selettività, evitando al contempo la fuoriuscita della miscela liquida da esso. Tuttavia ci sono diverse possibilità per migliorare le prestazioni di tale membrana. Ad esempio, in condizioni prolungate di temperatura elevata, come in un'auto parcheggiata al caldo o in condizioni domestiche con riscaldamento in funzione, troppa fragranza può evaporare dal dispositivo, influenzando la longevità dell'esperienza del profumo per il consumatore; un altro problema risiede nella mancanza di controllo sulla velocità con cui le note di testa (parte più volatile del profumo) e le note di fondo (parte meno volatile del profumo) evaporano dalla membrana, dando origine ad una percezione alterata del profumo, poiché le note di testa escono molto più velocemente di quelle di fondo. Per ottenere un migliore equilibrio dello spettro complessivo di fragranze presenti nel dispositivo, consentendo di distribuire il profumo al consumatore secondo il disegno desiderato, sarebbe preferibile una membrana che potesse essere regolata per impostare la velocità di evaporazione a seconda della volatilità dei componenti presenti nel prodotto.

Una possibile soluzione ad alcuni di questi problemi potrebbe risiedere nel rivestimento della membrana con nuovi polimeri adeguatamente

funzionalizzati, che potrebbero fungere da "gate" (porta) selettivo, consentendo o impedendo il rilascio del materiale volatile sotto determinati stimoli. I cambiamenti reversibili di polarità e conformazione impartiti ad un sistema polimerico fotocromatico mediante fotoirradiazione possono essere applicati al controllo del trasferimento di massa attraverso le membrane. Ad esempio, é stato riportato, che i sistemi a base di azo-benzene possono agire con successo come membrana innescata dalla luce.

A livello molecolare, l'isomerizzazione E-Z porta a un cambiamento sostanziale nella conformazione e nelle dimensioni geometriche. D'altra parte è anche noto che l'interazione di alcuni gruppi polimerici con il dipolo di forma azobenzenica Z può portare a un cambiamento nella bagnabilità e nel grado di gonfiore di una membrana, modificando così la sua permeabilità ai composti a basso peso molecolare. Dalla letteratura è ben noto che gli azobenzeni sono molto ricettivi all'inclusione in diversi tipi di materiali. Questa brillante proprietà li rende utili nella preparazione di diverse membrane fotoattive. Inoltre, la lunghezza d'onda che induce l'"apertura" della membrana e il successivo rilascio del profumo, potrebbe essere regolata progettando correttamente la struttura della molecola azobenzenica. L'oscurità e / o l'aumento della temperatura porterebbero le unità di azobenzene alla configurazione E più stabile, inibendo così il rilascio. Inoltre, poiché il polimero precisamente funzionalizzato è più polare quando è nella sua forma Z, la membrana "aperta" favorirebbe il rilascio di fragranze idrofile su quelle idrofobe, contribuendo così ad un certo equilibrio nel rilascio delle note di testa e di fondo.

In conclusione, l'obiettivo di questo progetto di dottorato è migliorare le prestazioni dei dispositivi Air Care sviluppando una membrana in grado di rilasciare le materie prime profumate caricate all'interno del resevoir senza essere eccessivamente influenzate dalle fluttuazioni di temperatura dell'ambiente esterno, così come avviene, invece, con l'uso della membrana utilizzata nei prodotti attualmente in commercio. A tale scopo, la membrana principale sará rivestita con un polimero modificato con nuove frazioni di azobenzene. Questo sistema potrebbe essere attivato dalla luce per fungere da porta intelligente per la diffusione del profumo nell'ambiente domestico / automobilistico, migliorando sia la selettività che il controllo del rilascio delle materie prime profumate. Inoltre, con una corretta progettazione dell'unità

funzionalizzante, la temperatura potrebbe fungere da ulteriore stimolo esterno, in grado di innescare convenientemente (o ridurre) la permeabilità della membrana attraverso la retroisomerizzazione termica.

Resumen:

Durant aquest segle molts estudis es van centrar al voltant dels materials intel·ligents com una manera prometedora per impulsar i sorgir les prestacions dels dispositius utilitzats en la nostra vida diària. Com a interès, aquests polímers s'utilitzen en aplicacions com ara subministrament de medicaments, diagnòstics, biotecnologia, sensors, actuadors i sistemes òptics, així com recobriments, tèxtils i béns de consum. Els científics estan creant un sistema que pugui ser cada cop més versàtil i "intel·ligent", segons les condicions dels entorns on se situen.

L'objectiu d'aquest projecte de doctorat és millorar el rendiment dels dispositius Air Care per a entorns i cotxes petits, produïts per l'empresa Procter & Gamble. Es tracta de dispositius passius que funcionen de forma contínua evaporant fragàncies d'una membrana porosa. Aquesta membrana representa el nucli del producte i permet la difusió dels materials volàtils amb una mala selectivitat, alhora que evita les fuites de la barreja líquida amb una taxa de lliurament de fragàncies més alta per unitat d'àrea.

Tot i això, hi ha diverses possibilitats de millorar les prestacions d'aquesta membrana. Per exemple, en condicions de temperatura més llarga, com en un cotxe estacionat o en una condició domèstica, es pot evaporar massa fragància, afectant la longevitat de l'experiència d'olor al consumidor; un altre problema rau en la manca de control sobre la velocitat que les notes superiors (part més volàtil del perfum) i les notes inferiors (part menys volàtil del perfum) s'evaporen de la membrana, cosa que dóna lloc a una percepció alterada del perfum, ja que les notes superiors surten molt més ràpides que les de baix. Per aconseguir un millor equilibri de l'espectre del perfum, permetent el lliurament del perfum al consumidor segons el disseny desitjat, es preferiria una membrana que es podia ajustar per establir la velocitat d'evaporació, depenent de la volatilitat dels components del perfum.

Una possible solució a alguns d'aquests problemes podria consistir en el recobriment de membrana amb polímers nous i correctament funcionalitzats, que podrien actuar com a "porta" selectiva, permetent o impedint l'alliberament del material volàtil sota certs estímuls. De fet, es poden aplicar els canvis reversibles de polaritat i conformació donats a un sistema de polímer

fotocròmic per fotoirradiació per controlar la transferència de massa a través de membranes. Per exemple, s'ha informat que els sistemes basats en azobenzè poden actuar amb èxit com a membrana desencadenada per la llum. A nivell molecular, la isomerització E-Z condueix a un canvi substancial en la conformació i mida geomètriques. D'altra banda, també se sap que la interacció d'alguns grups polímers amb el dipol de la forma d'azobenzè Z pot provocar un canvi en la humectació i el grau d'inflor d'una membrana, modificant així la seva permeabilitat a compostos de massa molar baixa. A partir de la lletra es coneix que els azobenzenes són molt receptius a la inclusió en diferents tipus de materials. Aquesta brillant propietat dels azobenzenes els fa útils en la preparació de diferents membranes fotoresponsives. D'altra banda, es pot ajustar la longitud d'ona que indueix l'obertura de la membrana i el posterior alliberament dissenyant adequadament l'estructura del fragment portant azoic. La foscor i / o l'augment de temperatura provocarien les unitats d'azobenzene a la configuració E més estable, inhibint així l'alliberament. A més, atès que el polímer tan funcionalitzat és més polar quan en la seva forma Z, la membrana "oberta" afavoriria l'alliberament de fragàncies hidròfiles sobre les hidrofòbiques, contribuint així a certs aplanaments de les notes superiors i inferiors.

Com a conclusió, l'objectiu d'aquest projecte de doctorat és millorar el rendiment dels dispositius Air Care Febreze que desenvolupen una membrana que pot alliberar les matèries primeres de perfum carregades a l'interior del resvoir sense que es vegi extremadament afectada per les fluctuacions de temperatura del medi extern, sent així molt menys significativa. sensible a la temperatura que la membrana actual usada en els productes actuals. Per fer-ho, la principal membrana es recobrirà amb un polímer modificat amb nous fragments d'azobenzen.

Aquest sistema es pot desencadenar per la llum perquè actuï com a porta intel·ligent per a la difusió del perfum, millorant tant la selectivitat com alliberant el control de les matèries primeres de perfum a l'entorn de la llar / cotxe. A més, mitjançant un disseny adequat de la unitat funcionalitzadora, la temperatura podria actuar com a estímul extern addicional, capaç de desencadenar convenientment (com reduir) la permeabilitat de la membrana mitjançant una isomerització tèrmica posterior.

Chapter 1. General introduction and objectives

1.1 General overview of stimuli-responsive polymers

The response to a stimulus is the basic process of living systems. Many biological systems are considered smart due to this ability. Humans are highly intelligent species due to their ability to remember and analyze logically large amount of information and act consequently. Many animals, are regarded as intelligent because of their aptitude to communicate, understand instructions, learn, analyze, and produce appropriate responses.[1] A cell, the basic unit of complex biological organisms, can be considered to have a primitive form of intelligence. Despite being small (i.e., micrometer sized), it is a highly complex system that performs a wide range of advanced extracellular and intracellular functions responding to external and internal environmental variations (Fig. 1.1).

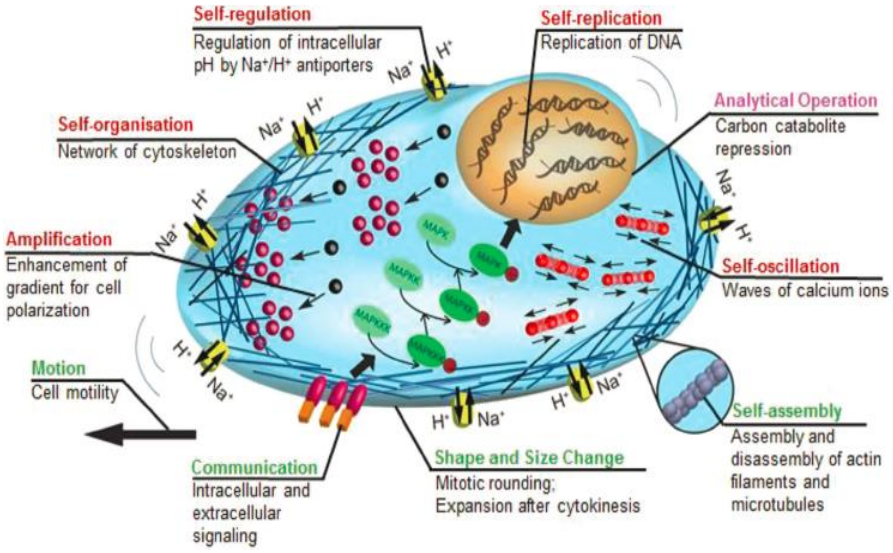

Figure 1.1 - Various functions of a cell. Reprinted with permission from [2]

Moreover, it is well known that common biopolymers, as proteins or nucleic acids, react very perceptively to changes in their surrounding environment. Thus, sensitivity toward the environment is fundamental for the biological systems to preserve themselves and manage their processes.

Based on these evidences, mimicking biological systems behavior became a very important field of research during the past decades to achieve new and smart materials for revolutionary technologies. One possible approach

toward creating smartness in materials is to use stimuli-responsive molecules. These molecules are usually considered smart because of their ability to sense and interact with their surroundings and produce a simple and direct response.

Researchers around the world have created many interesting systems that are remarkably smart and functional by using stimuli-responsive molecules as the building blocks for constructing new polymers, or to modify the ones already commercially available. These polymers can respond to external stimuli manifesting the response as impressive changes in one of the following: shape, surface characteristics, solubility, a sol-to-gel transition or a formation of an intricate molecular self-assembly, ecc.[2]

Despite the many types of molecules that are available for selection, most of the smart devices fabricated by material scientists are usually based on a few common types of stimuli-responsive molecules. The responsiveness of these common types of molecules can broadly be grouped into three main categories: change in molecular structure, bond formation and/or cleavage, and response to external fields (Fig. 1.2.). Several stimuli-responsive molecules undergo a change in molecular structure when they are exposed to an appropriate stimulus.[3–7] A common class of light-responsive molecules is based on spiropyran derivatives.[4–6] Upon exposure to UV, this type of molecule undergoes a ring opening process as illustrated in part (i) of Figure 2a. Exposure to visible light allows the molecule to undergo the reverse (i.e., the ring-closing) process. Significantly, this transformation allows the molecule to have a relatively large change in polarity. When the ring opens, the molecule splits into a moiety with a positive charge and a moiety with a negative charge. The formation of charged groups increases the polarity of the molecule.

In terms of temperature-responsive molecules, poly(N-isopropylacrylamide) (PNIPAM) is commonly used. Below its lower critical solution temperature (LCST), PNIPAM forms hydrogen bonds with water molecules in the solution; hence, it adopts an extended chain conformation (part (ii) of Figure 2a). Increasing the temperature above the LCST dehydrates the polymer chains and allows the polymeric chains to form hydrogen bonds intra- and inter-chains. These interactions result in a collapsed conformation of the polymeric chains.[8]

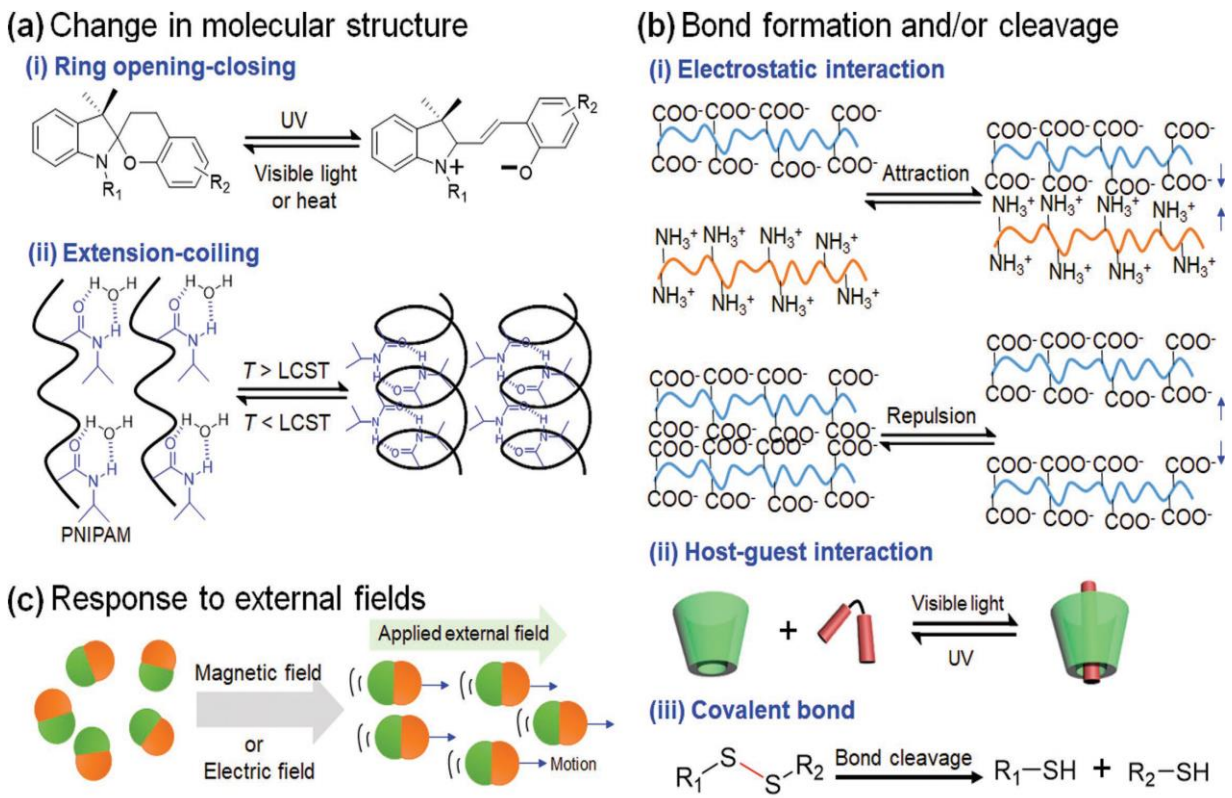

Figure 1.2 - Stimuli-responsive molecules/particles. After detecting an external stimulus, the stimuli-responsive molecules may: a) undergo a change in molecular structure, or b) result in bond formation and/or cleavage. c) Particles produce a response to external. Reprinted with permission from [2]

Stimulus can be also used for forming or breaking intra- or inter-molecular bonds. The type of bond formation and/or cleavage includes electrostatic attraction or repulsion, hydrophobic interaction, hydrogen bonding, host–guest interaction, and covalent bond (Figure 2b).[9–11] Part (i) of Figure 2b illustrates the case when two molecules undergo electrostatic attraction or repulsion. In order to achieve these interactions, the molecules need to have ionic or ionizable functional groups. Two widely used functional groups are the carboxylic acid (-COOH) and the amine ($-NH_2$) groups. When these functional groups are exposed to an appropriate pH, the -COOH group deprotonates to form the negatively charged carboxylate, while the $-NH_2$ group protonates to form the positively charged ammonium group. For example, if one polymeric chain bears carboxylate groups and another polymeric chain bears the ammonium groups, the chains attract electrostatically. If the two polymeric chains have only one type of charged group, the chains repel themselves.

Another useful type of molecular interaction is the host–guest interaction. Commonly used molecules include the β-cyclodextrin (β-CD) and azobenzene derivatives. β-CD has a high binding affinity with the trans-azobenzene derivatives and a low binding affinity with the cis-azobenzene derivatives.[12–14] Therefore, the host-guest interaction can be controlled reversibly by UV and visible light (part (ii) of Figure 3b).

A stimulus can be also used to cleave covalent bonds. A common example is the cleavage of the disulfide bond by glutathione (GSH).[15,16] Magnetic and electric fields are also commonly used as a stimulus for stimuli-responsive materials (Figure 3c). For example, if a material contains molecules that are magnetic or charged, it can orient and move with the externally applied field.

However, there are some fundamental aspects to consider to proper plan and develop smart polymers for the right application, on top of the selected specific ability of the stimuli-responsive molecules. The nature of the environmental stimuli, for example, is of high importance to successfully direct and control the function of the material in its appropriate environment. There are three main categories in which a stimulus can be classified: physical stimuli (e.g., temperature, ultrasounds, electromagnetic radiation (UV, light), mechanical stress/strain, electric fields), chemical stimuli (e.g., pH, redox

reactions, ionic strength), and biological stimuli (e.g., enzymes interactions, affinity ligands, biochemical agents).

All of them can have a direct effect on the interaction between the polymer chains themselves or between the polymer chains and the solvent molecules. These microscopic changes are the basis for explaining the smart behavior.

Another fundamental aspect in the creation of smart materials is the type of architectures that can be selected to produce a smart system. There is a broad range of architectures and structures that can be selected; they can cover not only different geometries but also several orders of magnitude in size (Fig. 1.3): starting from a single macromolecule in solution, proceeding with self-assembled systems (micelles, vesicles, ecc.) as well as cross-linked systems including capsules and polymeric gels. A large variety of processing strategies has been developed for the fabrication of smart polymers and a lot of attention has been addressed on systems like polymeric membranes used for microcapsules and coatings. Nano-sized micelles and microcapsules, for instance, are appropriate vehicles for targeted drug delivery systems.[17] Smart micelles, composed of hydrophilic and/or hydrophobic blocks, and microcapsules with functionalized shells, are able to respond to a plethora of stimuli in order to release their cargo.[18] The therapeutic agents, which can be entrapped in these structures, are released during the conformational changes triggered by the stimulus.[18–20]

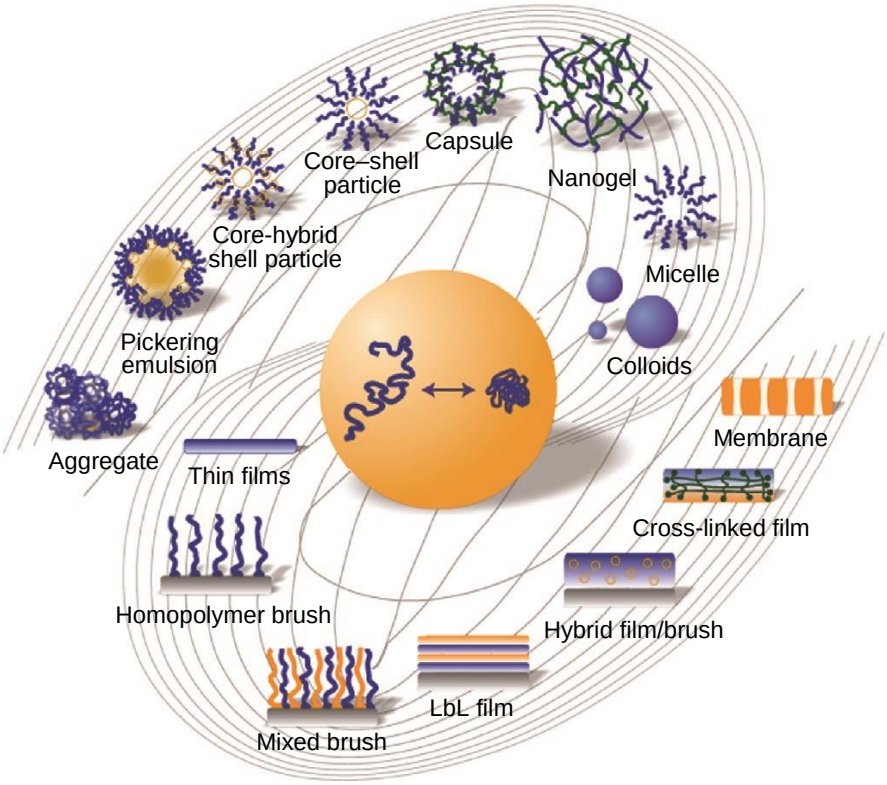

Figure 1.3 - 'Galaxy' of the architectures of stimuli-responsive polymer materials: from thin films (polymer brushes, multilayered films made of different polymers, hybrid systems that combine polymers and particles, thin films of polymer networks, and membranes that are thin films with channels/pores) to nanoparticles (micelles, nanogels, capsules and vesicles, core–shell particles, hybrid particle-in-particle structures, and their assemblies in solutions and at interfaces in emulsions and foams). Reprinted with permission from [21]

In drug delivery systems, the research community has placed a great deal of focus on sensitivity to temperature and light.[22,23] Many techniques are used to produce these versatile carriers and nowadays scientists are more and more involved to improve the methods to include these technologies in consumer goods and therapeutic devices efficiently. Smart materials have attracted special interest also for coating and membranes with stimuli-responsive properties that can be used in the protection of pre-existing materials or in ultra, micro-filtration and phase separation.[21,24–27] Smart coatings are designed to remain passive unless prompted to perform a stimuli-based function and can repeat the process over and over, up to thousands of cycles or more, spanning over several years. The surface property is directly dependent on the nature of

the polymers, grafting density, and surface roughness.[28] Moreover, a polymeric material can be easily functionalized on a surface using post- or pre-polymerization methods or modified with stimuli responsive moieties and used to cast self-standing membranes or to coat existing substrates. Techniques like spin coating, casting via solvent evaporation or layer-by-layer (LbL) deposition methods have been industrialized and adapted for their production.

Both the ability to respond to various stimuli and the numerous possible architectures are prerequisites for a broad range of applications covering the fields of drug delivery,[29] diagnostics,[30] biotechnology,[21,29–31] sensors,[32,33] actuators and optical systems,[34] as well as coatings and textiles.[35]

The behavior of stimuli-responsive polymers is often investigated either in bulk (e.g. polymer films) or in solution. Here a general overview will be provided of the most extended responsive polymers that can be grouped into four different classes: pH-responsive, temperature-responsive, electric field-responsive, and photo-responsive.

1.1.1 pH-responsive polymers:

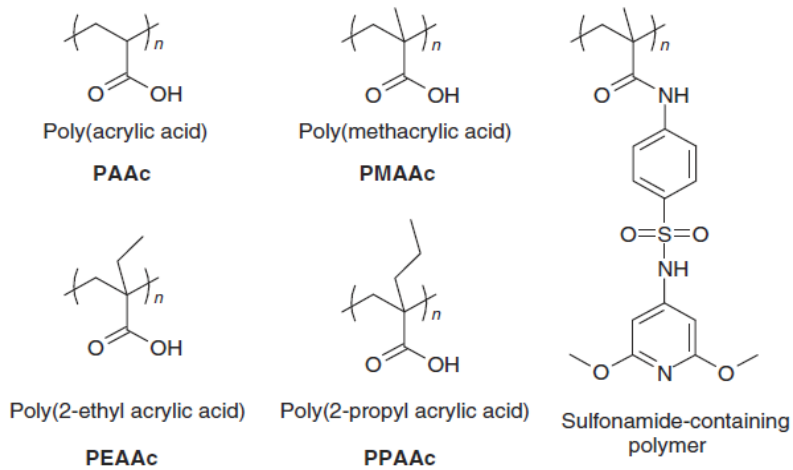

Figure 1.4 - pH-responsive polyacids. Reprinted with permission from [36]

pH-sensitive polymers are typically polyelectrolytes that accept or release protons in response to changes in environmental pH. Their side chain acidic or basic groups undergo reversible ionization and therefore they can be in a neutral or in a charged state. More importantly, changes between charged and

uncharged state significantly vary the hydrodynamic radius. The positively or negatively charged functional groups along the polymer backbone provoke electrostatic repulsions that result in an increase in the hydrodynamic volume of the polymer.[36–38] Polymers bearing carboxylic groups are the most common pH-responsive polyacids (Fig. 1.4). In Figure 1.5 some representatives for weak polybases are also illustrated, such as tertiary alkyl amines as well as aromatic amines. The amine groups accept protons at low pH values forming polyelectrolytes, whereas deprotonation occurs at higher pH resulting in uncharged species. Besides the polymers showed in Figure 6, intensive studies on pH-responsive degradable polymers, biopolymers, and artificial polypeptides are ongoing.[36]

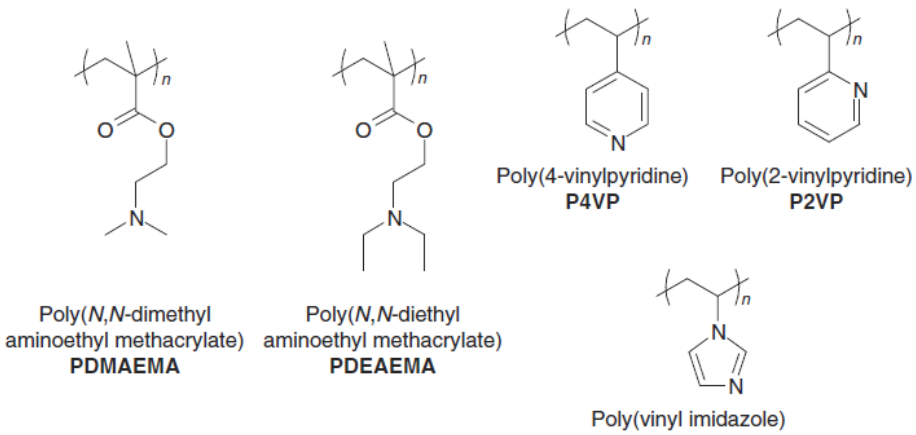

Figure 1.5 - pH-responsive polybases. Reprinted with permission from [36]

1.1.2. Thermo-responsive polymers:

Thermosensitive polymers exhibit reversible solubility variations because of changes in hydrophobic–hydrophilic balance induced by increasing temperature. Thermo-responsive polymers are typically uncharged polymers capable of forming hydrogen bonds with water molecules. However, upon increasing the temperature, the efficiency of hydrogen bonding between the polymer and water is significantly reduced. In this situation, a phase transition is observed in which the polymer changes from a hydrophilic state to a hydrophobic state. In fact, above this critical temperature, referred to as lower critical solution temperature (LCST), the polymer dehydrates and aggregates.

Otherwise, if phase separation is observed below a critical temperature, the polymer shows an upper critical solution temperature (UCST), also named higher critical solution temperature (HCST) behavior. In both cases, the phase separation is completely reversible and the smart polymer dissolves in water when the temperature is reduced below (or increased above, for HCST polymers) the transition temperature.

Three families of thermosensitive smart polymers are widely studied and used. First of all, poly(N-alkyl-substituted acrylamides) and the most well-known of them, poly(N-isopropyl acrylamide), have a transition temperature of 32 °C (depending on the polymer molecular weight).[39–44] The second example of these polymers is oligo(ethylene glycol) methacrylate (OEGMA) derivatives.[45–48] Finally, elastin-like polypeptides (ELP) are also among the most studied thermoresponsive systems.[49,50] These linear polypeptides are composed of repeating units of the pentapeptide valine-proline-glycine-X-glycine (with X corresponding to any amino acid, except proline) (Figure 1.6).

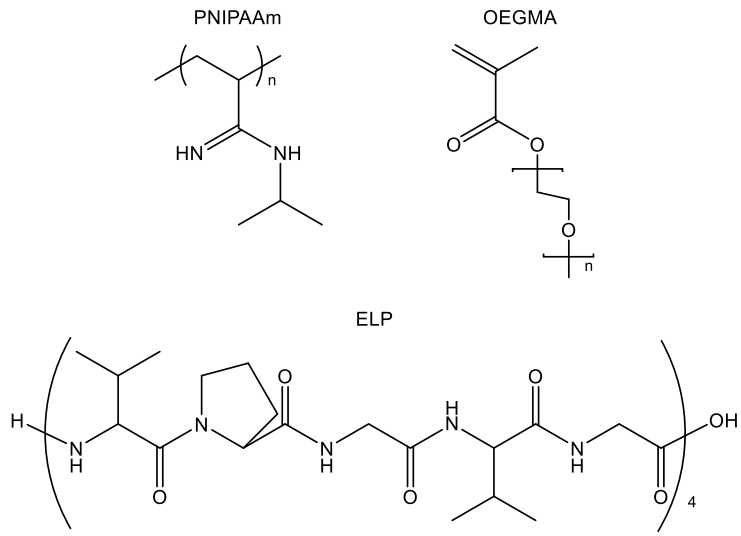

Figure 1.6 - Temperature responsive polymers. Reprinted with permission from [36]

1.1.3. Electric field-responsive polymers:

Some polymers can respond to static electric fields. In some cases, environmental changes such as pH or temperature could inflict undesired

consequences on the morphology of the material. An interesting approach to induce dynamic changes in polymeric systems concerns the use of electroactive polymers. In this case, the environment remains unaltered (e.g., solvent, electrolyte content, pH, temperature, and pressure). In general, the wettability of different polymer films in water increases by increasing the voltage between the water and an electrode placed below the polymer film. One of the pioneering studies was carried out by Berge et al.[52] who used poly(ethylene terephthalate) and observed a decrease on the contact angle up to 30° by applying high voltages. Reversible changes of electric potential have been employed also by Lahann et al.[53] to produce dynamic changes on the surface wettability of a polymeric film. For that purpose, the authors prepared a single layer of (16-mercapto) hexadecanoic acid (MHA). This molecule self-assembled as a single layer on gold with a carboxylate group (hydrophilic) capping the chain (hydrophobic), enabling the possibility for total system surface property alteration. Further, the molecules switched from a hydrophobic to a hydrophilic state *via* the conformational transitions that took place (Fig. 1.7).

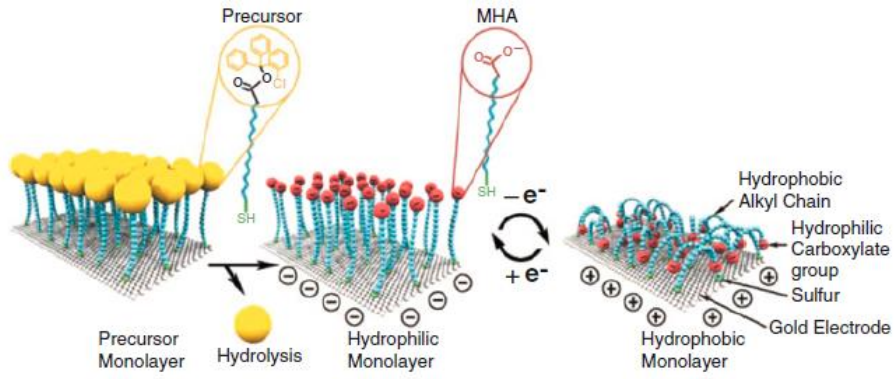

Figure 1.7 - Schematic representation of the transition between straight (hydrophilic) and bent (hydrophobic) molecular conformations. Reprinted with permission from [53]

More sophisticated systems reported translocation of molecules upon reduction/oxidation resulting in the control of the reversible hydrophilic and hydrophobic properties of the surface.[54] Recently, great attention have been

addressed also to electro-active systems that can be used as actuators and as coatings for corrosion protection of metals.[55,56]

1.1.4. Photo-responsive polymers:

Photochemical stimuli are very useful in generating responsive systems. Light control possesses intrinsic advantages compared to temperature, pH, electric and magnetic stimuli, as it: (i) employs non-contact and remote application, (ii) can be easily dosed in order to tune the strength of the response, and, (iii) allows accurate temporal and positional resolution of the response. Photosensitive substances are widely present in consumer goods like glass lenses, initially clear, which turn dark under sunshine. They are also present in trendy cosmetics and clothes. In addition to these objects that have been around for a long time, the digital age has tremendously expanded the fields, where photosensitive materials may play a role. The broad and current interest is transmitting, gating, and storing digital data.[57] Due their reversible feature, photosensitive species match the requirement of the rewritable recording media (CD-RW, DVD-RW), where memory bits must commute between the two binary states (“0” and “1”) upon request.[58,59] Different aspects of photo-responsive polymers have recently been studied and grouped in many interesting publications: Schumers et al. summarized reported work on photo-responsive block copolymers;[60] Zhao reported their light-induced self-assembly;[61,62] Theato and coworkers reviewed photosensitive polymers containing photoremovable groups;[63] Ikeda and coworkers described photo-responsive liquid crystalline polymers and their application as actuators;[64,65] Heinze and coworkers reviewed photosensitive polysaccharides.[66] Al-Malaika et al.[67] described photodegradable systems and Pasparakis et al.[68] reviewed their applications in biotechnology. Therefore, these types of materials are very versatile and effective in the creation of futuristic systems with different functions and applications.

Accordingly, photo-responsive polymers undergo a change in their properties in response to a light stimulus.[69–71] Different molecular properties can be light-regulated, including conformation,[72–77] polarity,[78–82] amphiphilicity,[83–86] charge,[87] optical chirality,[88,89] conjugation,[90,91] etc. The light-

induced molecular change is reflected in a macroscopic change of material properties like shape (i.e., contraction or bending), wettability, solubility, optical properties, conductivity, adhesion and so on. The functionality and, ultimately, the application potential of such a polymer are mainly determined by three parameters: (i) the magnitude of the property change after light triggering, (ii) the rate at which this change occurs, and (iii) the reversibility of the process.

In general, an ideal responsive polymer is the one that exhibits instantaneous and drastic property variation upon light exposure. Depending on the application, a modulation of the response with the light intensity or a reversible property change may be also advantageous. To obtain photo-responsive polymers, a photo-responsive functional group (chromophore) needs to be linked to a polymer as part of the main chain (as a monomer) or as a side chain group. Many types of chromophores are present in nature, or can be synthesized artificially in laboratory, and they can be classified in two categories: reversible and irreversible.

Reversible chromophores, often named molecular switches or photo-switches, undergo a reversible isomerization upon light excitation at a specific wavelength. The photochromic interconversion between isomeric forms allows switching the properties of the polymeric material by irradiation at two different wavelengths. To better describe the photochromic interconversion, the most common model introduced is a simple two-way reaction between two molecular species A and B. Although it may sometimes involve other species, the reaction is assumed to be unimolecular (Figure 1.8a).

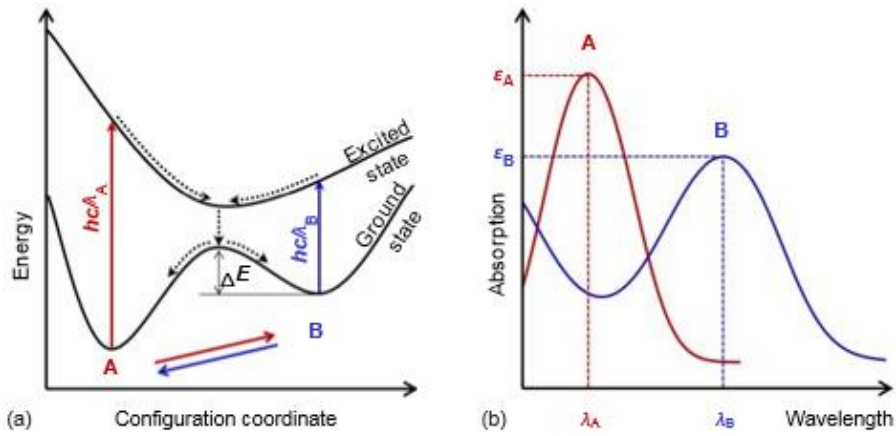

Figure 1.8 - Photochromism: a two-way light-induced reaction between two molecules A and B. (a) Potential energy diagram and (b) the related schematic absorption spectra.

The energy levels of the two isomers, A and B, are separated by a potential barrier (ΔE). If this barrier is low, B is metastable and can revert spontaneously to A. Such systems are called T-type referring to the thermally induced reaction from B to A. On the contrary, a high barrier features a bi-stable system. In this case, only photons can cause the reaction, and such systems are called P-type. In other words, nothing changes in the absence of light. This last characteristic is important since it makes the difference between photochromic bi-stable systems and others, such as ferroelectric or (ferro)magnetic systems. In the latter, shuttling between the two states of the bi-stable system does not follow the same route, displaying the well-known hysteresis, when the polarization or the magnetization is plotted versus the electric or the magnetic field. In photochromic systems, no concept of hysteresis is involved in the rationale of bi-stability. In usual photochromic systems, A absorbs in the UV or near-UV, with a characteristic absorption band at wavelength (λ_A). The absorption coefficient of A at this wavelength is ε_A. When a photon at λ_A is absorbed, A is excited from the ground to the excited state. The excited A yields B with a probability $\phi_{A\rightarrow B}$, known as the quantum yield. On the other hand, B reverts to A, with an analogous pattern, provided that B is excited at λ_B, where it absorbs. The spectral position of the absorption bands gives an indication of the color of light needed to induce the reaction

(Figure 1.8b). Reversibility is important in many applications such as information storage,[92] artificial muscles,[65] and actuators.

Irreversible chromophores are mainly applied to photodegradable materials and used in systems for drug delivery. The advantage of irreversible chromophores is the possibility of 100% photoconversion, since no equilibrium between two states is involved. This leads to effective release of drugs[61] or to drastic decrease of the molecular weight in applications requiring degradation.[68]

In Figure 9 some examples of reversible and irreversible chromophores are presented. Azobenzene can switch between planar *E*-form and bent *Z*-form *via* light-induced isomerization of the N=N bond.[93] When coupled to a polymer chain, azobenzene has switching of hydrophilicity,[62] chirality,[94] optical properties,[95–97] and coordinative interaction[98] enabled in polymer materials. On the other hand, spiropyran changes from an unconjugated spiroheterocycle to a charged planar merocyanine form with extended conjugation.[99] The light-induced change of a neutral to a charged system has been applied to control wettability,[100] vesicle dissociation,[101] molecular recognition,[102] polymer chain solubility,[103] and ion penetration.[104] Diarylethene exists as either anti-parallel or parallel rotamers. Under light exposure, the anti-parallel rotamer undergoes closing of the six-membered ring within its core.[105] When attached to a polymer chain, cyclization can induce an extension of conjugation structure and rigidization. This leads to a change in the photoelectric properties of the polymer, that is, oxidation properties of polythiophene, conductivity of polyfluorene or fluorescence quantum efficiency of a photochromic system.[106] These three examples involve light-induced intramolecular transitions. Coumarin derivatives undergo reversible intermolecular dimerization to form thermally stable and colorless isomers in response to light.[107] Dimerization has been applied to adjust the lower critical solution temperature (LCST) of polymers, or to stabilize polymersomes by intramolecular or intermolecular cross-linking.

Typical examples of irreversible chromophores include photolabile protecting groups (o-nitrobenzyl and coumarin-4-ylmethyl derivatives), pyrenylmethyl and 2-napthoquinone -3-methides.[61,108–111] Photolabile groups are cleaved from the polymer chain upon light exposure. Depending on the

position in the chain where the chromophore has been inserted, different light induced molecular processes can occur: charge generation in side groups,[112–114] depolymerization and chain shortening,[63] activation of catalyst and 'click' reactant, formation of active groups, etc.[115]

As shown in Figure 1.9, o-Nitrobenzyl derivatives undergo light-induced intramolecular oxidation resulting in the released (uncaged) functionality and a nitrosocarbonyl by-product, while coumarin-4-ylmethyl leaves a solvent-trapped coumarin by-product.[116] 2-naphthoquinone-3-methides generate a highly reactive radical which can selectively react with vinyl compounds incorporating an electron-donating group (e.g. oxygen) *via* very rapid Diels–Alder addition reaction, resulting in the coupling of two species.[108–111] Incorporating this group on polymer side chains enables light-induced reactivity which is useful in photolithography.

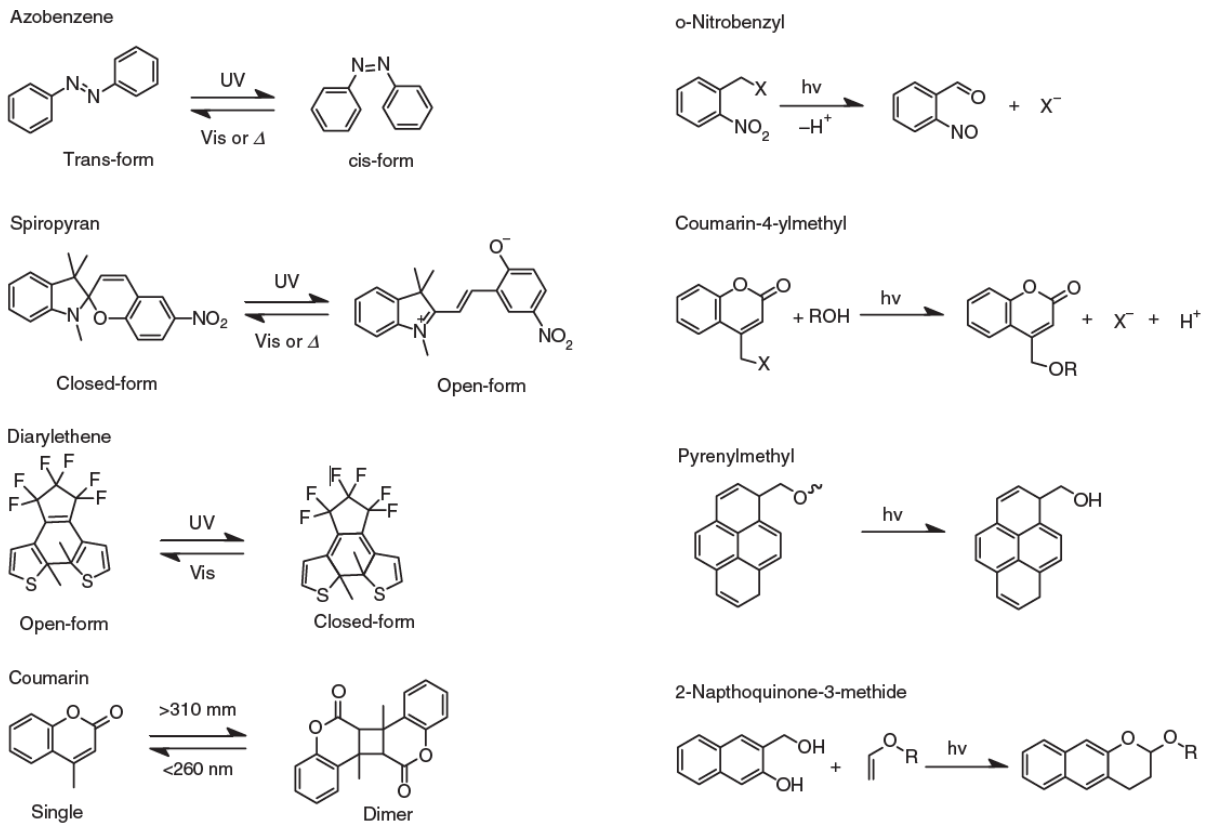

Figure 1.9 - Typical examples of reversible and irreversible photo-response groups

1.2. Azobenzene molecules

Among all the species of photo-active molecules described so far, azobenzenes are the most studied due to their simple preparation procedures, good processability, high thermal and chemical stability.[117] This family of organic photo-switchers gained a lot of attention during the last decades for the broad range of applications in which they can be used and for the simplicity with which their structure can be custom-made or modified to reach the correct response to the stimulus.

Azobenzenes are organic molecules that have two aromatic rings linked by an azo group (N=N). They are highly colored compounds and belong to the group of so-called FD&C (food, drug and cosmetics) dyes. Azobenzene was described for the first time in 1834,[118] and in 1937 – one century later – G.S. Hartley published a study on the influence of light on the configuration of N=N double bonds,[119] The exposure of a solution of azobenzene in acetone to light allowed the discovery of the *cis* isomer. This was the starting point of the development of one of the best organic molecular switches described so far. Nowadays, azobenzene dyes represent approximately 60% of the world production of industrial dyes.[120]

Like a C=C double bond, azobenzenes have two geometric isomers around the N=N double bond; the *E* isomer is ~12 kcal/mol more stable than the *Z* isomer.[121] The energy barrier of the photoexcited state is ~23 kcal/mol, such that the *E* isomer is predominant in the dark at room temperature.[122]

The *E* azobenzene easily isomerizes to the *Z* isomer by irradiation of the *E* isomer with a wavelength between 320 and 350 nm. The reaction is reversible, and the *E* isomer is recovered when the *Z* isomer is irradiated with light around 400 – 450 nm, or heated. For many azobenzenes, the two photochemical conversions occur on the scale of picoseconds, while the thermal relaxation of the *Z* isomer to the *E* isomer is much slower (milliseconds to days). The photo-induced isomerization of the azobenzenes leads to a remarkable change in their physical properties, such as molecular geometry, dipole moment or absorption spectrum.[123,124] The isomerization process involves a decrease in the distance between the two carbon atoms in position four of the aromatic rings of azobenzene, from 9.0 Å in the *E* form to 5.5 Å in

the *Z* form (Figure 1.10).[125] The *E* azobenzene is almost flat and has no dipole moment, whereas the *Z* isomer presents an angular geometry and a dipole moment of ~3.0 D. One of the rings rotates to avoid steric repulsions caused by the facing of one of the π clouds of one aromatic ring to the other. The UV-vis absorption spectrum of azobenzene presents two characteristic absorption bands corresponding to $\pi \rightarrow \pi^*$ and $n \rightarrow \pi^*$ electronic transitions. The transition $\pi \rightarrow \pi^*$ is usually in the near UV region and is common to carbonate systems, such as stilbene.[126] The electronic transition $n \rightarrow \pi^*$ is usually located in the visible region and is due to the presence of a lone electron pair on nitrogen atoms.[127] Due to this second electronic transition, the dynamic photoisomerization process of azobenzenes is different to the carbonate compounds.[128] Azobenzene undergoes *E*-*Z* isomerization by $S_1 \leftarrow S_0$ and $S_2 \leftarrow S_0$ excitations and *Z*-*E* isomerization by exciting into the S_1 or S_2 state. The sum of the quantum yields is different to unity, which indicates multiple pathways for isomerization.[129]

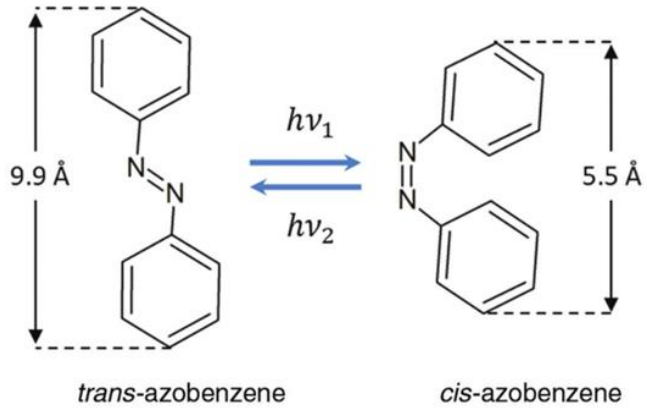

Figure 1.10 - Azobenzene photoisomerization.[130]

The isomerization process normally involves a color change to more intense colors. The absorption spectra of both isomers differ mostly in the following aspects (see Figure 1,11):[128]

- *E* isomer: the absorption band $\pi \rightarrow \pi^*$ is very intense, with a molar extinction coefficient (ε) ~ 2–3 × 10^4 $M^{-1} \cdot cm^{-1}$. The second band ($n \rightarrow \pi^*$) is much weaker (ε ~ 400 $M^{-1} \cdot cm^{-1}$) as this transition is not allowed in the E-*isomer* by symmetry rules.

- *Z* isomer: the absorption band $\pi \rightarrow \pi^*$ is shifted to shorter wavelengths (hypsochromic effect) decreasing significantly in intensity ($\varepsilon \sim 7–10 \times 10^3\ M^{-1}\cdot cm^{-1}$). The electronic transition $n \rightarrow \pi^*$ (380 – 520 nm) is allowed in the *Z* isomer, resulting in an increase in the intensity ($\varepsilon \sim 1500\ M^{-1}\cdot cm^{-1}$) with respect to the *E* isomer.

These differences allow a photochemical interconversion by irradiation with light of a certain wavelength, obtaining different concentration of the *Z* and *E* photostationary states. The photo stationary state is an *E*-*Z* steady-state composition that every photoswitchable sample in solution can reach after a certain period of time under the right illumination. Such composition, usually, depends on the competing effects of photoisomerization, thermal relaxation, and solvent nature. The kinetics of the isomerization and thermal relaxation processes, as well as the percentages of *Z* or *E* isomers, can be conveniently studied via absorption spectroscopy or NMR spectroscopy[131,132].

The excitation caused by the wavelength is dependent on the nature of the substituents of the aryl groups. In most cases, *E*→*Z* isomerization is promoted by irradiation with wavelengths between 320 and 380 nm, while exposures to $\lambda \sim 400–450$ nm favor the *Z*→*E* photoreversion. The mechanism is not well established. Several mechanistic studies have been performed on the isomerization reversal route *Z*→*E* of azobenzene to investigate the effect of the substituents on the benzene rings as well as the influence of several parameters.

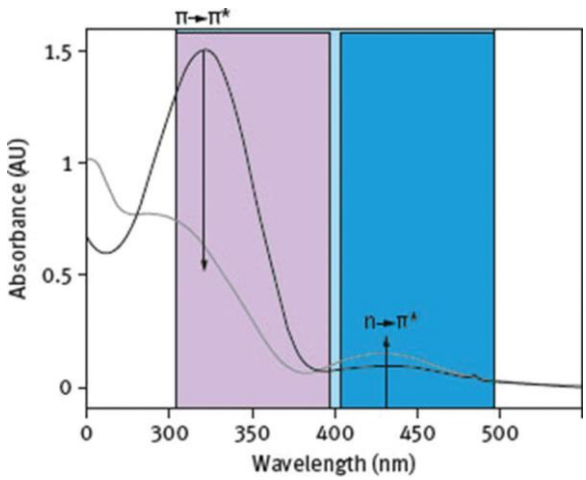

Figure 1.11 – UV-visible spectrum of azobenzene compounds.

The available data suggest that the isomerization of azocompounds can proceed through the reversal of one of the N–C bonds or by the rotation of the N=N bond. The lone pair of each nitrogen atom may lead to one $n \rightarrow \pi^*$ electronic transition ($S_0 \rightarrow S_1$) with inversion at the nitrogen atom (inversion mechanism). Conversely, the isomerization can also occur through a rotation mechanism, which involves a $\pi \rightarrow \pi^*$ transition ($S_0 \rightarrow S_2$) (Figure 1.12).[129,133,134]

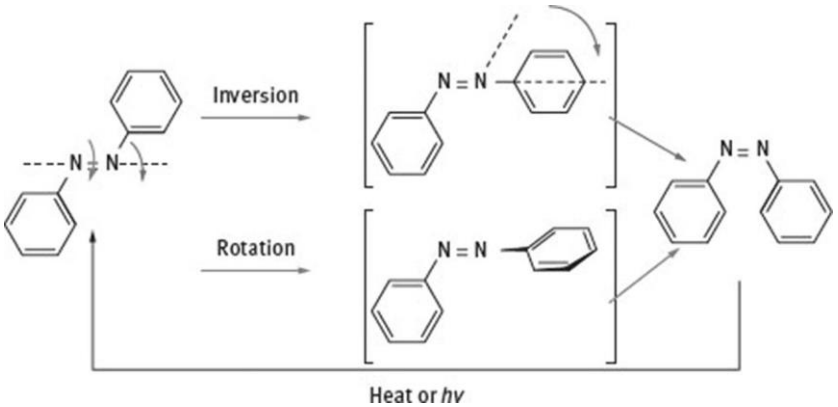

Figure 1.12 - Mechanistic proposals for the isomerization of azobenzenes.

1.2.1. Visible light-triggered azobenzenes

Despite all the useful properties and features described since so far, azobenzene molecules can have drawbacks regarding the applicability in some fields. The UV light photoisomerization of most azobenzenes, for example, can be considered as a limit for a wide range of *in vivo* or applications that comprise the biological systems. The UV light, actually, is considered unhealthy and can trigger unwanted responses, including cellular apoptosis. This is the main reason why the attention is particularly focused nowadays, on the modification of the azobenzene molecules to shift the isomerization process at different (higher) wavelengths. Photoisomerization that can occur entirely in the visible region would therefore be desirable, and considered as a benefit in many fields.[135] Many approaches for achieving longer wavelength switching have been tested as, for example, the coupling of azobenzene derivatives with upconverting nanophosphors[136] or the incorporation of electron-donor groups[137] which can dramatically red-shift the photoswitching wavelength. The

review from Merino et al. provides a comprehensive overview of the synthesis of azobenzene derivatives with special emphasis on the more recent ones and their mechanistic aspects.[138]

Although, the azobenzene chromophore family can be differentiated in three main clusters taking into account the electronic nature of the substituents present on the aromatic rings of the azobenzene, and was firstly proposed by Rau[121] (Fig. 1.13). The three groups are called: azobenzene derivatives, the amino-azobenzene derivatives and the push–pull azobenzene. This division depends principally on the order of their energetic electronic states $\pi \rightarrow \pi^*$ and $n \rightarrow \pi^*$[122].

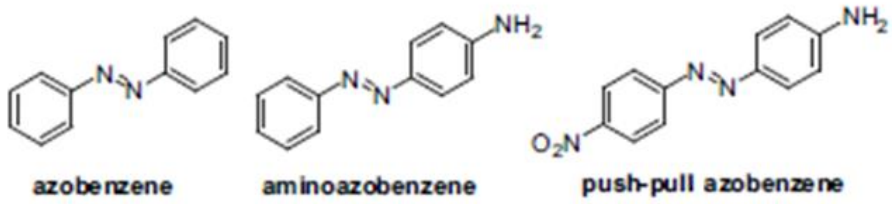

Figure 1.13 - Classification of azobenzenes compounds: un-modified azobenzene, aminoazobenzenes (azobenzene functionalized with one electron-donor group like -NH_2), push-pull azobenzenes (azobenzene functionalized with both electron-donor and electron acceptor groups like -NH_2 and NO_2).[121]

Those compounds all exhibit the central azobenzene structure while they differ for the ring substitution patterns; this helps to hold the common properties of azobenzene such as the strong electronic absorption, whilst the ring substitution leads to a modification of the absorption spectrum with a shift in the absorption wavelength;[139] moreover, depending on the nature of the substituents on the aromatic group, the equilibria between the *E* and *Z* isomers are variable. Each type of azobenzene also has a predominant color defined by the wavelength of the maximum absorption band (λ_{max}) (indicated in brackets in each case):

- Azobenzene type: the $\pi \rightarrow \pi^*$ band is very intense in the UV region and there is one $n \rightarrow \pi^*$ weaker in the visible region (yellow color). The electronic nature of the aromatic rings is very similar to simple azobenzene (Ph–N=N–Ph).

- Aminoazobenzene type (*o*- or *p*-(X)–C_6H_4–N=N-Ar): the π→π* and n→π* bands are very close or collapsing in the UV-vis region. In this case, the azocompounds have electron-donor substituents (X) in the *ortho* or *para* positions (orange color).
- Pseudo-stilbene type [(X)–C_6H_4–N=N–C_6H_4–(Y)]: the absorption band corresponding with π→π* transition is shifted to red, changing the appearance order with respect to the band n→π*. The azocompounds of this type present electron-donor substituents (X) and electron acceptors (Y) at the 4 and 4′ positions, respectively (push/pull system) (red color).

A large number of azobenzene derivatives are known in which enhanced electron-donating nature of ring substituents increases both the wavelength of absorption of the *E* isomer and the rate of thermal back-isomerization from *Z* to *E*.[140] This phenomenon has been attributed to similarities between the electronic excited state of the *E* isomer and the thermal transition state of back-relaxation that have both strong dipolar character (Figure 1.14)

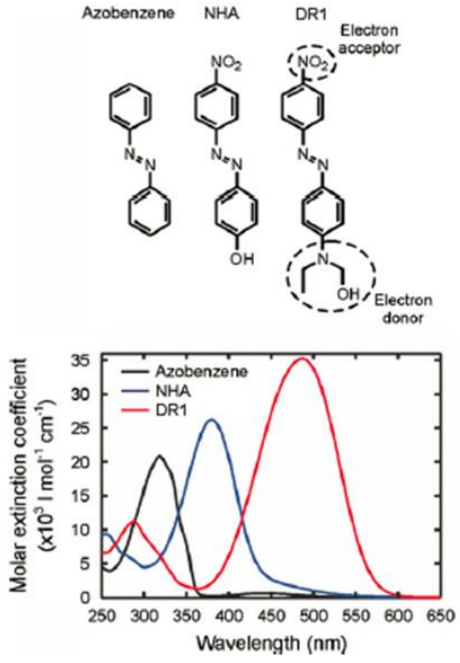

Figure 1.14 - Examples of azobenzenes and their absorption spectra measured from dilute tetrahydrofuran solution. The compounds are classified according to the weak or strong electron-donor behavior of the substituents and hence, to the absorption spectrum.

Due to their dipolar nature, the electronic excited state of the *E* isomer and the thermal transition state of back-relaxation can be really sensitive to the solvent polarity. This sensitiveness can influence different properties of azobenzene molecule, influencing these two states, like the photostationary state composition and the half-life of the *Z* isomer in the dark. In the work from Jerca et al. a detailed isomerization studies of a series of substituted azobenzenes is conducted by UV–Visible spectroscopy in different solvents.[141] They showed that isomerization and relaxation rates strongly depend on the polarity of the solvent and how the mechanisms of isomerization (rotation or inversion) depend on the chemical nature of the substituents and on the solvent polarity. Through spectroscopic measurements they developed a theoretical calculation for the study of the kinetics of photoisomerization and thermal relaxation. The kinetic parameters determined for the thermal *Z* to *E* relaxation processes confirm that the mechanism depends on the electron withdrawing capability of the substituent groups and on the solvent nature as well.

1.3. Smart controlled release membranes and their use in Febreze devices

As explained in the previous sections, during these years many studies were focused around the smart materials as promising way to boost and arise the performances of devices used in our daily life. As matter of interest, these polymers are being used in application like drug delivery, diagnostics, biotechnology, sensors, actuators and optical systems, as well as coatings, textiles and consumers goods. Scientists are creating system that could be more and more versatile and “smart”, depending on the conditions of the environments in which they are placed.

The aim of this PhD project is to improve, in fact, the performance of the Air Care devices produced by Procter & Gamble company.[142] Air care devices deliver a volatile material in a continuous or intermittent manner and may be passive or active. A crucial part of some of such devices consists of a porous membrane which allows the diffusion of the volatile material with poor selectivity, while avoiding leakage of the liquid mixture from the device with

higher fragrance delivery rate per unit area (Fig. 1.15). This membrane may be eventually sandwiched between coating layers.

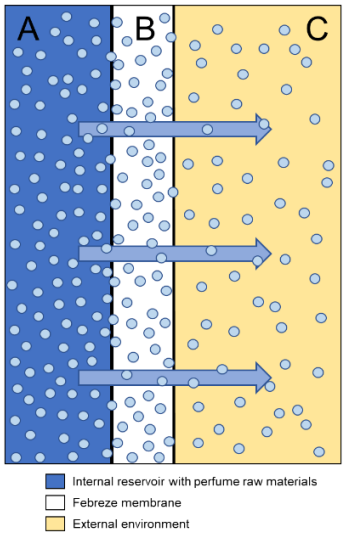

Figure 1.15 - Schematic rappresentation of Febreze Air Care device. A) the parfume moves from the internal reservoir to the membrane interface; B) the membrane is filled by the perfume raw materials; C) the perfume raw materials evaporate gradually from the membrane. The rate of the evaporation is affected by the temperature fluctuations of the extranal environment. [142]

However, there are several possibilities of improving the performances of this membrane. For instance, in conditions of prolonged higher temperature, like in a hot parked car or household condition, too much fragrance can evaporate, affecting the longevity of scent experience to the consumer; the membrane itself does not have an intensity control system and it is working continuously; another problem lies in the lack of control on the rate at which the top notes (more volatile part of the perfume) and the bottom notes (less volatile part of the perfume) evaporate from the membrane, which gives rise to an altered perception of the perfume, since the top notes come out much faster than the bottom ones. To get a better perfume spectrum balance, enabling the perfume to be delivered to the consumer according to the desired design, it would be preferred a membrane that could be tuned to set the rate of evaporation, depending on the volatility of the perfume components.

A possible solution to some of these problems could lie in membrane coating with new and properly functionalized polymers, which could act as a

selective “gate”, allowing or preventing the release of the volatile material under certain stimuli. As a matter of fact, the reversible changes of polarity and conformation imparted to a photochromic polymer system by photoirradiation can be applied to controlling mass transfer through membranes. For instance, it has been reported that azo-benzene based systems can successfully act as light-triggered membrane.[143] At a molecular level, *E-Z* isomerization leads to a substantial change in geometric conformation and size. On the other hand, it is also known that the interaction of some polymer groups with the dipole of *Z* azobenzene form can lead to a change in the wettability and swelling degree of a membrane, thus modifying its permeability to low molar mass compounds. This effect was proved in some blends even at azobenzene-functionalized content as low as 0.06 weight %.[144,145] From the letterature is well known that azobenzenes are very receptive to inclusion in different types of materials. This brilliant property of azobenzenes makes them useful in the preparation of different photoresponsive membranes. For this purpose, an azo molecule or chromophore can be directly blended into a polymer matrix or grafted (covalently attached) to a polymer. Also, polymeric membranes help in the study of these molecules to better understand their photoresponse so that they can be further used for the development of photoresponsive devices having applications in diverse fields. However, although the blending method is suitable, it shows instabilities in the photoresponse of the membranes attributable to the mobility of the azobenzenes in the polymer matrix and the tendency of the dipolar azobenzene molecules to form aggregates. Therefore, grafting is the most suitable method for the preparation of photoresponsive membranes with azobenzenes. In a recent study, azobenzene was grafted over the pore walls of a novel family of periodic mesoporous organosilicas.[146] In this study, bis(4-triethoxysilyl) azobenzene, bis(2,6-dimethyl-4-triethoxysilyl) azobenzene, and bis(2,6-diisopropyl-4-triethoxysilyl) azobenzene, three novel bis-silylated azobenzenes, were synthesized by using lithium-iodine exchange from their diiodoazobenzene derivatives. Further, these three bis-silylated azobenzenes were used to synthesize three novel azobenzene-bridged periodic mesoporous organosilica materials by using octadecyltrimethylammonium chloride (C_{18}TMACl) as a structure-directing agent under basic conditions. This resulted in the successful formation of

mesoporous materials with pore sizes in the range of 3.7 – 4.6 nm, and specific surface area in the range of 400 – 700 m^2/g. These materials are promising for reversible gas adsorption under the influence of light. Therefore, these materials can be used for the preparation of light-responsive membranes for gas-separation applications. This implies that release of volatile substances is possible and it can be triggered by light upon coating the vapor release surface of the porous membrane with a photochromic molecule-functionalized polymers. Moreover, the wavelength which induces the opening of the membrane, and subsequent release, could be adjusted by properly design the structure of the azo-bearing moiety. Darkness and/or temperature increase would drive the azobenzene units back to the more stable *E* configuration, thus inhibiting release. Moreover, since the so functionalized polymer is more polar when in its *Z* form, the "open" membrane would favor the release of hydrophilic fragrances over the hydrophobic ones, thus contributing to some flattening of the top and bottom notes.

1.4 Objectives

The objective of this PhD project is to improve the performance of Air Care Febreze devices produced by Procter & Gamble company; developing a membrane that can release the perfume raw materials inside the resevoir without being extremely affected by temperature fluctuations of the external environment, thus, being significantly less temperature sensitive than the current by used P&G ones.[142] In order to do this the main polyolefin/silica membrane will be coated with a polymer modified with novel azobenzene moieties.

This system could be triggered by light to act as an intelligent gate for the perfume diffusion, improving both selectivity and releasing control of the perfume raw materials in the home/car environment. In addition, by a proper design of the functionalizing unit, temperature could act as an additional external stimulus, able to conveniently trigger (i.e. reduce) membrane permeability through thermal back-isomerization.

The objectives of this thesis can be summarized as follows:

- Synthesis and characterization of the proper azobenzene moiety and characterization of its properties;
- Modification of commercial EVOH with the desired groups. Characterization of the resulting systems and study of the light/temperature response;
- Preparation of membranes out of modified EVOH by means of different techniques. Membranes characterization without and under external stimuli;
- Process selection for implementation of the stimuli-responsive membrane in the device and testing in the final prototype.

The main hypothesis which reinforce the objectives are:

- Azobenzene: The wavelength which induces the opening of the membrane, and subsequent release, could be adjusted by properly design the structure of the azo-bearing moiety. Darkness and/or temperature increase would drive the azobenzene units back to the more stable *E* configuration, thus inhibiting release. Moreover, since the so functionalized polymer is more polar when in its *Z* form, the "open" membrane would favor the release of hydrophilic fragrances over the hydrophobic ones, thus contributing to some flattening of the top and bottom notes;
- Polymer: reversible changes of polarity and conformation imparted to a photochromic polymer system by photoirradiation can be applied to controlling mass transfer through membranes. It has been reported that azo-benzene based systems can successfully act as light-triggered membrane;
- Membrane: the interaction of some polymer groups with the dipole of *Z* azobenzene form can lead to a change in the wettability and swelling degree of a membrane, thus modifying its permeability to low molar mass compounds;
- Prototypes: Release of volatile substances can be triggered by light upon coating the vapor release surface of the porous membrane with

a photochromic molecule-functionalized polymers with a specific thickness.

References

1. Schull, J. *et al.* Are species intelligent? *Behav. Brain Sci.* **13**, 63–75 (1990).
2. Zhang, X. *et al.* The Pathway to Intelligence: Using Stimuli-Responsive Materials as Building Blocks for Constructing Smart and Functional Systems. *Adv. Mater.* **31**, 1804540 (2019).
3. Fuß, W. *et al.* The Photochemical cis–trans Isomerization of Free Stilbene Molecules Follows a Hula-Twist Pathway. *Angew. Chem. Int. Ed.* **43**, 4178–4182 (2004).
4. Minkin, V. I. *et al.* Photo-, Thermo-, Solvato-, and Electrochromic Spiroheterocyclic Compounds. *Chem. Rev.* **104**, 2751–2776 (2004).
5. Chen, L. *et al.* A Light-Responsive Release Platform by Controlling the Wetting Behavior of Hydrophobic Surface. *ACS Nano* **8**, 744–751 (2014).
6. Berkovic, G. *et al.* Spiropyrans and Spirooxazines for Memories and Switches. *Chem. Rev.* **100**, 1741–1754 (2000).
7. Bandara, H. M. D. *et al.* Photoisomerization in different classes of azobenzene. *Chem. Soc. Rev.* **41**, 1809–1825 (2012).
8. Schild, H. G. *et al.* Poly(N-isopropylacrylamide): experiment, theory and application. *Prog. Polym. Sci.* **17**, 163–249 (1992).
9. Lu, W. *et al.* Supramolecular shape memory hydrogels: a new bridge between stimuli-responsive polymers and supramolecular chemistry. *Chem. Soc. Rev.* **46**, 1284–1294 (2017).
10. Aznar, E. *et al.* Gated Materials for On-Command Release of Guest Molecules. *Chem. Rev.* **116**, 561–718 (2016).
11. Yang, Y.-W. *et al.* Switchable Host–Guest Systems on Surfaces. *Acc. Chem. Res.* **47**, 1950–1960 (2014).
12. Murakami, H. *et al.* Light-Driven Molecular Shuttle Based on a Rotaxane. *J. Am. Chem. Soc.* **119**, 7605–7606 (1997).
13. Murakami, H. *et al.* A Multi-Mode-Driven Molecular Shuttle: Photochemically and Thermally Reactive Azobenzene Rotaxanes. *J. Am. Chem. Soc.* **127**, 15891–15899 (2005).

14. Inoue, Y. *et al.* Thermal and Photochemical Switching of Conformation of Poly(ethylene glycol)-Substituted Cyclodextrin with an Azobenzene Group at the Chain End. *J. Am. Chem. Soc.* **129**, 6396–6397 (2007).
15. Smith, C. V. *et al.* Compartmentation of Glutathione: Implications for the Study of Toxicity and Disease. *Toxicol. Appl. Pharmacol.* **140**, 1–12 (1996).
16. F. Quinn, J. *et al.* Glutathione responsive polymers and their application in drug delivery systems. *Polym. Chem.* **8**, 97–126 (2017).
17. Yokoyama, M. *et al.* Drug targeting with nano-sized carrier systems. *J. Artif. Organs* **8**, 77–84 (2005).
18. Miyata, K. *et al.*Polymeric micelles for nano-scale drug delivery. *React. Funct. Polym.* **71**, 227–234 (2011).
19. Rodríguez-Hernández, J. *et al.* Toward 'smart' nano-objects by self-assembly of block copolymers in solution. *Prog. Polym. Sci.* **7**, 691–724 (2005).
20. Mohamed, S. *et al.* Polymeric nano-micelles: versatile platform for targeted delivery in cancer. *Ther. Deliv.* **5**, 1101–1121 (2014).
21. Stuart, M. A. C. *et al.* Emerging applications of stimuli-responsive polymer materials. *Nat. Mater.* **9**, 101–113 (2010).
22. Akimoto, J. *et al.* Temperature-responsive polymeric micelles for optimizing drug targeting to solid tumors. *J. Controlled Release* **193**, 2–8 (2014).
23. Roy, D. *et al.* New directions in thermoresponsive polymers. *Chem. Soc. Rev.* **42**, 7214–7243 (2013).
24. Nagappan, S. *et al.* Bio-inspired, multi-purpose and instant superhydrophobic–superoleophilic lotus leaf powder hybrid micro–nanocomposites for selective oil spill capture. *J. Mater. Chem. A* **1**, 6761–6769 (2013).
25. Chen, J.-K. *et al.* Fabrications and Applications of Stimulus-Responsive Polymer Films and Patterns on Surfaces: A Review. *Materials* **7**, 805–875 (2014).
26. Mano, J. F. *et al.* Stimuli-Responsive Polymeric Systems for Biomedical Applications. *Adv. Eng. Mater.* **10**, 515–527 (2008).

27. Uhlmann, P. *et al.* Surface functionalization by smart coatings: Stimuli-responsive binary polymer brushes. *Prog. Org. Coat.* **55**, 168–174 (2006).
28. Minko, S. *et al.* Responsive Polymer Brushes. *J. Macromol. Sci. Part C* **46**, 397–420 (2006).
29. Bawa, P. *et al.* Stimuli-responsive polymers and their applications in drug delivery. *Biomed. Mater.* **4**, 022001 (2009).
30. Lai, J. J. *et al.* Dynamic bioprocessing and microfluidic transport control with smart magnetic nanoparticles in laminar-flow devices. *Lab. Chip* **9**, 1997–2002 (2009).
31. Börner, H. G. *et al.* Making “smart polymers” smarter: Modern concepts to regulate functions in polymer science. *J. Polym. Sci. Part Polym. Chem.* **48**, 1–14 (2010).
32. Guenther, M. *et al.* Chemical sensors based on multiresponsive block copolymer hydrogels. *Sens. Actuators B Chem.* **126**, 97–106 (2007).
33. Wang, C. *et al.* A pH-sensitive molecularly imprinted nanospheres/hydrogel composite as a coating for implantable biosensors. *Biomaterials* **31**, 4944–4951 (2010).
34. Fernández-Barbero, A. *et al.* Gels and microgels for nanotechnological applications. *Adv. Colloid Interface Sci.* **147–148**, 88–108 (2009).
35. Tokarev, I. *et al.* Molecular-engineered stimuli-responsive thin polymer film: a platform for the development of integrated multifunctional intelligent materials. *J. Mater. Chem.* **19**, 6932–6948 (2009).
36. Gil, E. S. *et al.* Stimuli-reponsive polymers and their bioconjugates. *Prog. Polym. Sci.* **29**, 1173–1222 (2004).
37. Philippova, O. E. *et al.* Interaction of Hydrophobically Modified Poly(acrylic acid) Hydrogels with Ionic Surfactants. *Macromolecules* **29**, 2822–2830 (1996).
38. Tonge, S. R. *et al.* Responsive hydrophobically associating polymers: a review of structure and properties. *Adv. Drug Deliv. Rev.* **53**, 109–122 (2001).
39. Berndt, E. *et al.* Synthesis of block copolymers for surface functionalization with stimuli-responsive macromolecules. *Polymer* **50**, 5181–5191 (2009).

40. Alarcón, C. *et al.* Bioadhesion at micro-patterned stimuli-responsive polymer brushes. *J. Mater. Chem.* **15**, 2089–2094 (2005).
41. Kaholek, M. *et al.* Fabrication of Stimulus-Responsive Nanopatterned Polymer Brushes by Scanning-Probe Lithography. *Nano Lett.* **4**, 373–376 (2004).
42. Matsuda, N. *et al.* Tissue Engineering Based on Cell Sheet Technology. *Adv. Mater.* **19**, 3089–3099 (2007).
43. Mizutani, A. *et al.* Preparation of thermoresponsive polymer brush surfaces and their interaction with cells. *Biomaterials* **29**, 2073–2081 (2008).
44. Ernst, O. *et al.* Tuning of Thermo-responsive Self-Assembly Monolayers on Gold for Cell-Type-Specific Control of Adhesion. *Langmuir* **24**, 10259–10264 (2008).
45. Yamamoto, S. *et al.* ATRP Synthesis of Thermally Responsive Molecular Brushes from Oligo(ethylene oxide) Methacrylates. *Macromolecules* **40**, 9348–9353 (2007).
46. Lutz, J.-F. *et al.* Biocompatible, Thermoresponsive, and Biodegradable: Simple Preparation of “All-in-One” Biorelevant Polymers. *Macromolecules* **40**, 8540–8543 (2007).
47. Lutz, J.-F. *et al.* About the Phase Transitions in Aqueous Solutions of Thermoresponsive Copolymers and Hydrogels Based on 2-(2-methoxyethoxy)ethyl Methacrylate and Oligo(ethylene glycol) Methacrylate. *Macromolecules* **40**, 2503–2508 (2007).
48. Becer, C. R. *et al.* Libraries of methacrylic acid and oligo(ethylene glycol) methacrylate copolymers with LCST behavior. *J. Polym. Sci. Part Polym. Chem.* **46**, 7138–7147 (2008).
49. Meyer, D. E. *et al.* Quantification of the Effects of Chain Length and Concentration on the Thermal Behavior of Elastin-like Polypeptides. *Biomacromolecules* **5**, 846–851 (2004).
50. Fernández-Trillo, F. *et al.* Reversible Immobilization onto PEG-based Emulsion-templated Porous Polymers by Co-assembly of Stimuli Responsive Polymers. *Adv. Mater.* **21**, 55–59 (2009).
51. Gil, E. S. *et al.* Stimuli-reponsive polymers and their bioconjugates. *Prog. Polym. Sci.* **29**, 1173–1222 (2004).

52. Vallet, M. *et al.* Electrowetting of water and aqueous solutions on poly(ethylene terephthalate) insulating films. *Polymer* **37**, 2465–2470 (1996).
53. Lahann, J. *et al.* A Reversibly Switching Surface. *Science* **299**, 371–374 (2003).
54. Katz, E. *et al.* Electromechanics of a Redox-Active Rotaxane in a Monolayer Assembly on an Electrode. *J. Am. Chem. Soc.* **126**, 15520–15532 (2004).
55. Bar-Cohen, Y. *et al.* Artificial muscles using electroactive polymers (EAP): capabilities, challenges and potential. (2005).
56. Bar-Cohen, Y. *et al.* 8 - Electroactive polymers as actuators. in *Advanced Piezoelectric Materials* (ed. Uchino, K.) 287–317 (Woodhead Publishing, 2010). doi:10.1533/9781845699758.1.287.
57. Szaciłowski, K. *et al.* Digital Information Processing in Molecular Systems. *Chem. Rev.* **108**, 3481–3548 (2008).
58. Corredor, C. C. *et al.* Photochromic Polymer Composites for Two-Photon 3D Optical Data Storage. *Chem. Mater.* **19**, 5165–5173 (2007).
59. Toriumi, A. *et al.* Reflection confocal microscope readout system for three-dimensional photochromic optical data storage. *Opt. Lett.* **23**, 1924–1926 (1998).
60. Schumers, J.-M. *et al.* Light-Responsive Block Copolymers. *Macromol. Rapid Commun.* **31**, 1588–1607 (2010).
61. Zhao, Y. *et al.* Photocontrollable block copolymer micelles: what can we control? *J. Mater. Chem.* **19**, 4887–4895 (2009).
62. Zhao, Y. *et al.* Light-Responsive Block Copolymer Micelles. *Macromolecules* **45**, 3647–3657 (2012).
63. Zhao, H. *et al.* o-Nitrobenzyl Alcohol Derivatives: Opportunities in Polymer and Materials Science. *Macromolecules* **45**, 1723–1736 (2012).
64. Yu, H. *et al.* Photocontrollable Liquid-Crystalline Actuators. *Adv. Mater.* **23**, 2149–2180 (2011).
65. Ikeda, T. *et al.* Photomechanics of Liquid-Crystalline Elastomers and Other Polymers. *Angew. Chem. Int. Ed.* **46**, 506–528 (2007).
66. Wondraczek, H. *et al.* Photoactive polysaccharides. *Carbohydr. Polym.* **83**, 1048–1061 (2011).

67. Al-Malaika, S. *et al.* Photodegradable Polymers. in *Photochemistry and Photophysics of Polymer Materials* 603–626 (John Wiley & Sons, Ltd, 2010). doi:10.1002/9780470594179.ch16.
68. Pasparakis, G. *et al.* Photodegradable Polymers for Biotechnological Applications. *Macromol. Rapid Commun.* **33**, 183–198 (2012).
69. Shibaev, V. *et al.* Photoactive liquid crystalline polymer systems with light-controllable structure and optical properties. *Prog. Polym. Sci.* **28**, 729–836 (2003).
70. Zhao, Y. *et al.* Rational design of light-controllable polymer micelles. *Chem. Rec.* **7**, 286–294 (2007).
71. Krauss, U. *et al.* LOVely enzymes – towards engineering light-controllable biocatalysts. *Microb. Biotechnol.* **3**, 15–23 (2010).
72. Shinkai, S. *et al.* Photoresponsive complexation of metal cations with an azobenzene-crown-azobenzene bridge immobilized in polymer supports. *J. Am. Chem. Soc.* **104**, 2933–2934 (1982).
73. Lai, C.-T. *et al.* Aggregation-Induced Emission in Tetraphenylthiophene-Derived Organic Molecules and Vinyl Polymer. *J. Phys. Chem. B* **114**, 10302–10310 (2010).
74. Gupta, S. *et al.* Immobilization of Silver Nanoparticles on Responsive Polymer Brushes. *Macromolecules* **41**, 2874–2879 (2008).
75. Ruchmann, J. *et al.* Photoresponse of Complexes between Surfactants and Azobenzene-Modified Polymers Accounting for the Random Distribution of Hydrophobic Side Groups. *Macromolecules* **44**, 604–611 (2011).
76. Everlof, G. J. *et al.* Stimuli-responsive polymers. 4. Photo- and thermo-regulated chiroptical behavior in azobenzene-modified polymers fitted with main chain spirobiindane turns and chiral binaphthyl bends. *Polymer* **41**, 6527–6536 (2000).
77. Irie, M. *et al.* Properties and applications of photoresponsive polymers. *Pure Appl. Chem.* **62**, 1495–1502 (1990).
78. Zakhidov, A. A. *et al.* Photogeneration of charge carriers in organic superlattices with polarization double barriers. *Synth. Met.* **71**, 1875–1876 (1995).

79. Wu, Y. *et al.* Photoinduced Alignment of Polymer Liquid Crystals Containing Azobenzene Moieties in the Side Chain. 5. Effect of the Azo Contents on Alignment Behavior and Enhanced Response. *Macromolecules* **32**, 3951–3956 (1999).
80. Sajti, Sz. *et al.* Response function for the characterization of photo-induced anisotropy in azobenzene containing polymers. *Appl. Phys. B* **75**, 677–685 (2002).
81. Pandey, S. *et al.* Siloxane polymers containing azo moieties synthesized by click chemistry for photo responsive and liquid crystalline applications. *J. Polym. Sci. Part Polym. Chem.* **50**, 1205–1215 (2012).
82. Wang, Y. *et al.* Self-assembly and photo-responsive behavior of novel ABC2-type block copolymers containing azobenzene moieties. *Soft Matter* **8**, 3131–3138 (2012).
83. Chen, C. *et al.* Photo-responsive, biocompatible polymeric micelles self-assembled from hyperbranched polyphosphate-based polymers. *Polym. Chem.* **2**, 1389–1397 (2011).
84. He, J. *et al.* Light-responsive polymer micelles, nano- and microgels based on the reversible photodimerization of coumarin. *Dyes Pigments* **89**, 278–283 (2011).
85. Chen, C.-J. *et al.* Construction of photo-responsive micelles from azobenzene-modified hyperbranched polyphosphates and study of their reversible self-assembly and disassembly behaviours. *New J. Chem.* **36**, 694–701 (2012).
86. Han, D. *et al.* Block Copolymer Micelles with a Dual-Stimuli-Responsive Core for Fast or Slow Degradation. *Langmuir* **28**, 2327–2331 (2012).
87. Fries, K. H. *et al.* Spectroscopic Analysis of Metal Ion Binding in Spiropyran Containing Copolymer Thin Films. *Anal. Chem.* **82**, 3306–3314 (2010).
88. Mayer, S. *et al.* A new chiral polyisocyanate: an optical switch triggered by a small amount of photochromic side groups. *Macromol. Chem. Phys.* **199**, 1675–1682 (1998).
89. Zhang, W. *et al.* Unpolarized-Light-Driven Amplified Chiroptical Modulation Between Chiral Aggregation and Achiral Disaggregation of

an Azobenzene-alt-Fluorene Copolymer in Limonene. *Macromolecules* **44**, 5105–5111 (2011).

90. Kim, E. *et al.* Photoswitching of Diarylethene Polymers Synthesized by TEMPO Mediated Polymerization. *Mol. Cryst. Liq. Cryst.* **430**, 135–145 (2005).
91. Uchida, K. *et al.* Picosecond laser photolysis studies on a photochromic oxidation polymer film consisting of diarylethene molecules. *J. Mater. Chem.* **15**, 2128–2133 (2005).
92. Feringa, B. L. *et al.* Chiroptical Molecular Switches. *Chem. Rev.* **100**, 1789–1816 (2000).
93. Barrett, C. J. *et al.* Photo-mechanical effects in azobenzene-containing soft materials. *Soft Matter* **3**, 1249–1261 (2007).
94. Maxein, G. *et al.* Photochemical Inversion of the Helical Twist Sense in Chiral Polyisocyanates. *Macromolecules* **28**, 8438–8440 (1995).
95. Kravchenko, A. *et al.* Optical Interference Lithography Using Azobenzene-Functionalized Polymers for Micro- and Nanopatterning of Silicon. *Adv. Mater.* **23**, 4174–4177 (2011).
96. Alicante, R. *et al.* Matrix Order Influence on the Non-Linear Optical Properties of Dispersed Chromophore-Azopolymer Systems. *Macromol. Chem. Phys.* **213**, 776–783 (2012).
97. Schab-Balcerzak, E. *et al.* Poly(etherimide)s and poly(esterimide)s containing azobenzene units: Characterization and study of photoinduced optical anisotropy. *Opt. Mater.* **34**, 733–740 (2012).
98. Barille, R. *et al.* Cooperative interaction in azopolymers upon irradiation. *New J. Chem.* **33**, 1207–1210 (2009).
99. Paramonov, S. V. *et al.* Spiropyran, chromene or spirooxazine ligands: Insights into mutual relations between complexing and photochromic properties. *J. Photochem. Photobiol. C Photochem. Rev.* **12**, 209–236 (2011).
100. Anastasiadis, S. H. *et al.* Reversibly Photo-Responsive Polymer Surfaces for Controlled Wettability. *J. Adhes. Sci. Technol.* **22**, 1853–1868 (2008).
101. Lee, H. *et al.* Light-Induced Reversible Formation of Polymeric Micelles. *Angew. Chem. Int. Ed.* **46**, 2453–2457 (2007).

102. Andersson, J. *et al.* Photoswitched DNA-Binding of a Photochromic Spiropyran. *J. Am. Chem. Soc.* **130**, 11836–11837 (2008).
103. Szilágyi, A. *et al.* Rewritable Microrelief Formation on Photoresponsive Hydrogel Layers. *Chem. Mater.* **19**, 2730–2732 (2007).
104. Nayak, A. *et al.* An Optically Reversible Switching Membrane Surface. *Angew. Chem. Int. Ed.* **45**, 4094–4098 (2006).
105. Walko, M. *et al.* The isolation and photochemistry of individual atropisomers of photochromic diarylethenes. *Chem. Commun.* 1745–1747 (2007) doi:10.1039/B702264F.
106. Luo, Q. *et al.* Recent progress on photochromic diarylethene polymers. *Polym. Chem.* **2**, 2435–2443 (2011).
107. Cardenas-Daw, C. *et al.* Reversible Photocycloadditions, a Powerful Tool for Tailoring (Nano)Materials. *Macromol. Chem. Phys.* **213**, 144–156 (2012).
108. Arumugam, S. *et al.* Photochemical Generation and the Reactivity of o-Naphthoquinone Methides in Aqueous Solutions. *J. Am. Chem. Soc.* **131**, 11892–11899 (2009).
109. Arumugam, S. *et al.* Light-Induced Hetero-Diels−Alder Cycloaddition: A Facile and Selective Photoclick Reaction. *J. Am. Chem. Soc.* **133**, 5573–5579 (2011).
110. Arumugam, S. *et al.* Patterned Surface Derivatization Using Diels–Alder Photoclick Reaction. *J. Am. Chem. Soc.* **133**, 15730–15736 (2011).
111. Arumugam, S. *et al.* Photoreactive Polymer Brushes for High-Density Patterned Surface Derivatization Using a Diels–Alder Photoclick Reaction. *J. Am. Chem. Soc.* **134**, 179–182 (2012).
112. Brown, A. A. *et al.* Photoresponsive Polymer Brushes for Hydrophilic Patterning. *Langmuir* **25**, 1744–1749 (2009).
113. Cui, J. *et al.* Polymer Brushes with Phototriggered and Phototunable Swelling and pH Response. *Macromol. Rapid Commun.* **32**, 1699–1703 (2011).
114. Brown, A. A. *et al.* Polymer brush resist for responsive wettability. *Soft Matter* **5**, 2738–2745 (2009).
115. Mayer, G. *et al.* Biologically Active Molecules with a “Light Switch”. *Angew. Chem. Int. Ed.* **45**, 4900–4921 (2006).

116. Goeldner, M. *et al. Dynamic Studies in Biology: Phototriggers, Photoswitches and Caged Biomolecules*. (John Wiley & Sons, 2006).
117. Silong, S. *et al.* Synthesis and characterization of side-chain liquid-crystalline polyacrylates containing azobenzene moieties. *J. Appl. Polym. Sci.* **86**, 2653–2661 (2002).
118. Demselben *et al.* Ueber das Stickstoffbenzid. *Ann. Pharm.* **12**, 311–314 (1834).
119. Hartley, G. S. *et al.* The *Cis*-form of Azobenzene. *Nature* **140**, 281 (1937).
120. Zollinger, H. *et al. Color Chemistry: Syntheses, Properties, and Applications of Organic Dyes and Pigments*. (John Wiley & Sons, 2003).
121. Rabek, J. F. *et al. Photochemistry and Photophysics*. (CRC Press, 1989).
122. Brown, E. V. *et al.* Cis-trans isomerism in the pyridyl analogs of azobenzene. Kinetic and molecular orbital analysis. *J. Am. Chem. Soc.* **97**, 621–627 (1975).
123. Morgenstern, K. *et al.* Isomerization Reactions on Single Adsorbed Molecules. *Acc. Chem. Res.* **42**, 213–223 (2009).
124. Dürr, H. *et al. Photochromism: Molecules and Systems*. (Elsevier, 2003).
125. Koshima, H. *et al.* Mechanical Motion of Azobenzene Crystals upon Photoirradiation. *J. Am. Chem. Soc.* **131**, 6890–6891 (2009).
126. Sension, R. J. *et al.* Femtosecond laser studies of the cis-stilbene photoisomerization reactions. *J. Chem. Phys.* **98**, 6291–6315 (1993).
127. Bédard, M. *et al.* Optically Driven Encapsulation Using Novel Polymeric Hollow Shells Containing an Azobenzene Polymer. *Macromol. Rapid Commun.* **28**, 1517–1521 (2007).
128. Ladányi, V. *et al.* Azobenzene photoisomerization quantum yields in methanol redetermined. *Photochem. Photobiol. Sci.* **16**, 1757–1761 (2017).
129. Merino, E. *et al.* Control over molecular motion using the cis–trans photoisomerization of the azo group. *Beilstein J. Org. Chem.* **8**, 1071–1090 (2012).
130. Oscurato, S. *et al.* From nanoscopic to macroscopic photo-driven motion in azobenzene-containing materials. *Nanophotonics* (2018) doi:10.1515/nanoph-2018-0040.

131. Magennis, S. W. *et al.* Two-Photon-Induced Photoisomerization of an Azo Dye. *Chem. Mater.* **17**, 2059–2062 (2005).
132. Beltrame, P. L. *et al.* Thermal cis-trans isomerization of azo dyes in poly(methyl methacrylate) matrix: A kinetic study. *J. Appl. Polym. Sci.* **49**, 2235–2239 (1993).
133. Tamai, N. *et al.* Ultrafast Dynamics of Photochromic Systems. *Chem. Rev.* **100**, 1875–1890 (2000).
134. Crecca, C. R. *et al.* Theoretical Study of the Isomerization Mechanism of Azobenzene and Disubstituted Azobenzene Derivatives. *J. Phys. Chem. A* **110**, 8188–8203 (2006).
135. Beharry, A. A. *et al.* Azobenzene Photoswitching without Ultraviolet Light. *J. Am. Chem. Soc.* **133**, 19684–19687 (2011).
136. Wu, W. *et al.* NIR-Light-Induced Deformation of Cross-Linked Liquid-Crystal Polymers Using Upconversion Nanophosphors. *J. Am. Chem. Soc.* **133**, 15810–15813 (2011).
137. Mourot, A. *et al.* Tuning Photochromic Ion Channel Blockers. *ACS Chem. Neurosci.* **2**, 536–543 (2011).
138. Merino, E. *et al.* Synthesis of azobenzenes: the coloured pieces of molecular materials. *Chem. Soc. Rev.* **40**, 3835–3853 (2011).
139. Mahimwalla, Z. *et al.* Azobenzene photomechanics: prospects and potential applications. *Polym. Bull.* **69**, 967–1006 (2012).
140. Nishimura, N. *et al.* Thermal Cis-to-Trans Isomerization of Substituted Azobenzenes II. Substituent and Solvent Effects. *Bull. Chem. Soc. Jpn.* **49**, 1381–1387 (1976).
141. Jerca, V. V. *et al.* Advances in understanding the photoresponsive behavior of azobenzenes substituted with strong electron withdrawing groups. *Opt. Mater.* **48**, 160–164 (2015).
142. Gruenbacher, D. P. *et al.* Method for delivering a volatile material. (2010).
143. Tylkowski, B. *et al.* Preparation of a new lightly cross-linked liquid crystalline polyamide by interfacial polymerization. Application to the obtainment of microcapsules with photo-triggered release. *Eur. Polym. J.* **45**, 1420–1432 (2009).

144. Ishihara, K. *et al.* Photoinduced permeation control of proteins using amphiphilic azoaromatic polymer membrane. *J. Polym. Sci. Polym. Lett. Ed.* **22**, 515–518 (1984).

145. Tylkowski, B. *et al.* Light-Induced Switching of the Wettability of Novel Asymmetrical Poly(vinyl alcohol)-co-ethylene Membranes Blended with Azobenzene Polymers. *Langmuir* **26**, 14821–14829 (2010).

146. Abboud, M. & Sayari, A. Novel family of periodic mesoporous organosilicas containing azobenzene within the pore walls. *Microporous Mesoporous Mater.* **249**, 157–164 (2017).

Chapter 2. Design, synthesis and chemical characterization of novel asymmetrical azobenzene compounds

2.2 Introduction

The parent azobenzene molecule, as already mentioned in Chapter 1, can bear different chemical groups on the phenyl rings in order to fine-tune the optical properties and response time of the isomerization.[1] These substituents will also dramatically change the spectroscopic properties, affecting the relative position and intensity of the absorption bands in UV–Vis spectra. Several studies have already demonstrated that the introduction of ring substituents significantly influences the absorption wavelength of both isomers of azobenzene.[2] This shift has been attributed to three factors: I) electron-donor group on the rings lead to a red-shift of the absorbance of the *E* isomer, due to raising the relative energy of the HOMO in the *E* form,[3] II) steric interactions reduces the sp^2 character of the N atoms, also raising the HOMO energy, leading to the red-shifted absorbance,[4] and III) electron-withdrawing groups, such as F atoms, can lower the n-orbital energy of the *Z* isomer by reducing the electron density in the nearby N=N bond, red-shifting the absorbance of the *E* isomer either.[5] In Table 2.1. several examples of the modification of azobenzene molecules and thus, of the corresponding absorption spectra, are schematically reported.

Table 2.1. - Visible Light-responsive symmetric azobenzene derivatives reported in literature.

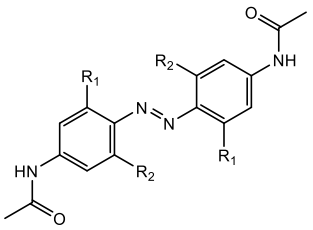

R_1	R_2	λ_{max} *E* isomer [nm]	λ_{max} *Z* isomer [nm]
H	H	364	348 (π→π*), 473 (n→π*)
Methoxy	Methoxy	338 (π→π*), 480 (n→π*)	330 (π→π*), 444 (n→π*)
Piperidine	H	445	-
F	F	364 (π→π*), 370 (n→π*)	314 (π→π*), 450 (n→π*)

According to the table and to what already explained in Chapter 1, increasing electron density can be a good strategy to red-shift the absorption and lower the energy barrier for the *E-Z* isomerization. This last feature of the azobenzene-type molecules is a very promising tool that allows fine-tuning of the optical response and that can broad the fields of applications in which these molecules can be used when, for example, the isomerization driven by UV light irradiation is a problem (e.g., *in vivo* applications).

The main idea of this thesis work is to design, synthesize and study novel asymmetrical azobenzene compounds with specific substitutional pattern, bearing one reactive site. The specific properties derived from their substitutional pattern and the single reactive site could make them good candidates for the chemical modification of commercial polymers, thus giving them stimuli responsive properties for the creation of a smart material.

To the best of our knowledge, the synthesis of the azo-derivatives, that will be described in this chapter, has not been reported in literature. These systems were well-designed to achieve *E-Z* isomerization when irradiated by visible light and a thermal back isomerization when heated above room temperature.

First, the entire procedure to synthesize the azo-compounds was planned, following a molecular design approach. The molecular design consists of four passages leading to the moieties in acyl-chloride form with which the selected copolymer would be modified through an esterification reaction. The structure of the final azo-compound was designed in order to include electron-donor substituents in orto position to the azo-bound, as to induce photoisomerization in the visible region and possibly thermal back-isomerization in a proper temperature range.

The procedure consists four steps, that are:

- Azo coupling reaction between an aromatic amine and a phenolic compound, giving 4-((2-hydroxy-5-methylphenyl)diazenyl)-3-methoxybenzoic acid (**AZO1**);
- Methylation of the alcoholic and carboxylic groups, giving methyl 3-methoxy-4-((2-methoxy-5-methylphenyl)diazinyl) benzoate (**AZO2**);

- Hydrolysis of the methyl ester group, giving 3-methoxy-4-((2-methoxy-5-methylphenyl)diazenyl)benzoic acid (**AZO3**);
- Conversion to acyl-chloride, giving 3-methoxy-4-((2-methoxy-5-methylphenyl)diazenyl)benzoyl chloride (**AZO4**).

The products derived from the four reaction steps were studied and characterized by NMR ^{1}H, ^{13}C analysis and FT-IR analysis. The reactions were adjusted and redefined to increase their yields and the purity of the products to meet the industrial needs and be suitable for a future industrial scale-up.

2.2 Experimental

2.2.1. Materials

4-Amino-3-methoxybenzoic acid (TCI, Tokyo Chemical Industries, ≥99% pure), 4-methylphenol (p-Cresol) (TCI, Tokyo Chemical Industries, ≥98% pure), methyl iodide (CH_3I), sodium hydride (NaH, 50% dispersion in oil), sodium hydroxide (NaOH), potassium hydroxide (KOH), sodium nitrite ($NaNO_2$), thionyl chloride ($SOCl_2$), triethylamine were purchased by Merck and used without any further purification. All the solvents were supplied by Scharlau, Merck and Fluka and used without previous purification as received. Aqueous solutions were prepared using distilled water. Tetrahydrofuran (THF) was dried according to standard procedures.

2.2.2. Methods and characterization techniques

Nuclear Magnetic Resonance (NMR):

Nuclear Magnetic Resonance (NMR) spectroscopy is an analytical chemistry technique used in quality control and research for the determination of the purity of a sample, its molecular structure as well as the content of a specific species in a mixture. NMR spectroscopy is thus, one of the main techniques utilized for the study of molecular structures of organic compounds; it is a non-destructive technique and it requires 5-30 mg of samples depending on the accuracy desired on the final spectrum.

The principle behind NMR is that every nucleus has a characteristic spin and all nuclei are electrically charged. The spin can be integral, fractional or

equal to zero. The most relevant and interesting isotopes, which will be analyzed in this thesis work, are ^{1}H and ^{13}C which both have a fractional spin equal to ½. When an external magnetic field is applied, two opposite spin energy states are possible for each isotope, ±1/2: the one +1/2 aligned with the external field and the other one -1/2 antiparallel to the external field. Between these two spins states an energy transfer is possible. Figure 2.1 illustrates that the two spin states have the same energy when the external field is zero but diverge as the field increases. At a field equal to B_x the energy difference is given by Equation 2.1:

$$\Delta B = \frac{\mu B_x}{I} \qquad \textit{Eq.2.1}$$

where I=1/2 and μ is the magnetic moment of the nucleus in the field.

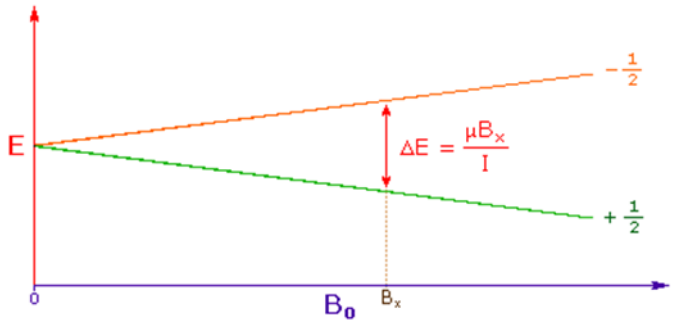

Figure 2.16. - Energy diagram which explains the principle behind NMR spectroscopy: spin energy states as a function of the external applied magnetic field.

For NMR purposes, this small energy difference (ΔE) is usually given as a frequency in units of MHz ranging from 20 to 900 MHz, depending on the magnetic field strength and the specific nucleus being studied.

Irradiation of a sample with a radio frequency (rf) energy corresponding exactly to the spin state separation, will cause excitation of the nuclei from the +1/2 state to the higher -1/2 spin state. The energy transfer takes place at a wavelength that corresponds to rf and, when the spin returns to its level base, energy is emitted at the same frequency. The signal that matches this transfer is measured and processed to yield an NMR spectrum for the nucleus

concerned. The exact resonant frequency of the energy transition of a specific atom is dependent on the effective magnetic field, that is on the electron shielding which is in turn dependent on its chemical environment. Information about the nucleus chemical environment can thus be derived from its resonant frequency. In general, the more electronegative the nucleus is, the higher the resonant frequency. Unlike infrared and UV-Visible spectroscopy indeed, where absorption peaks are uniquely located by a frequency or wavelength, the location of different NMR resonance signals is dependent on both the external magnetic field strength and the rf frequency. Since two magnets with the same exact fielddo not exist, resonance frequencies will vary accordingly and an alternative method for characterizing and specifying the location of NMR signals is needed. To solve this problem, it is customary to adopt tetramethylsilane (TMS) as the proton reference frequency. As a standard compound, TMS is added to every sample analyzed and its signal is used as reference. To eliminate the dependence on the magnetic field thus, it is convenient to express each NMR signal not in frequency but in terms of the chemical shift δ defined as follow:

$$\delta = \frac{v - v_{ref}}{v_{ref}} \qquad \text{Eq.2.2}$$

where v_{ref} is the resonant frequency of the reference signal and v is the frequency of the sample signal. This operation gives a locator number called the chemical shift, having units of parts-per-million (ppm), and designated by the symbol δ.

^{1}H NMR and ^{13}C NMR spectra of all the molecules synthesized in this work, were recorded at 400 and 100.4 MHz, respectively. A Varian Gemini 400 spectrometer was used, with proton noise decoupling for ^{13}C NMR. Measurements were carried out at room temperature using 5-10 mg or 30-40 mg of sample respectively for ^{1}H and ^{13}C analysis; the samples were dissolved in deuterated dimethylsulfoxide (d-DMSO). The chemical shifts were given in parts per million from TMS (Tetramethylsilane) in ^{1}H NMR spectra, while the central peak of the solvent was taken as the reference in the case of ^{13}C NMR

spectra. For ^{1}H-NMR measurements, the retention time between consecutive pulses (d1) was set between 1 and 16 seconds, while ^{13}C-NMR spectra were recorded with a lower d1, between 0.5 and 0.2 seconds. The ^{13}C NMR spectra of the organic molecules were recorded with a flip angle of 45˚, and the number of transients ranged from 20,000 to 40,000.

Fourier-Transform Infrared-Spectroscopy (FT-IR):

Infrared (IR) spectroscopy is one of the most common and widely used spectroscopic techniques employed mainly by inorganic and organic chemists to determine specific structures of compounds. Chemical compounds have different chemical properties due to the presence of different functional groups. In this technique infrared light interact with a sample which can be solid or liquid and, while a certain aliquot of the incident light goes through the sample, a certain amount gets absorbed by the molecules inside the sample. The absorption of IR light can be analysed in three ways by measuring absorption, emission and reflection. IR Spectroscopy measures the vibrations of atoms boundings and, based on this, it is possible to determine the functional groups. Generally, stronger bonds and light atoms will vibrate at a high stretching frequency or wavenumber. A common FTIR spectrometer consists of a source, interferometer, sample compartment, detector, amplifier, A/D convertor, and a computer as schematized in Figure 2.2. The source generates radiation which passes the sample through the interferometer which is used to split one beam of light into two, so that the paths of the two beams are different and then they recombine into the detector.

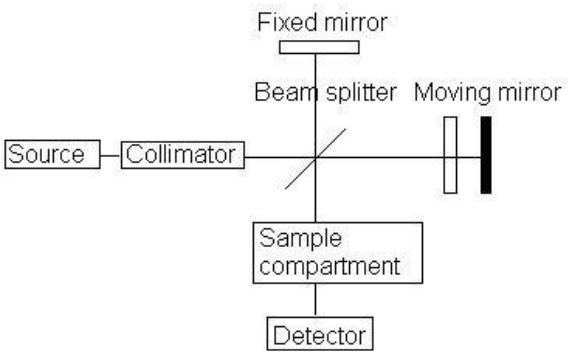

Figure 2.17. - Schematized FT-IR spectrometer.

Then the signal is amplified and converted to digital signal by the amplifier and analog-to-digital converter, respectively. The signal is transferred to a computer in which Fourier transform is carried out. The term Fourier-transform infrared spectroscopy originates from the fact that a Fourier transform is required to convert the raw data into the actual spectrum. The interferogram obtained is a plot of the intensity of signal versus the optical path difference (OPD). Since a Fourier transform can be viewed as the inversion of independent variables of a function, the Fourier transform of the interferogram can be viewed as the inversion of the OPD. The unit of OPD is centimeter, so the inversion of OPD has a unit of inverse centimeters also known as wavenumbers.

In this work the infrared spectroscopy has been used qualitatively to determine mainly the progress of the reaction of chlorination, the hydrloisis degree and the functionalization of molecules. Fourier-transformed infrared spectra were recorded on an FTIR-ATR 680 PLUS spectrophotometer from JASCO with a resolution of 4 cm^{-1} in the absorbance mode and transmittance modes and scanning speed of 2 mm/s. This device is equipped with an attenuated total reflection accessory (ATR) with thermal control and a diamond crystal (Golden Gate heated single reflection diamond ATR from Specac-Teknokroma). The spectra were recorded at room temperature from the liquid samples.

2.2.3. Synthesis of novel asymmetrical azobenzene moieties

The synthesis of the azo-compounds for the modification of the commercial polymer was planned to be performed in 4 steps: azo coupling reaction between aromatic amine and phenol compounds (**AZO1**); methylation of the alcoholic and carboxylic groups (**AZO2**); hydrolysis of the methyl ester group (**AZO3**); conversion to acyl chloride (**AZO4**). All steps were monitored by Thin Layer Chromatography (TLC), Proton Nuclear Magnetic Resonance Spectroscopy (^{1}H NMR) and Fourier-Transform Infrared-Spectroscopy (FT-IR). All the procedure was performed in red-light environmenr laboratories in order to prevent any accidental isomerization occurring from visible light irradiation of the samples.

Synthesis of 4-((2-hydroxy-5-methylphenyl)diazenyl)-3-methoxybenzoic acid (**AZO1**) (Scheme 2.1.):

For the synthesis of 4-((2-hydroxy-5-methylphenyl)diazenyl)-3-methoxybenzoic acid (**AZO1**), 12 mmol of 4-Amino-3-methoxybenzoic acid, 80 mL water, and 7 mL 35% hydrochloric acid were introduced in a 100 mL beaker and mildly heated to 40 °C to get the amine chlorohydrate.

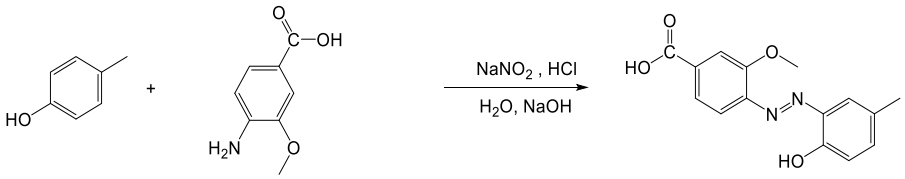

p-Cresol 4-amino-3-methoxybenzoic acid 4-((2-hydroxy-5-methylphenyl)diazenyl)-3-methoxybenzoic acid (**AZO1**)

Scheme 2.1 - Synthesis of 4-((2-hydroxy-5-methylphenyl)diazenyl)-3-methoxybenzoic acid (**AZO1**).

The resulting suspension was then cooled to 0°C in an ice bath. Meanwhile, 1.35 g (19.6 mmol) sodium nitrite were dissolved in 2.8 mL water and added dropwise to the first suspension to obtain the corresponding diazonium salt (solution A). Solution B was prepared by dissolving 1.616 g (15 mmol) 4-methylphenol in 14 mL of water with 2.10 g (52.5 mmol) of sodium hydroxide. Solution B was then carefully added dropwise to solution A at 0 °C. A dark red precipitate was obtained, which was then filtered and dried in oven at 45°C. The crude product was dissolved in 200 mL of a 10% aqueous solution of sodium hydroxide, the solution was diluted with 800 mL of water and then 20 mL 37% hydrochloric acid were added carefully. The product precipitated as a pure dark red solid which was then filtered and dried in oven at 45°C, yield 58%; m.p.: 262.7 °C (deg.).

^{1}H NMR (DMSO-d6) δ: 12.32 (s, 1H), 7.79 (d, J = 8.3 Hz, 1H), 7.75 (d, J = 1.5 Hz, 1H), 7.66 (dd, J = 3.8, 1.2 Hz, 2H), 7.63 (d, J = 1.6 Hz, 1H), 7.26 (m, 1H), 6.96 (d, J = 8.4 Hz, 1H), 4.02 (s, 3H), 2.32 (s, 3H).

^{13}C NMR (DMSO-d6) δ: 167.0 (s); 155.9 (s); 151.9 (s); 142.1 (s); 134.6 (s); 129.3 (s); 118.5 (s); 114.1 (s); 56.7 (s); 20.3 (s).

Synthesis of methyl-3-methoxy-4-((2-methoxy-5-methylphenyl)diazinyl) benzoate (**AZO2**) (Scheme 2.2.):

For the methylation of the hydroxyl groups of the previous molecule and the production of methyl-3-methoxy-4-((2-methoxy-5-methylphenyl)diazinyl) benzoate (**AZO2**), to 7.4 mmol of AZO1 in 50 ml of dry THF, 0.83 g of NaH (60% dispersion in oil) were added followed by 1.73 mL (27 mmol) of methyl iodide. The mixture was stirred at 80°C for 24 hours. The solvent was evaporated with rotavapor obtaining a light orange solid, which was recrystallized from 2-propanol. Yield: 49%, m.p.: 138.4 °C

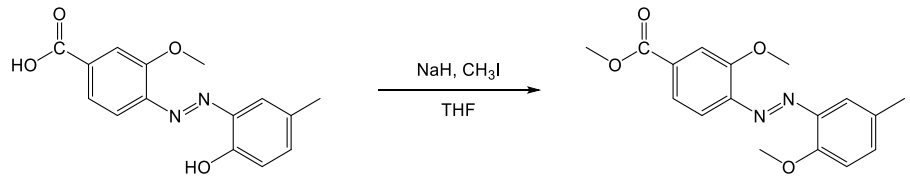

4-((2-hydroxy-5-methylphenyl)diazenyl)-3-methoxybenzoic acid (**AZO1**)

methyl 3-methoxy-4-((2-methoxy-5-methylphenyl)diazenyl)benzoate (**AZO2**)

Scheme 2.2. - Synthesis of methyl 3-methoxy-4-((2-methoxy-5-methylphenyl)diazinyl) benzoate (**AZO2**).

^{1}H NMR (DMSO-d6) δ: 7.76 (d, J = 1.3 Hz, 1H), 7.56 (dd, J = 8.2, 1.4 Hz, 1H), 7.37 (d, J = 8.2 Hz, 1H), 7.31 (dd, J = 8.4, 1.9 Hz, 1H), 7.26 (d, J = 1.8 Hz, 1H), 7.15 (d, J = 8.5 Hz, 1H), 3.97 (s, 3H), 3.92 (s, 3H), 2.29 (s, 3H).

^{13}C NMR (DMSO-d6) δ: 169.5 (s); 156.4 (s); 155.2 (s); 144.9 (s); 142.6 (s); 142.1 (s); 133.4 (s); 129.8 (s); 121.8 (s); 117.0 (s); 115.8 (s); 113.9 (s); 113.7 (s); 56.5 (s); 56.2 (s); 20.5 (s).

Synthesis of 3-methoxy-4-((2-methoxy-5-methylphenyl)diazenyl)benzoic acid (**AZO3**) (Scheme 2.3.):

Methyl-3-methoxy-4-((2-methoxy-5-methylphenyl)diazinyl) benzoate (**AZO2**) was hydrolyzed to the parent carboxylic acid obtaining the 3-methoxy-4-((2-methoxy-5-methylphenyl)diazenyl)benzoic acid (**AZO3**). 1 g (2.9 mmol)

of methyl-3-methoxy-4-((2-methoxy-5-methylphenyl)diazinyl) benzoate (**AZO2**) was dissolved in 30 ml of methanol (MeOH) and heated to 70 °C. Then 0.45 g potassium hydroxide (KOH) dissolved in 3 ml of water was added. Reaction mixture was refluxed under constant stirring for 30 minutes. The solution was cooled to room temperature and then poured to 600 ml of ice-water mixture. The system was acidified with 1.5 M hydrochloric acid reaching pH≈1, the product precipitate as a reddish solid. Reaction mixture was filtered, washed with hexane and dried at room temperature. Yield: 69%, m.p.:187°C.

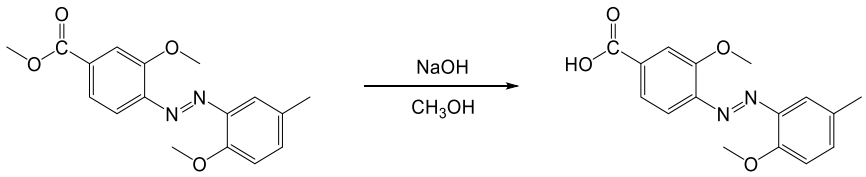

methyl 3-methoxy-4-((2-methoxy-5-methylphenyl)diazenyl)benzoate (**AZO2**)

3-methoxy-4-((2-methoxy-5-methylphenyl)diazenyl)benzoic acid (**AZO3**)

Scheme 2.3. - Synthesis of 3-methoxy-4-((2-methoxy-5-methylphenyl)diazenyl)benzoic acid (**AZO3**).

^{1}H NMR (DMSO-d6) δ: 13.25 (s, 1H), 7.73 (d, J = 1.6 Hz, 1H), 7.62 (dd, J = 8.2, 1.6 Hz, 1H), 7.45 (d, J = 8.2 Hz, 1H), 7.37 (ddd, J = 8.5, 2.3, 0.6 Hz, 1H), 7.29 (dd, J = 2.2, 0.7 Hz, 1H), 7.18 (d, J = 8.5 Hz, 1H), 4.01 (s, 3H), 3.93 (s, 3H), 2.29 (s, 3H).

Synthesis of 3-methoxy-4-((2-methoxy-5-methylphenyl)diazenyl)benzoyl chloride (**AZO4**):

To get 3-methoxy-4-((2-methoxy-5-methylphenyl)diazenyl)benzoyl chloride (**AZO4**), 1 g (3.36 mmol) of 3-methoxy-4-((2-methoxy-5-methylphenyl) diazenyl)benzoic acid (AZO3) was mixed with 10 mL of thionyl chloride ($SOCl_2$) and 0.07 mL of triethylamine. The mixture was heated on an oil bath up to 60 °C for three hours. Then, the solution was stirred overnight at room temperature. Unreacted thionyl chloride was removed under reduced pressure and the residue was washed with dry n-hexane (100 mL) and dried under vacuum at 40 °C. The yield obtained for this reaction is 94%.

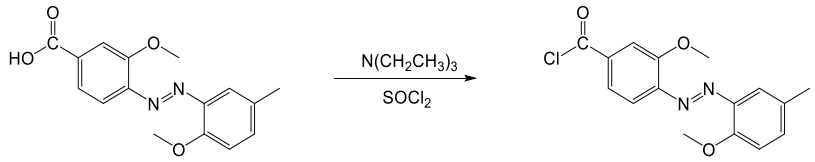

3-methoxy-4-((2-methoxy-5-methylphenyl)diazenyl)benzoic acid (**AZO3**)

3-methoxy-4-((2-methoxy-5-methylphenyl)diazenyl)benzoyl chloride (**AZO4**)

Scheme 2.4. - Synthesis of 3-methoxy-4-((2-methoxy-5-methylphenyl)diazenyl)benzoyl chloride (**AZO4**).

^{1}H- and ^{13}C-NMR spectra of the 3-methoxy-4-((2-methoxy-5-methylphenyl)diazenyl)benzoyl chloride are not reported due to the ease of hydrolyzation of this molecule, but the reaction progress was checked via FT-IR. In the Figure 2.6. the spectra of the modified azo-carboxylic acid (AZO3, green dotted and dashed line) and of the corresponding obtained chloride (AZO4, purple line) are reported together to prove the completion of the chemical reaction.

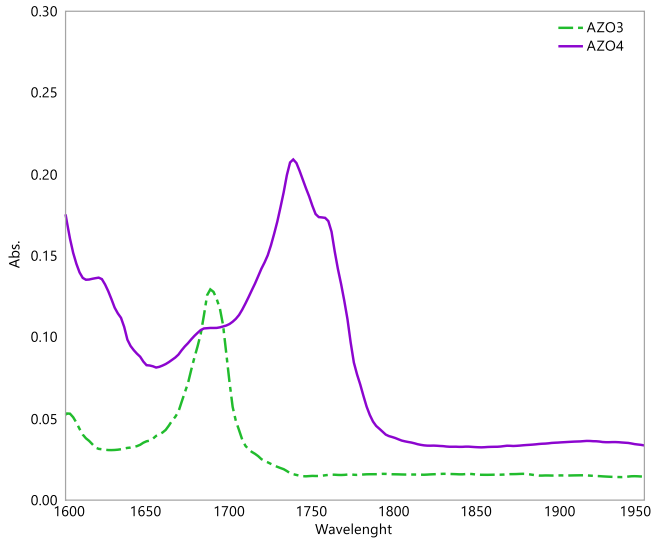

Figure 2.3. - FT-IR spectra of 3-methoxy-4-((2-methoxy-5-methylphenyl) diazenyl)benzoic acid (AZO3) and 3-methoxy-4-((2-methoxy-5-methylphenyl)diazenyl)benzoyl chloride (AZO4).

2.3. Results & discussions

2.3.1. Molecular design of the azo-derivatives

Azo compounds are usually synthesized with procedures like: azo coupling reaction (coupling of diazonium salts with activated aromatic compounds), Mills reaction (reaction between aromatic nitroso derivatives and anilines) and Wallach reaction (transformation of azoxybenzenes into 4-hydroxy substituted azoderivatives in acid media).[5] They are mostly produced with symmetric structures that have two potential reactive sites that offer the possibility to combine them with other monomers; in this way polymers capable to react when irradiated by an electromagnetic irradiation can be produced. They are typically sensitive to UV light irradiation and they can have unstable *Z* form that can convert back to the more stable *E* form within even picoseconds.

In order to produce an organic molecule that could be a suitable candidate for a polymeric modification, a preliminary study on the possible substitution pattern for the novel azobenzene compounds was performed.

The major points to focus on for the design of the novel asymmetric moieties were the followings:

- Produce a molecule with only one reactive site for further modifications and being used as a side-chain group;
- Move the excitation wavelength of the *E-Z* isomerization from the UV region of the absorbance spectrum to the visible light one;
- Enhance the stability of the *Z* form once obtained after irradiation with white light.

The 4-((2-hydroxy-5-methylphenyl)diazenyl)-3-methoxybenzoic acid (**AZO1**) was obtained by an azo coupling reaction between p-cresol and 4-amino-3-methoxybenzoic acid. Further, AZO1 was converted into methyl 3-methoxy-4-((2-methoxy-5-methylphenyl)diazenyl) benzoate (**AZO2**) by methylation of the hydroxyl groups with sodium hydride and methyl iodide in dry THF at 80°C for 24 hours. A saponification was necessary in order to obtain 3-methoxy-4-((2-methoxy-5-methylphenyl)diazenyl)benzoic acid (**AZO3**).

Subsequently, 3-methoxy-4-((2-methoxy-5-methylphenyl)diazenyl)benzoyl chloride (**AZO4**) was prepared from AZO3 with a chlorination reaction in $SOCl_2$, following the procedure highlighted in Scheme 2.2. All the synthetic procedures used in this Chapter were taken from literature and slightly modified to produce the selected novel compounds.[6–9]

To successfully synthesize the first compound (**AZO1**), an azo coupling reaction procedure was chosen with p-cresol and 4-amino-3-methoxybenzoic acid as precursors. In this specific electrophilic aromatic substitution reaction, a p-cresol with a methyl group in *para* position was selected as the activated arene. Due to the size of the attacking species, substitution occurs typically in *para* to the activating group. Therefore, ortho substitution takes place when the *para* position is already occupied by another substituent.

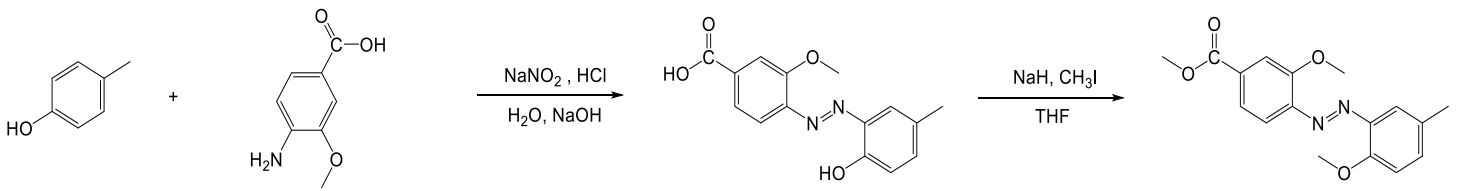

p-Cresol

4-amino-3-methoxybenzoic acid

4-((2-hydroxy-5-methylphenyl)diazenyl)-3-methoxybenzoic acid (**AZO1**)

methyl 3-methoxy-4-((2-methoxy-5-methylphenyl)diazenyl)benzoate (**AZO2**)

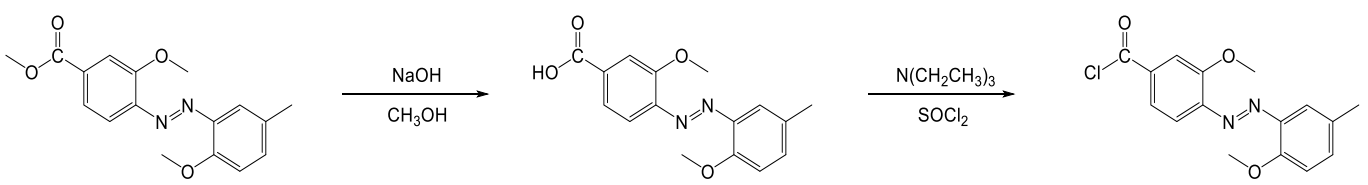

methyl 3-methoxy-4-((2-methoxy-5-methylphenyl)diazenyl)benzoate (**AZO2**)

3-methoxy-4-((2-methoxy-5-methylphenyl)diazenyl)benzoic acid (**AZO3**)

3-methoxy-4-((2-methoxy-5-methylphenyl)diazenyl)benzoyl chloride (**AZO4**)

Scheme 2.5. - Global synthetic path of azo-moieties. Azo coupling reaction between aromatic amine and phenol compounds (AZO1); methylation of the alcoholic and carboxylic groups (AZO2); hydrolysis of the methyl ester group (AZO3); conversion to acyl chloride (AZO4)

The 4-amino-3-methoxybenzoic acid was chosen to give the molecule the desired asymmetry and a reactive site for further modifications. In addition, the presence of an electron donor group on the aromatic ring, like the methoxy one, we aimed to move the isomerization wavelength to the visible region of the absorption spectrum to trigger the isomerization with white light irradiation.[10] Finally, it was reported[11] that the methyl group could enhance the stability of the *Z* isomer, prolonging its half-life in the darkness.

The conditions of the reaction were carefully controlled both in pH and temperature due to the instability of the diazonium salts formed during the process (Scheme 2.6.). A mildly acidic or neutral solution is usually needed when an aromatic amine is involved in this reaction: nevertheless, if the solution is too acidic, the concentration of free amine becomes too small and the reaction does not occur. the more reactive phenoxide ion is a better initiator to generate the target azobenzene, when slightly alkaline conditions are present. However, neither amines nor phenols, can react in moderately alkaline solution because the diazonium ions are converted into the corresponding diazo hydroxide.[12]

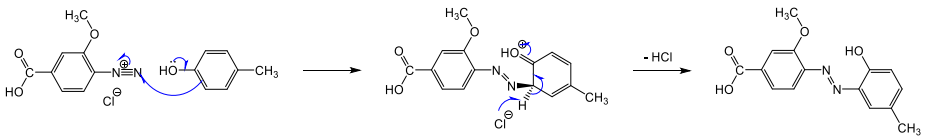

Scheme 2.5. - AZO1 reaction mechanism.

The AZO1 compound was then methylated to give AZO2. This modification generates a structure with two electron donor groups in ortho position on both the phenyl rings, changing the conjugation of the electrons on the -N=N- double bound. The optical properties of the synthesized compounds, as a consequence of this substitution pattern, will be fully reported and described in Chapter 3. The mechanism of the reaction is showed in Scheme 2.7.

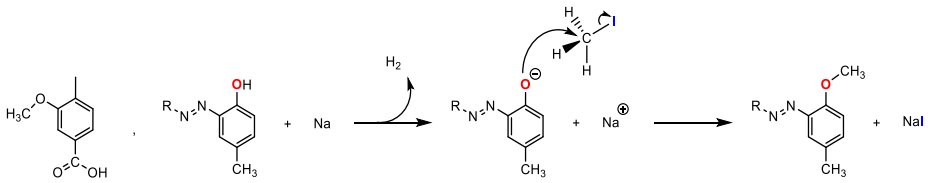

Scheme 2.6. - AZO2 reaction mechanism.

To produce AZO3, the carboxylic ester (AZO2) was hydrolyzed to the parent carboxylic acid and an alcohol. This reaction leads to acyl-oxygen cleavage. The hydroxide anion reacts with the carbonyl group of the ester. The immediate product is called an orthoester.

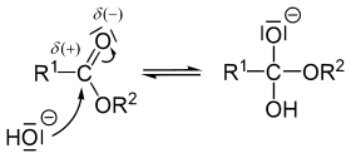

Expulsion of the alkoxide generates a carboxylic acid:

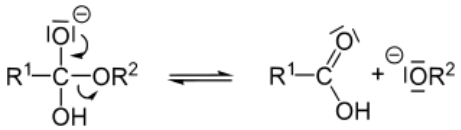

The alkoxide ion is a strong base so that the proton is transferred from the carboxylic acid to the alkoxide ion creating an alcohol:

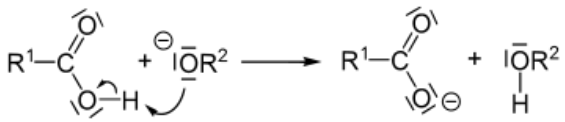

For the conversion of AZO3 in the corresponding acyl chloride (AZO4), thionyl chloride was used as reagent and solvent in the same reaction. This reaction is propaedeutic for the preparation of the azo-moiety to produce photosensitive polymers which will be examined in Chapter 4. The previously synthesized AZO3 was dried carefully and, once all the residual water was eliminated, it was dissolved in thionyl chloride. Triethylamine was employed as a base, to neutralize the hydrogen chloride produced during the reaction of chlorination and remove it from the reaction mixture, facilitating the reaction to proceed to completion.

2.3.2. ^{1}H-NMR Characterizations and ^{13}C-NMR Characterization

^{1}H-NMR spectra of AZO1 and AZO2 molecules dissolved in deuterated DMSO are showed in Figure 2.7. The proton spectra exhibited similarities for both the molecules. The peaks corresponding to the aromatic hydrogens are present and are highlighted in the insets showing the δ region between 7.0 ppm and 8.0 ppm. The peaks related to the hydrogen atoms of the methoxy and methyl groups are present in the region from 2.0 to 4.0 ppm. A peak corresponding to the -OH of the carboxylic group is visible at 12.18 ppm (Fig. 2.7.A). After the conversion to methyl ester, this peak disappeared as it is evident in the Figure 2.7.B. On the other hand, a peak corresponding to the new methyl ester group is present at 3.91 ppm. All the peaks of the aromatic rings were shifted after the methylation, but the number remained unchanged, as expected. From these evidences one can conclude that the methylation of the AZO1 molecule was successfully accomplished. The small peak at 3.33 ppm, present in both spectra, is characteristic of the residual water in d-DMSO. A similar description can be made for the ^{1}H spectra of AZO2 and AZO3, compared in Figure 2.8. Also in this case the proton related to the aromatic rings are the expected number. Due to the asymmetry of the molecules, the proton signals of the two aromatic rings are well defined and not overlapped. The differences between these spectra are highlighted by the presence of the signal of the carboxylic proton (in AZO3 spectrum) and by the different chemical shift of the peaks in the aromatic zone. Thus, the hydrolysis of AZO2 was successfully achieved.

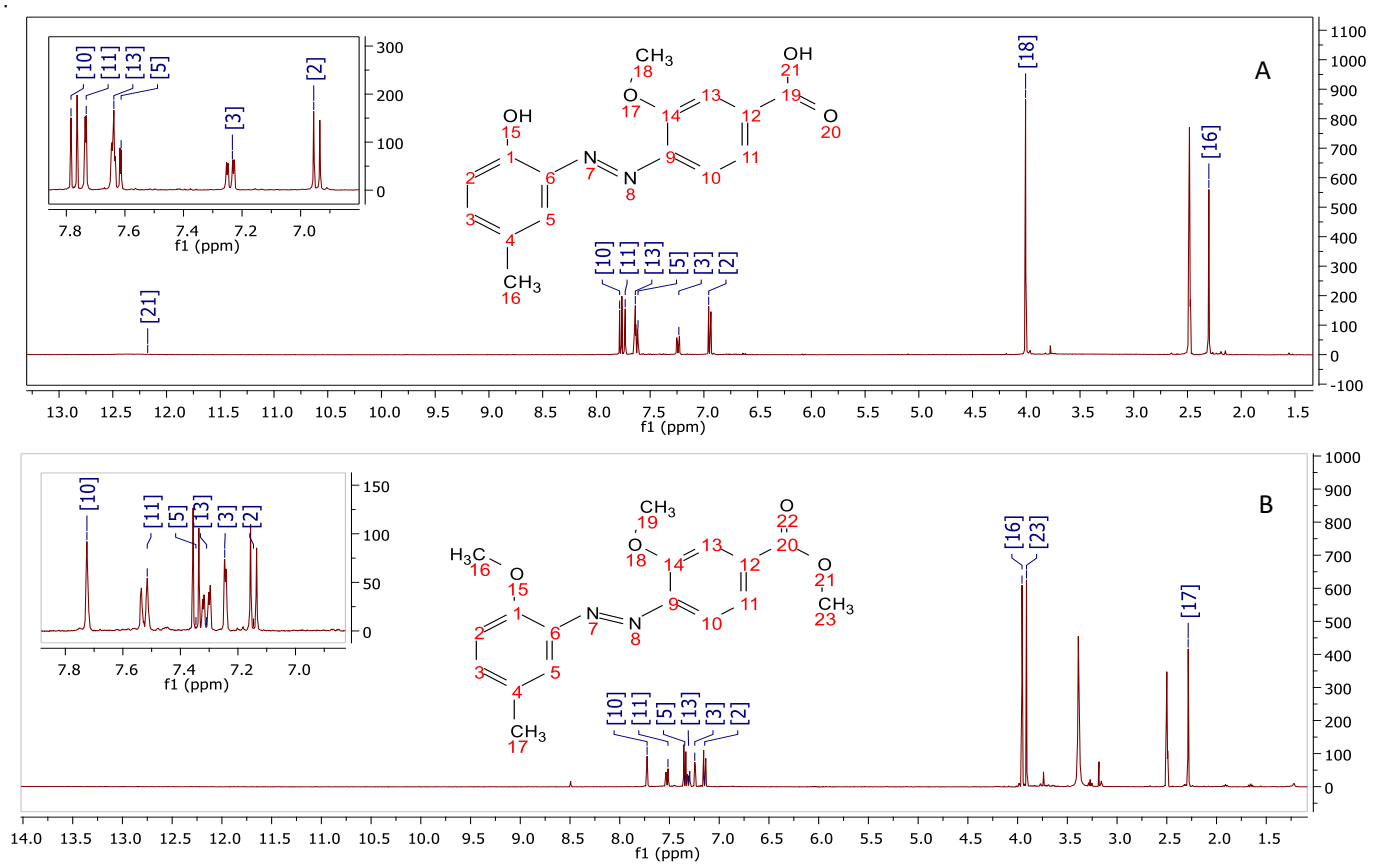

Figure 2.**4**. – AZO1 and AZO2 ^{1}H NMR spectra comparison: A) and B) respectively

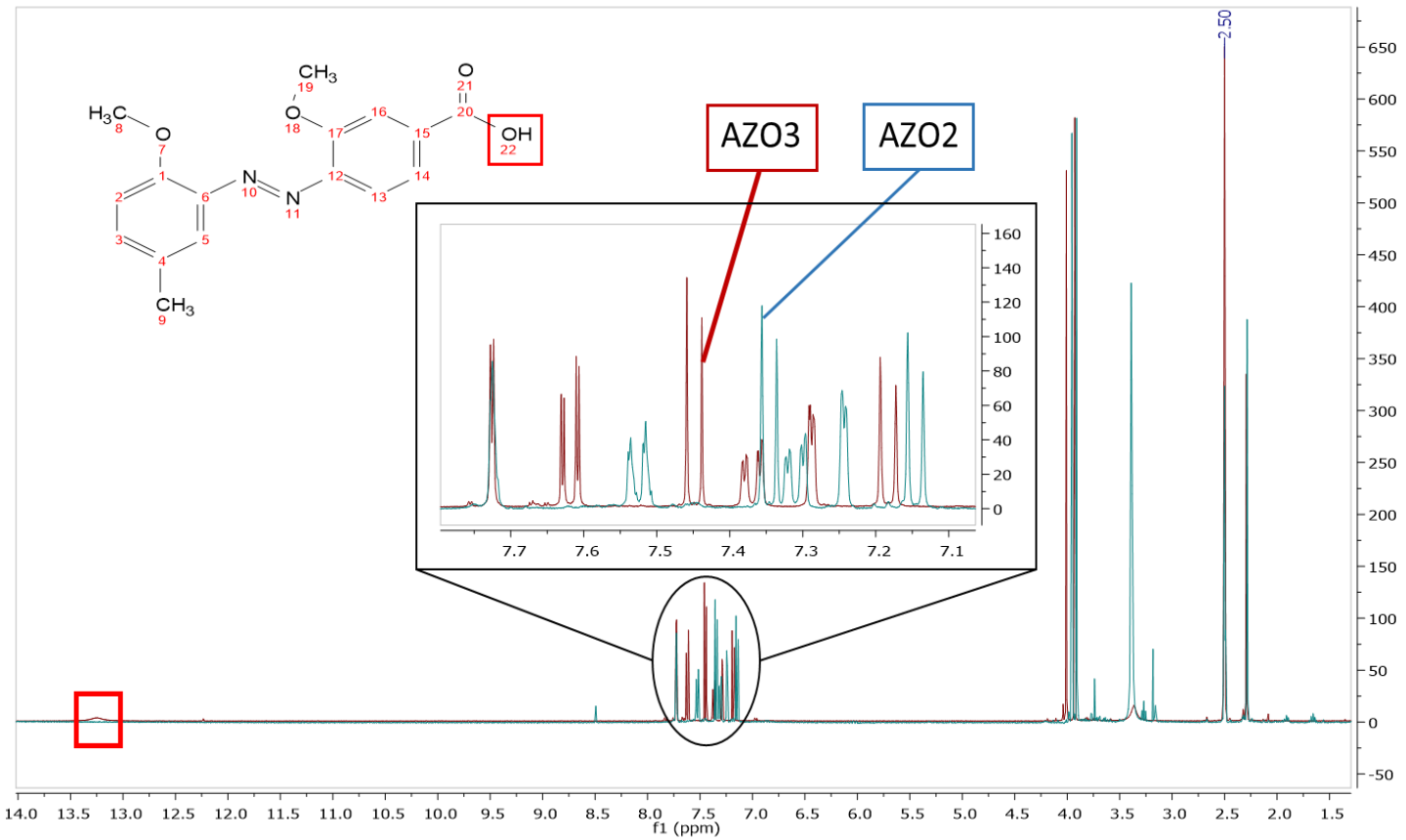

Figure 2.5. – AZO2 and AZO3 ^{1}H NMR spectra comparison.

The ^{13}C chemical shifts of the molecule AZO1 and AZO2 are given in Table 2.2. These two samples have been used as examples of the carbon NMR spectra of the azo compounds. AZO4 molecules have not been analyzed due to its instability to atmospheric environment.

Table 2.2. - AZO1 and AZO2 ^{13}C NMR chemical shifts comparison.

	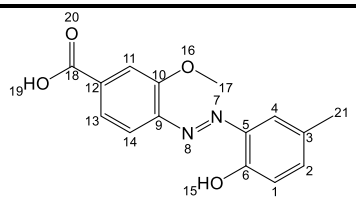 AZO1	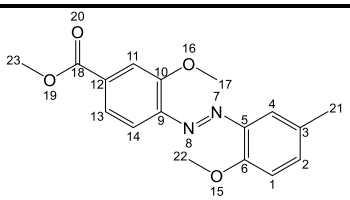 AZO2
1	118.2	113.3
2	135.1	133.0
3	134.2	129.4
4	128.1	113.6
5	141.7	142.2
6	151.7	144.5
9	138.1	141.7
10	155.5	154.8
11	113.7	116.6
12	128.9	156.0
13	122.0	121.4
14	116.1	115.4
17	56.3	55.8
18	166.7	169.1
21	19.9	20.1
22	-	56.1
23	-	55.8

From the data showed it is evident that two new signals appear after the methylation of AZO1, they can be related to the two carbons present in the AZO2 structure after AZO1 methylation.

2.3.3. FTIR Characterization

In Figure 2.9 a comparison of the FT-IR spectra of the four compounds is showed. The most interesting area is the one related to the spectral zone between 1500-1800 cm^{-1}.

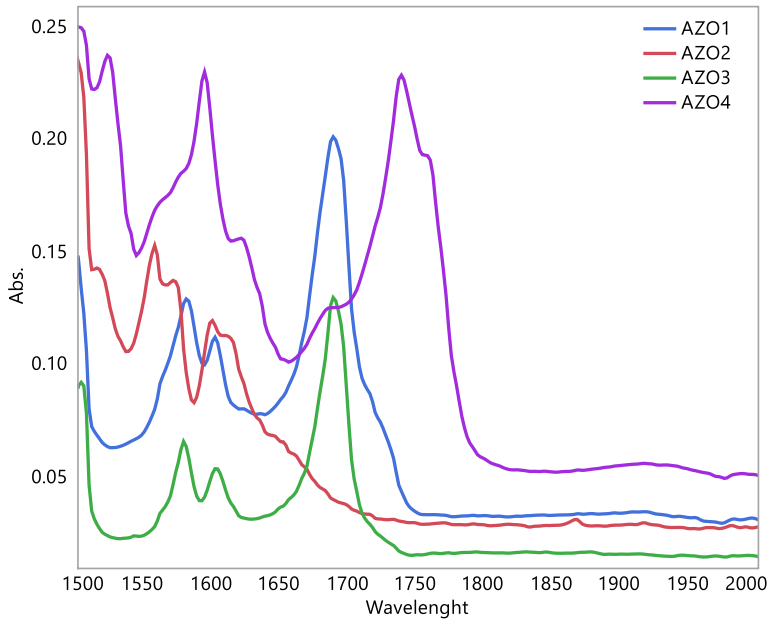

Figure 2.6. – FT-IR spectra comparison of all the AZOs in the spectral zone between 1500 and 2000 nm.

In this zone we can clearly distinguish when the carboxylic group is present in the molecule (case of AZO1 and AZO3 compounds), removed (in AZO2), or modified into the acyl chloride (in AZO4). The carbonyl stretching (C=O) absorption, in fact, is one of the strongest IR absorptions signal and, in the case of carboxylic acid, it should appear in the range 1780-1700 cm^{-1} as a singlet. In our case study, the peak relative to the C=O stretching is evident at 1690 cm-1 for AZO1 and AZO3 spectra (blue and green lines, respectively). This peak is shifted at lower wavenumbers, if compared to what expected, due to the nature of the substituents adjacent to the carboxylic group: in our case, the presence of the aromatic ring directly linked to the C=O double bound, the inductive and resonance effect shifts the absorption to lower wavenumbers.[13] The spectrum of AZO4 (purple line) is characteristic of the acyl-chloride and, in

this case, the peak relative to the carboxylic acid disappear leading to a new signal at 1760 cm^{-1}. The new signal, typical of the C=O stretching of the acid halides, demonstrates the formation of the new compound.

2.4. Conclusions

In this chapter the synthesis and characterization of the four azo-moieties AZO1, AZO2, AZO3 and AZO4 are reported. AZO4 was prepared from the chlorination of carboxylic acid (AZO3) and it is propaedeutic for the preparation of photosensitive branched polymers which will be explored in the Chapter 4.

The structure and the purity of the photosensitive compounds was characterized by means of ^{1}H and ^{13}C NMR spectroscopy, while FT-IR analyses were used to monitor the reactions and prove the acyl chloride formation. All the molecules studied from NMR spectra present the expected amount of peaks and the signals are correctly describing the planned structures.

An asymmetrical azobenzene structure was successfully synthesized, with two electron donor group in orto position to the azo bond. The carboxylic group acid form was successfully converted into the acyl chloride in order to get a suitable pending group for the creation of the stimuli responsive polymer.

The optical properties related to these molecules will be detailed described in detail in the next chapter, with a specific attention to AZO1 and AZO2 molecules. These two moieties, in fact, were selected upon the four, as model compounds. AZO3 was not fully characterized because it was used as a transition structure useful to reach the chloride form. AZO4 was impossible to study since it could be easily hidrolized.

2.5. References

1. Nicolescu, F. A. *et al* New Organic–Inorganic Hybrids with Azo-dye Content. *Des. Monomers Polym.* **13**, 437–444 (2010).
2. Jia, S. *et al.* Photoswitchable Molecules in Long-Wavelength Light-Responsive Drug Delivery: From Molecular Design to Applications. *Chem. Mater.* **30**, 2873–2887 (2018).
3. Forber, C. L. *et al.* Electronic spectra of cis- and trans-azobenzenes: consequences of ortho substitution. *J. Am. Chem. Soc.* **107**, 5884–5890 (1985).
4. Sadovski, O. *et al.* Spectral Tuning of Azobenzene Photoswitches for Biological Applications. *Angew. Chem. Int. Ed.* **48**, 1484–1486 (2009).
5. Merino, E. *et al.* Synthesis of azobenzenes: the coloured pieces of molecular materials. *Chem. Soc. Rev.* **40**, 3835–3853 (2011).
6. Peris, S. *et al.* Synthesis, characterization, and photoresponsive behavior of new azobenzene-containing polyethers. *J. Polym. Sci. Part Polym. Chem.* **47**, 5426–5436 (2009).
7. Stoochnoff, B. A. *et al.* The methylation of some phenols and alcohols with sodium hydride / methyl iodide in tetrahydrofuran at room temperature. *Tetrahedron Lett.* **14**, 21–24 (1973).
8. Saucă, S. *et al.* Flame retardant phosphorous-containing polymers obtained by chemically modifying poly(vinyl alcohol). *Polym. Degrad. Stab.* **98**, 453–463 (2013).
9. Tylkowski, B. *et al.* Photo-Triggered Microcapsules. *Macromol. Symp.* **360**, 192–198 (2016).
10. Dong, M. *et al.* Red-Shifting Azobenzene Photoswitches for in Vivo Use. *Acc. Chem. Res.* **48**, 2662–2670 (2015).
11. Nishioka, H. *et al.* Incorporation of methyl group on azobenzene for the effective photo-regulation of hybridization and suppression of thermal isomerization. *Nucleic Acids Symp. Ser.* **50**, 85–86 (2006).
12. Djedaini-Pilard, F. *et al.* Azobenzenes—synthesis and carbohydrate applications. *ResearchGate* **65**, 10105–10123 (2009).
13. Matczyszyn, K. *et al.* Influence of the environment on kinetics and electronic structure of asymmetric azobenzene derivatives — experiment

and quantum-chemical calculations. *J. Mol. Struct.* **565–566**, 53–57 (2001).

Chapter 3. Optical properties characterizations of novel asymmetrical azobenzene compounds

3.1. Introduction

The main interesting characteristic of azobenzene molecules is their facile and reversible isomerization of the double bond, between the more thermally stable *E* configuration and the meta-stable *Z* one.[1–5] This process drives to change the geometry of the molecule. As a matter of fact, while the *E* form is nearly planar, the *Z*-isomer is three-dimensional and has a ground state energy approximately 0.6 eV higher than the *E* one.[6–8] This interconversion between the two isomers makes the azobenzene the most used organic chromophore for technical applications, including optical waveguides and shutters,[9] optical memories,[10] photo-active artificial muscles,[11–14] photo triggered carriers and membranes,[15–19] etc.

Generally, an azo solution under illumination will achieve a photostationary state (PSS), with a steady-state *E*–*Z* composition based on the competing effects of photoisomerization and thermal relaxation back into the *E* state. The composition of the sample also depends on the irradiation wavelength, intensity, solvent-solute interactions and temperature. Moreover, the parent azobenzene molecule can bear different chemical groups in order to fine-tune the optical properties and response time of the isomerization, as mentioned in Chapter 1.[20] These substituents will also dramatically change the spectroscopic properties, affecting the relative position and intensity of the absorption bands in UV–Vis spectra. In addition, they have a great contribution on the percentage of each species (*E* and *Z*-isomer) present at the PSS. It is usually accepted that *Z*–*E* thermal relaxation may take place by means of two pathways that can be competitive (Figure 3.1.): rotation, or inversion of one of the nitrogen atoms. [21,22] Depending on the properties of the substituents bonded to one or both phenyl rings, and on the polarity of the reaction medium, one of these mechanism of relaxation may be favored over the other.[18,23]

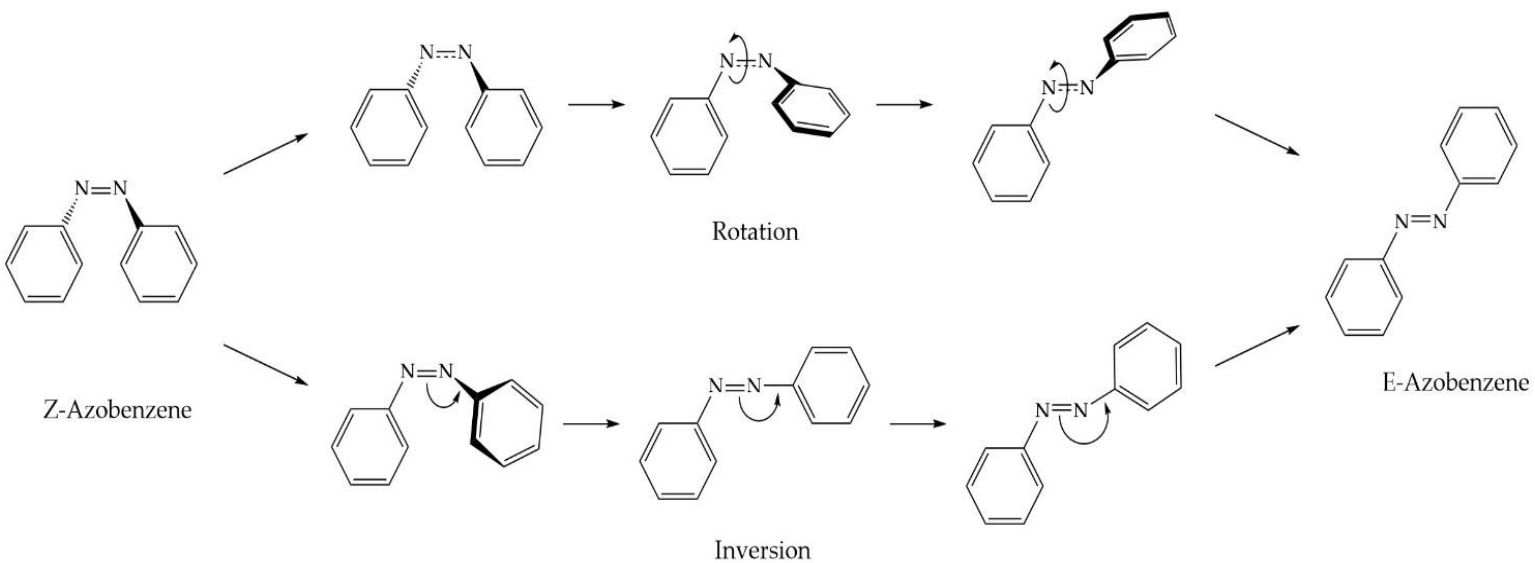

Figure 3.18. - Rotation and inversion thermal relaxation mechanisms for unsubstituted azobenzene

Understanding the isomerization kinetics of the different substituted azo-derivatives in solution is of great importance in order to gain control over the response time and design photo responsive materials for precise applications.

Thus, we focused our attention on the study of the *E–Z–E* isomerization kinetics of two on the four related novel azo-derivatives synthesized and studied in the previous Chapter, AZO1 and AZO2 respectively (Scheme 3.1.). The main objective of this section is to present an example on how the chemical modifications of the basic structure of the first novel azo derivate (AZO1) can change almost completely the optical properties of the system. Moreover, we selected AZO1 and AZO2 as candidates due to the major change produced from the chemical reaction on AZO1. The conversion of the hydroxyl group into a methoxy group, in fact, is exactly localized on the substituent in orto position to the -N=N- bound and, as can be found also in the literature, this change drives to the entire modification of the system photochemistry.[3,24,25]

Herein, we investigated the substituents nature of these two molecules and chromophore-solvent interactions, which control the photo responsive behaviour. Moreover, the conversion process was analyzed *in silico* through a static approach (Time Dependent DFT) and the photodynamics of isomer conversion through a multi-configurational wavefunction methodology (QD-NEVPT2) in order to have a complete understanding of the properties of such systems. In the course of our investigation, we discovered some unusual and unexpected photochemistry of this asymmetrical ortho substituted derivatives that has provided insight into underlying aspects of azobenzene isomerization as well as the possibility to reveal new applications for a well-known molecule.

3.2. Experimental part

3.2.1. Materials

Dimethyl sulfoxide (DMSO), N,N-dimethylformamide (DMF), dioxane, tetrahydrofuran (THF), chloroform and dichloromethane spectrophotometric grade, were purchased from Merck and used without previous purification as received.

3.2.2. Methods and characterization techniques

UV-Visible spectroscopy (UV-Vis)

UV-Visible spectrometers can be used to measure the absorbance of ultra violet or visible light for samples which contain either C bonds or atoms with non-bonding orbitals as the N and therefore can absorb light in the region from 200 - 800 nm. The measurement can be either at a single wavelength or a scan over a certain range in the spectrum. The technique can be used both quantitatively and qualitatively. A schematic diagram of a UV-visible spectrometer is shown in Figure 3.1. The light source (a combination of tungsten/halogen and deuterium lamps) provides the visible and near ultraviolet radiation covering the 200-800 nm. The output from the light source is focused onto the diffraction grating which splits the incoming light into its component colours of different wavelengths.

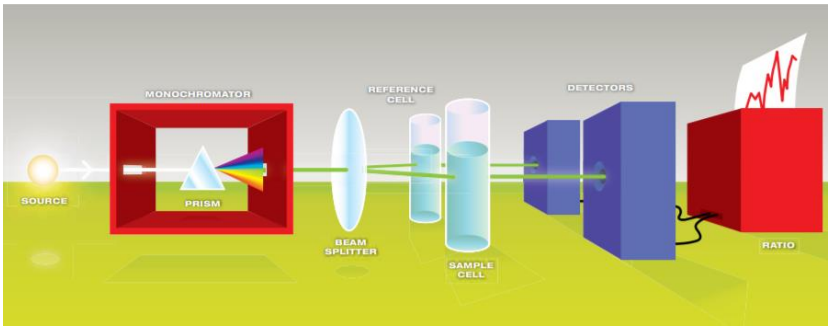

Figure 3.19. - Schematic diagram of a UV-Visible spectrometer.

For liquids the sample is held in an optically flat, transparent container, in our case in quartz, called a cell or cuvette. The reference cell or cuvette contains the solvent in which the sample is dissolved, and this is commonly referred to as the blank. For each wavelength the intensity of light passing through both a reference cell (I_o) and the sample cell (I) is measured. If $I \leq I_o$, then the sample has absorbed some of the light. The absorbance (A) of the sample is related to I and I_o according to the Equation 3.1:

$$A = log_{10} \frac{I_0}{I} \qquad \textit{Eq.3.1}$$

The detector converts the incoming light into a current, the higher the current the greater the intensity. The chart recorder usually plots the absorbance against the wavelength in the UV and visible region of the electromagnetic spectrum.

Photoisomerization was investigated by irradiating samples with a UV light source at 340 nm using a UV-1800 Shimadzu Spectrophotometer for the desired irradiation time and with scanning rate of 3,000 to 2 nm/min. The kinetics of photoisomerization and thermal relaxation were followed by the same instrument. The samples for UV-Visible spectroscopy were prepared via dilution of the sample into adequate solvent to give a final concentration in the range 0.9–1.3 g/L in red light room ($\lambda > 600$ nm), to assure that they were predominantly in *E* form. After maintaining the azo dye solutions in the dark overnight, the spectra were taken in a UV-grade quartz cell with optical beam path of 1 cm before and after irradiation with lamp iDual bulb Adaptative LED (11 W) with full spectrum visible light. The solution was analyzed after 5 minutes irradiation; the process was repeated several times since the photostationary state (PPS) was observed.

The *Z*–*E* thermal relaxation of solutions was studied after irradiating the samples reaching the photostationary state with the iDual lamp and then heating them in a TCC-100 Thermoelectrically Temperature Controlled cell holder for the analysis at different temperatures. The instruments collected the spectra each 2 minutes for 30 minutes. The temperatures used for the experiment were: 30°C, 40°C, 50°C and 60°C (± 1 °C). Background was performed on each of the solvents used both before and after light irradiation and confirmed that the solvents absorption spectrum did not affect the region between 250 and 600 nm.

Nuclear Magnetic Resonance (NMR)

A study of the kinetics of thermal back isomerization for the synthesized asymmetric azobenzene moiety was performed by using ^{1}H-NMR analysis. A Varian Gemini 400 MHz spectrometer equipped with a heating chamber was used for this purpose. The sample of the photo-sensitive solution was prepared using d-DMSO as solvent. Starting from a mixture of *E* and *Z* isomers, obtained through irradiation of the sample for 30 min by sunlight, the azo compound was

heated into the NMR spectrometer and kept at fixed temperature for 30 min. The spectra were recorded every 5 min to monitor how the concentration of the two isomers in the mixture changed. The described procedure was repeated at four different temperatures, namely 30, 40, 50, and 60 °C (± 2 °C), to study the thermal back isomerization and to calculate the activation energy E_a of this process.

3.2.3. Theory/calculations

The photoisomerization experimental data were analyzed according to Eq.3.2.

$$\ln \frac{A_0 - A_\infty}{A_t - A_\infty} = k_i t \qquad \text{Eq.3.2}$$

where t is the irradiation time, A_0, A_t and A_∞ are the E form absorbances corresponding to the time 0, t and PSS, respectively, and k_i is the rate constant of E–Z photoisomerization. In the case of thermal relaxation, the kinetics follow Eq.3.3, where k_r is the rate constant of the Z–E relaxation, A_0, A_t and A_∞ are the Z form absorbances corresponding to the time 0, t and photostationary state and t is the relaxation time.

$$\ln \frac{A_0 - A_\infty}{A_t - A_\infty} = k_r t \qquad \text{Eq.3.3}$$

The content of the Z-isomer at the PSS was determined using relation 3.4.

$$\alpha_Z = \frac{A_0 - A_{PSS}}{A_0} \qquad \text{Eq.3.4}$$

where A_0 and A_{PSS} represent the absorbances at k_{max} for E-isomer before and after irradiation with UV light, respectively. This formula assumes negligible absorption of the Z-isomer at E absorption maximum.

Activation parameters of the thermal back isomerization were determined by measuring the temperature dependence of the rate constant and fitting the

data with the Arrhenius equation (Eq.3.5.) or the Eyring equation (Eq.3.6.) to obtain the activation energy, E_a, the enthalpy of activation, $\Delta H^{\neq}$, and the entropy of activation, $\Delta S^{\neq}$.

$$\ln k = \ln A - \frac{E_a}{RT} \qquad \text{Eq.3.5}$$

where k is the thermal rate constant, R is the universal gas constant, T is the temperature in Kelvin, A is the steric factor and E_a is the activation energy.

$$\ln \frac{k}{T} = -\frac{\Delta H^{\neq}}{RT} + \ln \frac{k_b}{h} + \frac{\Delta S^{\neq}}{R} \qquad \text{Eq.3.6}$$

where $\Delta H^{\neq}$, is the enthalpy of activation, $\Delta S^{\neq}$ the entropy of activation, k_b is the Boltzmann constant, h is Planck constant.

3.2.4. Computational Methods

Density Functional calculations were performed using the ADF 2017 103 modelling suite employing[26] the Perdew, Burke and Ernzerhof hybrid functional (PBE0).[27–29] The basis sets consisted of all electron triple zeta Slater type orbitals with one polarization function (TZP). The COnductor like Screening MOdel (COSMO) dielectric continuum solvation scheme was employed in the calculations with default appropriate parameters for dimethylformamide, dimethyl sulfoxide and dichloromethane.[30] Geometry optimizations did not involve any symmetry constraints. Time Dependent (TD-PBE0) runs for the calculation of UV-Visible transitions required 60 singlet-singlet excitations.[31] Additional multiconfigurational self-consistent field calculations performed using the ORCA 4.0.1 software package.[32–34] The PES scans were carried out by relaxing the geometries of all systems in vacuo at the state average (six singlets) CASSCF(4,3) level to a minimum at every scan point. Each of the twenty scan points subsequently underwent a wavefunction perturbation through the Quasi-Degenerate N-Electron Valence Perturbation Theory (QD-NEVPT2) approach in the Nakano formulation.[35–37] The Ahlrichs def2-TZVP

contracted Gaussian type basis set[38] was employed for every element making use of the Resolution of the Identity (RI) Coulomb integral approximation scheme with the def2-TZVP/C correlation density fitting basis set.[39] Using the state average CASSCF wavefunction a non-SCF CI run was performed for the ground (S_0) and second excited (S_2) states which then underwent a density matrix analysis using the Natural Bond Orbital scheme (NBO 6 program.[40] The Natural Localized Molecular Orbitals were generated and their bond orders computed using the procedure devised by Schleyer et al.[41]

3.3. Results and discussions

3.3.1. Molecular design of the optical properties of the novel azo-derivatives

As already explained in Chapter 2, the novel azobenzene structures produced in this work were designed to have:

- One reactive site for further modifications to use the molecule as a pending group for polymers modification;
- Two electron donor groups in orto position to the azo-bound to move the excitation wavelength in the visible region of the absorption spectrum;
- One methyl group that could enhance the stability of the *Z*-isomer once produced by light irradiation.

In Figure 3.2. the changes between a basic azobenzenes molecule and the new asymmetrical azobenzenes, AZO1 and AZO2, are highlighted. We aimed to find a pathway to punctually modify the basic azobenzene structure and to produce a molecule crafted for our application needs. The green circle points the position of the carboxylic/ester groups; the red circles represent the positions of the methoxy/hydroxyl groups; the blue circle shows the position of the methyl group.

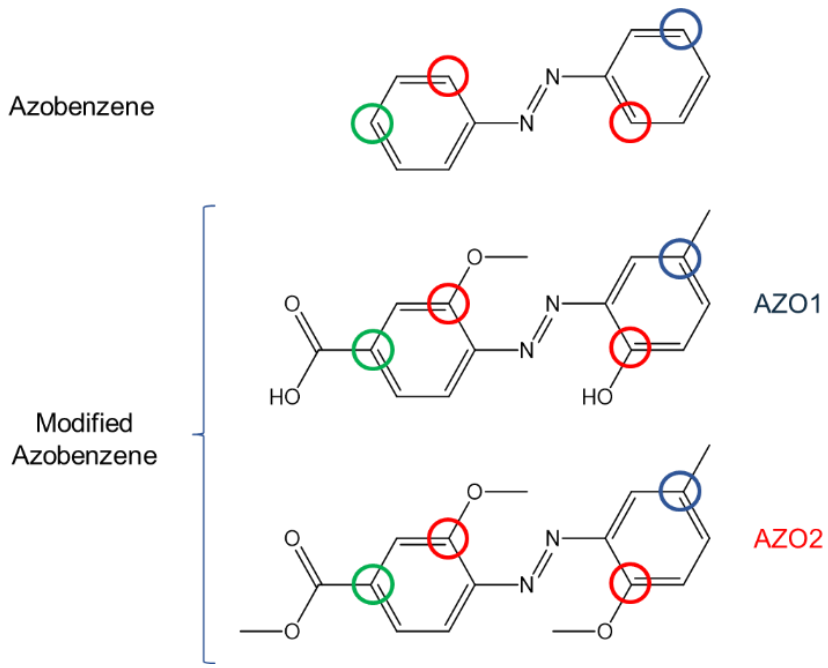

Figure 3.20. - Comparison of the structures of the azobenzene moieties. In green position of carboxylic/ester groups; in red position of methoxy/hydroxyl groups; in blue position of methyl group.

From the account given by Bandara et al. regarding a specific set of azobenzene derivatives the hydroxyl groups can hinder the isomerization by forming hydrogen bonds with the azo group, or other substituent on the opposite ring. We therefore envisaged to apply this same idea for the present work. The AZO1 compound was thus methylated to give AZO2. This modification generates a structure with two electron donor groups in ortho position on both the phenyl rings, changing the conjugation of the electrons on the -N=N- double bound. This modification was needed given the small isomerization conversion registered for AZO1 *E*-isomer when irradiated by white light, as shown in the following sections. As it will be explained, this modification unlocked the isomerization of the following molecule and gave to the AZO2 interesting optical properties. We recurred to the TD-DFT studies to confirm and investigate, this peculiar aspect of AZO1 molecule.

3.3.2. UV/Vis spectra interpretation

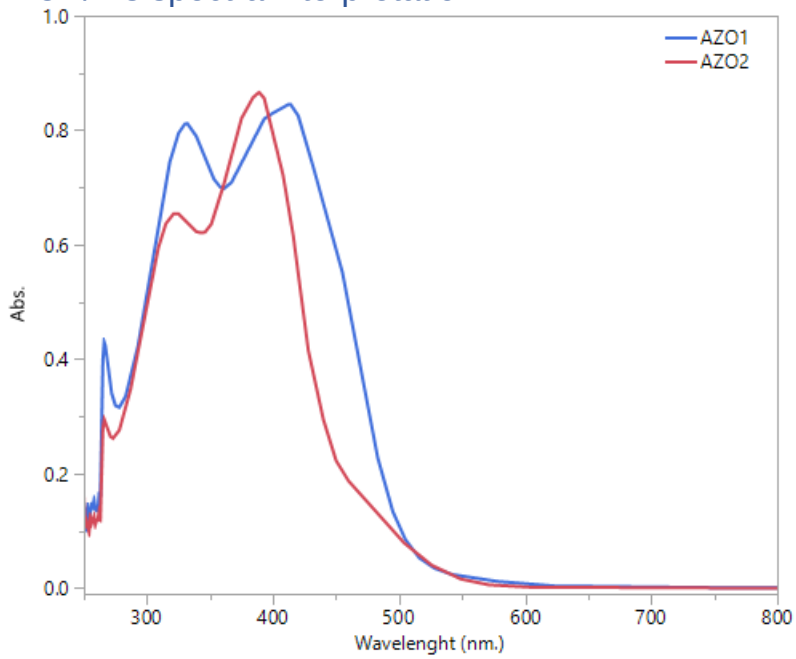

Figure 3.21. - UV/Vis spectra comparison of AZO1 and AZO2.

The UV–Vis absorption spectra of the azo-derivatives exhibit two characteristic absorption bands. The first characteristic absorption band related to the strong π–π* transitions of E isomer is present around 330–320 nm. The weak absorption, originating from the forbidden symmetry of n–π* transitions, is present around 412-325 nm.

Table 3.3. - Wavelength maxima and experimentally measured rate constants for isomerization (k_i), reverse isomerization (k_r) and the content of the *Z*-isomer at the PSS (α_Z). AZO1 and AZO2 optical properties comparison..

Sample	Solvent	λ_{max} (nm)	λ_{min} (nm)	k_i (s^{-1})	k_r (s^{-1})	α_Z (%)
AZO1	DMF	415	330	$1.5x10^{-4}$	-	3.2
AZO2	DMF	389	320	$3.08x10^{-3}$	$3.77x10^{-6}$	45.7

Comparing the absorption spectra, it is evident that the methoxy groups attached on both the phenyl rings of AZO2 are blue shifting the λ_{max} of 23 nm in DMF (tab. 3.1.). This can be explained by the lower conjugation effect that they induce on the -N=N- bound electrons. This group, in fact, has a less

pronounced electron donor behaviour than the hydroxyl group present in the AZO1 structure.

To understand the optical properties of the two compounds an in silico analysis was carried out with the Time Dependent Density Functional (TD-DFT) approach. A DFT geometry optimisation (see computational methods) was performed for the ground state for both structural isomers of AZO1 and AZO2. The simulated electronic vertical transitions of both molecules are displayed on Figure 3.4 and these will occur in the frontier orbital region mapped out in Figure 3.5. The calculated bands (TD-PBE0) compare favourably well to the experimental ones presenting a systematic redshift in the region of 20-50 nm. The relative intensities are incorrectly described likely due to solvent interaction effects.

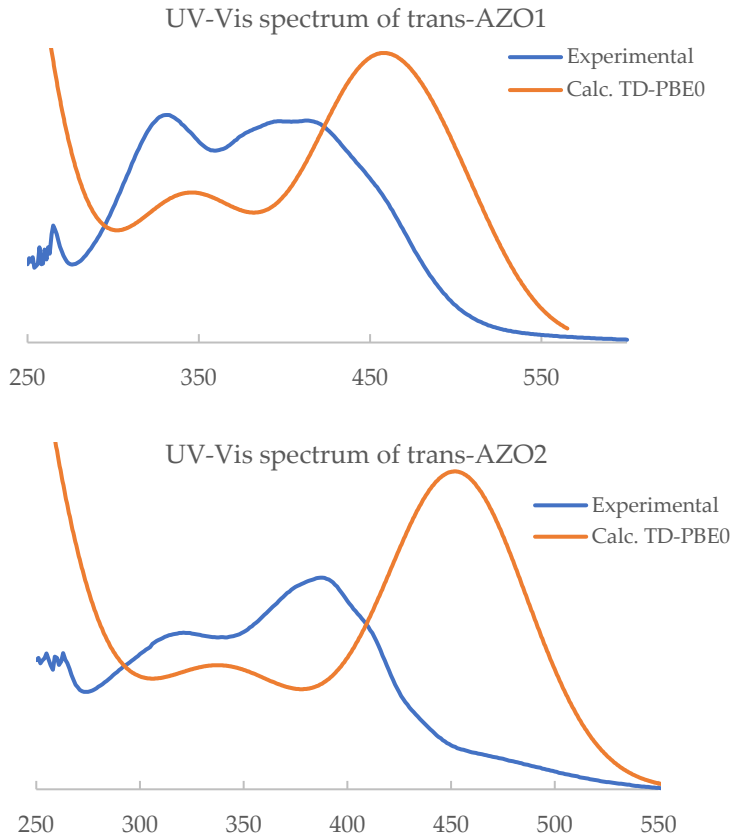

Figure 3.22. - Measured and calculated absorption spectra of *E*-AZO1 (left) and *E*-AZO2 (right) in dimethylformamide.

The band maxima correspond to the electronic excitations are listed in Table 3.2. and Table 3.3. for AZO1 and AZO2, respectively. The most intense transition in the visible region can be assigned to the second excited state for both *E*-AZO1 and *E*-AZO2 each showing oscillator strengths of 0.57 and 0.91 respectively. The conventional assignment of distinctly separate n→ π* and π→ π* transitions is not rigorously valid in the case of *E*-AZO1 since there is admixture of both transitions in the first two bands.

Table 3.4. - Calculated excitation energies, band maxima assignments and oscillator strengths (f_{osc}) of E-AZO1 (experimental values from UV/Vis analysis are shown in brackets).

Excited state #	Main Character	Excitation (nm)	f_{osc}
S_1	$\pi_2 \rightarrow \pi^*$ (48%) $n_1 \rightarrow \pi^*$ (37%) $n_2 \rightarrow \pi^*$ (12%)	489 (415)	0.34
S_2	$\pi_2 \rightarrow \pi^*$ (51%) $n_1 \rightarrow \pi^*$ (36%) $n_2 \rightarrow \pi^*$ (11%)	441 (399)	0.57
S_3	$n_2 \rightarrow \pi^*$ (76%) $n_1 \rightarrow \pi^*$ (23%)	379	6.9×10^{-2}
S_4	$\pi_1 \rightarrow \pi^*$ (98%)	338 (330)	0.33

Table 3.5. - Calculated excitation energies, band maxima assignments and oscillator strengths (f_{osc}) of E-AZO2 (experimental values from UV/Vis analysis are shown in brackets).

Excited state #	Main Character	Excitation (nm)	f_{osc}
S_1	$n_2 \rightarrow \pi^*$ (58%) $n_1 \rightarrow \pi^*$ (37%)	494	9.6×10^{-3}
S_2	$\pi_2 \rightarrow \pi^*$ (98%)	448 (389)	0.91
S_3	$n_1 \rightarrow \pi^*$ (59%) $n_2 \rightarrow \pi^*$ (39%)	372	6.6×10^{-2}
S_4	$\pi_1 \rightarrow \pi^*$ (98%)	333 (320)	0.30

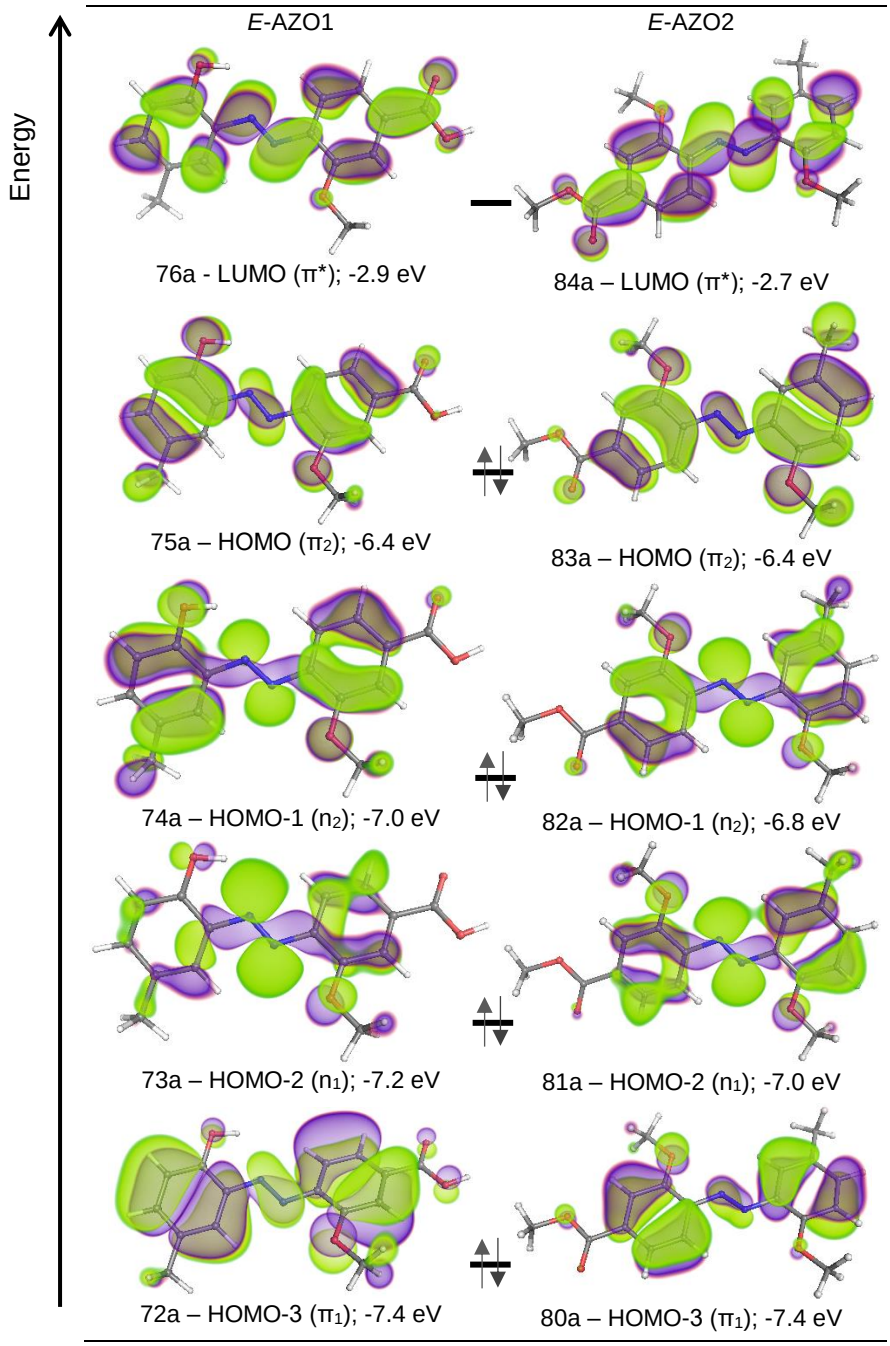

Figure 3.23. - Kohn-Sham molecular orbitals relevant to the electronic transitions of *E*-AZO1 and *E*-AZO2 in the visible region.

The first and second electronic transitions of *E*-AZO1 correspond to two maxima calculated to be at 489 and 441 nm and have a majority of $\pi_2 \rightarrow \pi^*$ character. The other band with significant oscillator strength in this compound is due to a $\pi_1 \rightarrow \pi^*$ transition occurring at 338 nm.

The spectral features of *E*-AZO2 are altogether significantly different in that $n \rightarrow \pi^*$ transitions do not admix with the π π^* type excitations. Since the former transitions are symmetry forbidden, they have a very low oscillator strength while the latter show up as very strong intensity bands. To broaden the study on the optical properties of the two moieties, the samples were dissolved in different solvents, according to the solubility of the different molecules. Figure 3.6 shows the dipole moments (in Debye) of each solvent compared to the wavelengths of the main peaks (λ_1, λ_2, λ_3) of the absorption spectra of the azo-derivatives.

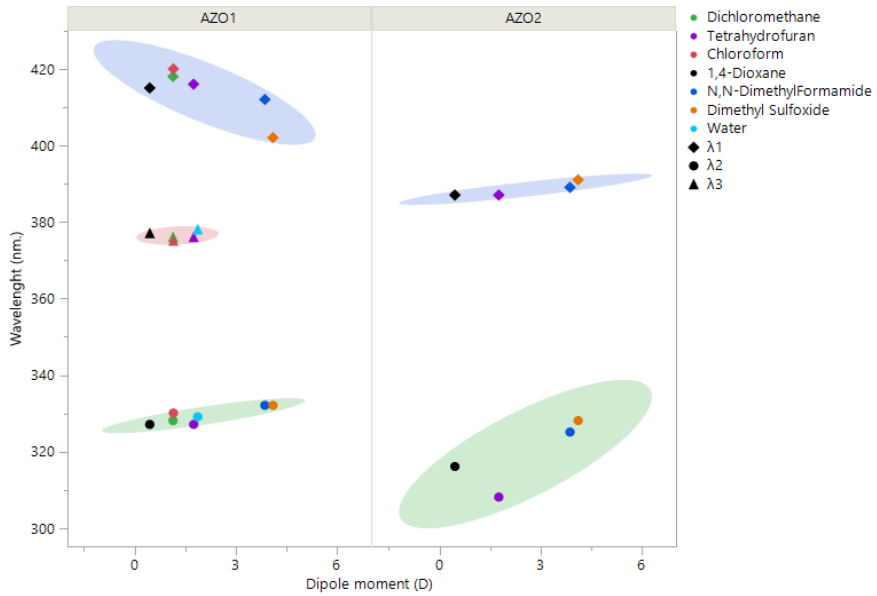

Figure 3.24. - Band absorption maxima of AZO1/AZO2 correlated with solvent dipole moment (Debye).

For AZO1 molecule, a broader range of solvents could be tested. The first peculiar aspect is that AZO1 main peak (λ_1) is splitting its signal passing from a more polar solvent like dimethyl sulfoxide to a less polar one like

dichloromethane. This can be ascribed to the different mechanism of excitation followed by the electrons involved in the azo double bound when irradiated by light. In more polar solvents the signal linked to this excitation are overlapped (λ_1), then their wavelength split (λ_1 and λ_3) being better resolved when the polarity of the solvent decreases. The second crucial aspect is highlighted by the hypsochromic shift of λ_1 and the bathochromic shift of λ_2 of AZO1 molecule in polar solvents. This can be related to the stabilization of the electronic cloud of AZO1, that is favoured by the presence of a less polar solvent like dioxane. This, in fact, can decrease the conjugation effect of the electrons of the azo double bond, shifting lambda to lower wavelengths. AZO2 λ_1 is slightly influenced by the solvent polarity, a bathochromic shift is registered passing from a less polar solvent to a more polar one.[24]

The UV-Vis spectrum was calculated for *E*-AZO1 in various implicit solvent dielectric media to determine how the effect that polarity shifts the visible band wavelengths. As may be seen from the values in Table 3.4 the values of λ_1 tend to increase when passing from the vacuum to the solvated environment.

Table 3.6. - Calculated band absorption wavelengths for the AZO1 system.

COSMO dielectric medium	λ_1(nm)	λ_3(nm)
DMSO	449	340
DMF	441	338
CH_2Cl_2	444	338
None	410	322

Neglecting dispersion interactions between solvent and solute represent the limiting case of solvation in non-polar media. However, the value of λ_1 changed only a few for the used selection of solvents, with varying degree of polarity differences. The observed trend for DMSO is not reproduced by the calculation and in fact the value is slightly higher with respect to CH_2Cl_2 and DMF, but the change is so small that barely any significance can be inferred from it. The failure to account for the experimental trend is a sign that explicit interactions between the solute and the solvent, which are not taken into account at this level of theory, are essential to explain the subtle band shifts.

3.3.3. E–Z photoisomerization

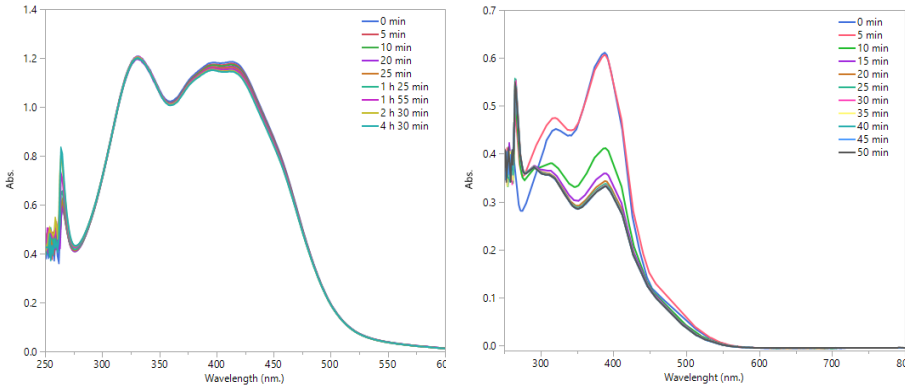

AZO1 AZO2

Figure 3.25. - UV/Vis Absorption changes upon irradiation of visible light. From left to right, A) AZO1 and B) AZO2 absorption spectra.

The photoisomerization kinetics of azo-derivatives was established by monitoring the absorbance of π-π* absorption band. Figure 3.7 shows the UV–Vis spectra of the AZO1 and AZO2 molecules after irradiation at different times. Under white light irradiation the intensity of the π-π* absorption band gradually decreases with the irradiation time, while the n–π* absorption band increases, until the photo-stationary state is reached. Both the solvent polarity and substituent nature influence the composition of the PSS. In fact, comparing the isomerization of both molecules, there are big differences that are easy to point out. First, only a slight change is visible in AZO1 absorption spectra (Fig. 3.7.A); the *E-Z* conversion rate is about 3.3 % after 4h 30 min of irradiation compared to 45.7 % of AZO2 after 50 minutes of irradiation. The kinetic constant of the isomerization for the two molecules differ by an order of magnitude (Table 3.5).

Table 3.7. - AZO2 *E-Z* photoisomerization rate constants at 303K. In this order: k_i, direct isomerization kinetic constant; k_r, thermal relaxation kinetic constant; α_Z, content of the *Z*-isomer at the PSS (photo-stationary state); $\tau_{1/2}$, half-life of *Z*-isomer in the dark.

Solvent	k_i (s^{-1})	k_r (s^{-1})	α_Z (%)	$\tau_{1/2}$
DMF	$3.08x10^{-3}$	$3.77x10^{-6}$	45.7	$1.84x10^{+5}$
DMSO	$6.38x10^{-3}$	$3.14x10^{-6}$	48.3	$2.21x10^{+5}$
DIOX	$8.51x10^{-4}$	$2.14x10^{-6}$	16.7	$3.24x10^{+5}$

Table 3.5. lists the photoisomerization rate constants calculated from UV–Vis experiments on AZO2 in different solvents at 303K. It can be observed that AZO2 k_i increases going from a less polar solvent like dioxane to a more polar one, such as DMSO. This evidence can be related to the photoisomerization mechanism. When rotation or inversion-assisted rotation pathway is preferred, an acceleration of the photoisomerization rate in polar solvents is noticed, due to the stabilization of the dipolar transition state. A change in the isomerization mechanism can be responsible for the lower percentage of *Z* fraction registered when AZO2 is dissolved in dioxane.[24]

3.3.4. Z–E thermal relaxation followed by UV/Vis analysis

The kinetic *Z–E* thermal relaxation of AZO1 and AZO2 were investigated at several temperatures in order to determine its thermodynamic parameters. However, in the case of AZO1, thermal relaxation was impossible to study due to the hindered isomerization. The rate of *Z–E* thermal relaxation of AZO2 molecule was monitored in the dark at the absorption maximum of its *E*-isomer. During thermal *Z–E* isomerization the intensity of the π-π* absorption band gradually increased with the relaxation time, while that of the n-π* absorption band, corresponding to *Z*-isomer, decreased. The thermal *Z* to *E* isomerization rate, summarized in Table 3.6, was determined for AZO2 at different temperatures and solvents. The process was found to be first order in all the studied solvents.

Table 3.8. - AZO2 k_r (in s^{-1}) constants in different solvents at different temperatures.

T (K)	DMF	DMSO	DIOX
303.15	$3.77x10^{-6}$	$3.14x10^{-6}$	$2.14x10^{-6}$
313.15	$1.18x10^{-5}$	$1.02x10^{-5}$	$6.23x10^{-6}$
323.15	$3.22x10^{-5}$	$3.01x10^{-5}$	$1.73x10^{-5}$
333.15	$5.59x10^{-5}$	$6.93x10^{-5}$	$3.81x10^{-5}$

Calculation of the first-order rate constants at various temperatures allowed us to estimate thermodynamic activation parameters such as the activation energy (E_a), activation enthalpy ($\Delta H^{\neq}$), and activation entropy ($\Delta S^{\neq}$)

for thermal *Z* to *E* reaction using Arrhenius and Eyring equations. We used the linear correlation between the enthalpy and the entropy of activation to determine the mechanism of AZO2 thermal relaxation. In all the solvents, the Arrhenius plots were linear, proving that there is no significant change in the reaction pathway over the examined temperature range. AZO2 compound has positive enthalpy of activation and negative entropy for all the solvents used (see Table 3.7.).

Table 3.9. - AZO2 thermodynamic activation parameters.

	Dipole moment (D)	A (s^{-1})	E_a (kJ mol^{-1})	$\Delta H^{\neq}$ (kJ mol^{-1})	$\Delta S^{\neq}$ (J mol^{-1} K^{-1})
DMF	3.9	$6.57x10^{+7}$	$76.6x10^{+3}$	74.0	-104.1
DMSO	4.1	$3.41x10^{+9}$	$87.2x10^{+3}$	84.5	-71.2
DIOX	0.4	$2.22x10^{+8}$	$81.3x10^{+3}$	78.6	-94.1

AZO2 in DMF has the highest $\Delta S^{\neq}$ absolute value and the lowest $\Delta H^{\neq}$; therefore exhibits the fastest thermal relaxation.[42,43] This is consistent with the calculation that will be shown below. In order to understand the dynamic photochemical and thermal processes involved in the isomerisation of AZO1 and AZO2 a choice of appropriate computational strategy was paramount. The employment of density functional theory is unsuitable in this instance because there is no guarantee, that at every stage in the transformation within the specific excited state hypersurface, the electron wavefunction of the ground state remains singly determinantal.

The best methodology is to adopt multi-configurational self-consistent field theory [32,44] with a posteriori perturbational corrections for a good description of dynamical electron correlation such as the NEVPT2 approach (see Computational Methods).[36,45] Two conventional mechanisms usually adopted to describe the isomer change involve the either the twisting of the ∡(N=N-C) angle (inversion) or a rotation of the planes that make up the ∡(C-N=N-C) dihedral (rotation). Only the latter was found to exhibit more favourable energies for the photochemical conversion.

This contradicts the hydrogen bonding inhibition scenario as presented by Bandara et al,[46] since rotation of the molecule around the -CNNC- dihedral planes does not necessarily require the termination of the intramolecular hydrogen bond with the adjacent hydroxyl group. An alternative explanation is given below to account for the slower rates of photo-switching. The alternative twisting scenario may be found in the supporting information section. More elaborate reaction coordinates combining angular and dihedral changes have been studied also for unsubstituted azobenzene.[47]

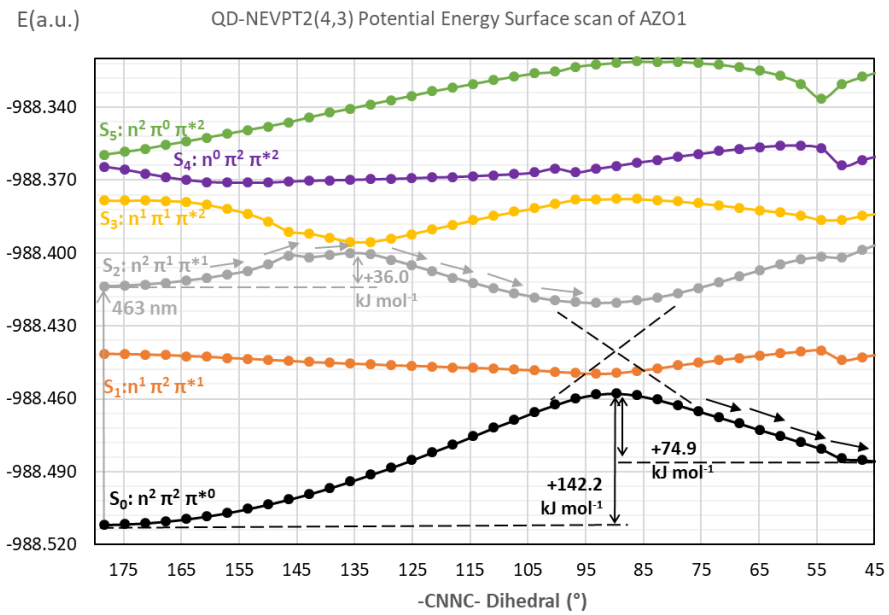

Figure 3.26. - QD-NEVPT2(4,3)//SA6-CASSCF(4,3)/def2-TZVP potential energy surface scan of the six lowest lying singlet states of AZO1. The S_2 and S_3 have an avoided crossing at approximately ∡(CNNC)=139° and some 8.6 kcal/mol above the S_2 minimum.

As seen from Tables 3.2.-3.3. the second excited state (S_2) presents the highest oscillator strength for both AZO1 and AZO2: this will be the most efficient conversion pathway. A relaxed potential energy surface (PES) scan of the -CNNC- dihedral at the QD-NEVPT2(4,3)//CASSCF(4,3)/def2-TZVP level of theory is presented in Figure 3.7. and in Figure 3.8. for AZO1 and AZO2, respectively. Therein the energies of each of the lowest six singlets were monitored throughout this reaction coordinate. The main composition of

the states at the beginning of the process (*E*-isomer) is qualitatively described with different colours. The curves are qualitatively similar to what was previously reported for azobenzene.[48] The photochemical process originates with the promotion of $S_0 \rightarrow S_2$ ($\pi^1\ \pi^{*1}$) which can allow the system enough flexibility to distort the dihedral once the π bond strength has a formal bond order of zero. However, due to orbital polarisation there still remains a marginally bonding interaction and some thermal energy is still required to break it. This barrier is computed to be 36.0 kJ mol^{-1} in the case of AZO1 and 27.4 kcal mol^{-1} for AZO2 and takes place at ∡(CNNC)=135° and ∡(CNNC)=143° respectively. One metric to measure the π symmetry bond strength from the electronic density is the Natural Localized Molecular Orbital (NLMO) bond order taken from the CASCI(4,3) density matrix. A comparative analysis of the azo bond orders in ground (S_0) and excited (S_2) states is displayed on Table 8. It may be seen that the calculated π bond order is fairly identical from the outset (S_0). The $S_0 \rightarrow S_2$ excitation suppresses the π bond strength differently in AZO1 and AZO2. In AZO1 the π bond remnant is stronger than in AZO2 thereby justifying the additional energetic requirement for the dihedral rotation and rendering AZO1 kinetically more inert in the S_2 state.

Table 3.10 – NLMO bond orders in the two states S_0 and S_2 at the ground state CASCI(4,3)/def2-TZVP level.

	NLMO π(N-N) bond order S_0	***NLMO π(N-N) bond order S_2***
AZO1	0.951	7.84×10^{-3}
AZO2	0.934	4.43×10^{-3}

Disregarding thermal contributions to the transition state energies, i.e. $\Delta E^{\ddagger}(S_2) \approx \Delta G^{\ddagger}(S_2)$ and assuming a high quantum yield for the S_2 excitation, the Eyring equation yields a $k_i(AZO1)/k_i(AZO2)$ ratio of 3.1×10^{-2} using the above calculated values which is reasonably close to experimental one (4.8×10^{-2}). Overall, a 9 kJ mol^{-1} energy difference leads to a decrease in the reaction rate constant close to two orders of magnitude.

Towards more acute angles one hallmark feature[48] of azobenzene derivatives comes to the fore, which is the conical intersection (CI) allowing S_2 to configurationally admix with S_0 leading to the cis isomer, in the region 80°<∡(-CNNC-)<100° as the lone pairs (n) become degenerate with the π orbitals. The energy gap in this nonadiabatic coupling (H_{02}) is 98.3 kJ mol^{-1} in AZO1 and 83.1 kJ mol^{-1} in AZO2. From the Landau-Zener relation[49] it is known that the probability of transition between the two adiabatic surfaces S_0 and S_2 can be given by $e^{-H_{02}^2/\alpha}$ where α is a collection of constants incorporating nuclear velocity, and the difference in reaction coordinate slope in each adiabatic state. H_{02} is the squared energy gap between the two states at the avoided crossing. As the values of H_{02} are considerable for both molecules (98.3 kJ mol^{-1} in AZO1 and 83.1 kJ mol^{-1} in AZO2) the probability of radiationless transition is practically zero. Thus, the $S_0 \rightarrow S_2$ transition will require the emission of one photon at 1217 nm (AZO1) and 1437 nm (AZO2) wavelength (infra-red region).

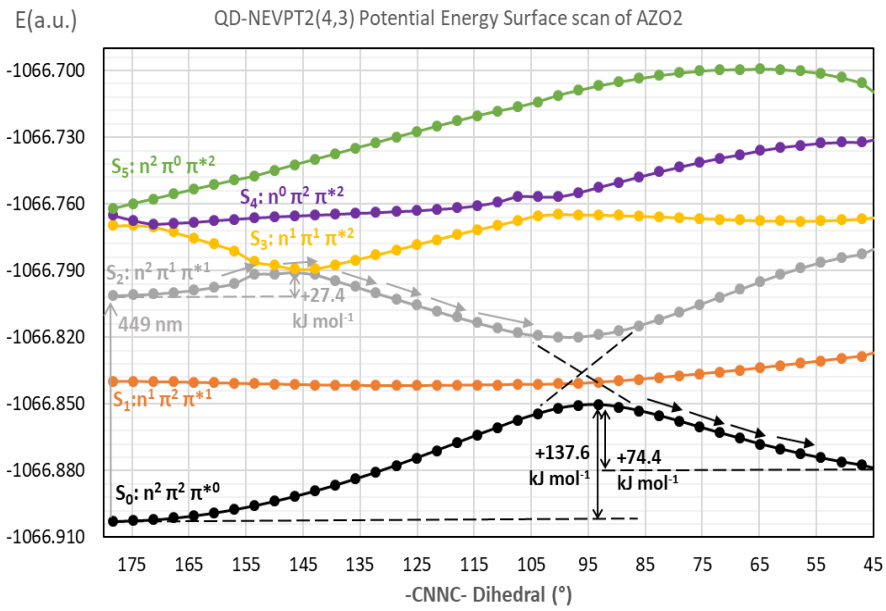

Figure 3.27. - QD-NEVPT2(4,3)//SA6-CASSCF(4,3)/def2-TZVP potential energy surface scan of the six lowest lying singlet states of AZO2. S_2 and S_3 states cross at approximately ∡(CNNC)=150°and 6.6 kcal/mol above the S_2 minimum.

The potential energy landscapes also afford an overview of the thermal back-isomerization which has the values +74.9 and +74.4 kJ mol^{-1}. These values are in good agreement with the relaxation activation energies determined experimentally even neglecting the necessary thermal corrections (zero point, vibrational, rotational and translational).

3.3.5. Z–E thermal relaxation followed by NMR analysis

In addition, the kinetic of thermal back isomerization was also studied *via* NMR spectroscopy.[50,51] The behaviour of *Z* ortho-substituted azobenzene in solution, kept in the dark, at 30, 40, 50, and 60 °C was studied recording ^{1}H-NMR spectra at each temperature, every 5 minutes, and assuming the isomerization process to have a first order kinetic (Equation 3.2).

In this case, in the Equation 3.1, *v* is the *Z*-*E* isomerization rate at each temperature, *k* is the rate constant and *A* is the area of the ^{1}H-NMR peak selected as reference for the calculation; it represents the concentration of a specific proton in the selected isomer. The same proton in the two isomers, *Z* and *E*, shows the signals at different ppms. It is worth, thus, to report, in this section, the ^{1}H-NMR spectra of the previously synthesized ortho-substituted azobenzene as an overlap between the irradiated and not irradiated sample (*Z* and *E* isomer respectively). From the comparison of the two spectra, it is possible to assign, to each proton, the corresponding peak related to its *E* or *Z* isomer.

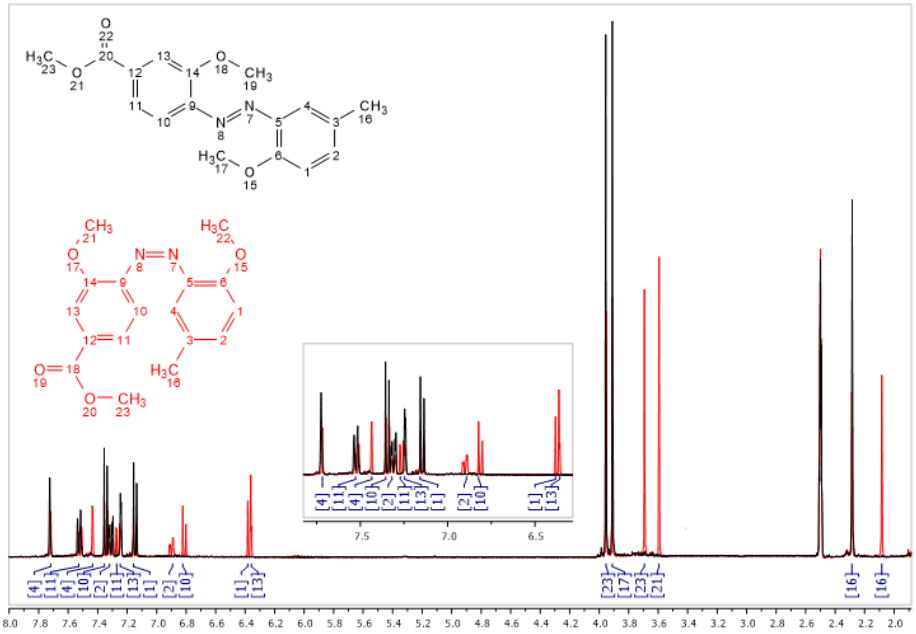

Figure 3.9 ^{1}H-NMR spectra of *E*- (black) and *Z*- (red) ortho-substituted azobenzene. In the inset are reported the ppms of the aromatic protons.

In Figure 3.9 it is reported, with a black curve, the spectrum of the isomer E; its chemical structure is also reported in black. In the same Figure, the red curve represents the spectrum of the irradiated isomer *Z*, which is indeed schematized in red. The inset shows a magnification of the aromatic peaks.

To study the kinetic of thermal back isomerization and to calculate the activation energy of the thermal relaxation process, the peak corresponding to the methoxy group at 3.61 ppm of the *Z* ortho-substituted azobenzene were selected as reference.

At room temperature (20 ± 2 °C), the comparison of the areas of the peaks at 3.92 ppm and 3.61 ppm (Equation 3.7), which corresponds to the protons of the methoxy group in the *E* and *Z* configuration, respectively, shows that, for the sample utilized in this experiment, after 30 min of sunlight exposure the AZO2 is 50 % in its *Z* form.

$$Z\%_{NMR} = \frac{A_Z}{A_Z + A_E} \qquad \textit{Eq. 3.7}$$

The experimental data of the thermal back isomerization were analysed considering a first order kinetic[21] and the values for the kinetic constants in d-DMSO were calculated according to the Equation 3.4-3.5 (Figure 3.9). The k_r values recorded at 30 and 60 °C, ranged between 1.1×10^{-3} and 1.2×10^{-2} s^{-1}, and are in agreement with literature findings.[52]

As expected, the thermal back relaxation at 30° is very slow and after 60 min only the 2.4 % of the *Z*-isomer in the starting mixture has reverted to *Z*. However, the kinetics at higher temperatures is much more representative of the thermic process: as a matter of example, Figure 3.10 shows the ^{1}H-NMR spectra in d-DMSO of AZO2 recorded in darkness at 70 °C at different times comprised between t=0 (soon afterwards 30 min sun exposure) and t=60 min. The inset shows the magnification of the peak at 3.61 ppm which corresponds to the methoxy group of the *Z*-AZO2 and which was selected as a reference to study the kinetic of thermal back isomerization. At this temperature, higher speed of isomerization was found and, after 60 min of heating, only approximately 9% of the *Z*-isomer remained in the studied mixture.

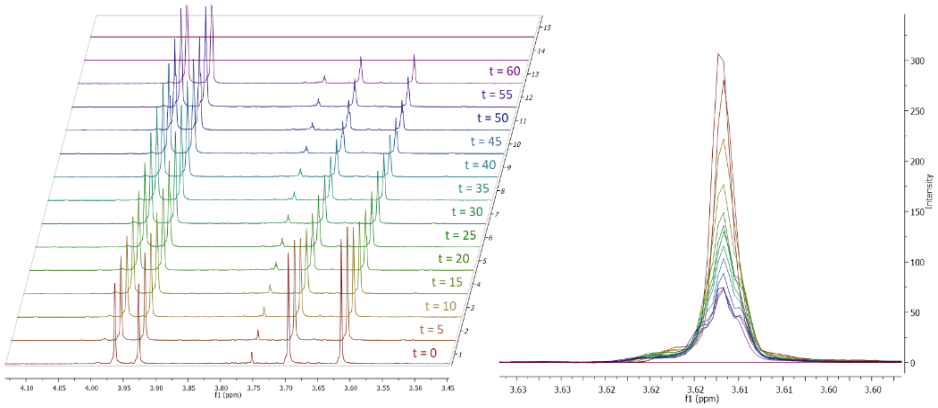

Figure 3.10 - Kinetic of thermal back isomerization calculated via ^{1}H-NMR at 70 ºC starting from a mixture of E and Z isomers of the ortho-substituted azobenzene.

In addition, the activation energy of the thermal back isomerization was determined by measuring the temperature dependence of the slope *k* and fitting the data with the Arrhenius equation (Equation 3.8):

$$k = Ae^{\frac{E_a}{RT}} \qquad \textit{Eq.3.8}$$

where E_a is the activation energy of the thermal process, R is the universal gas constant, k is the constant rate at each temperature T expressed in Kelvin. The activation energy E_a exhibited a value of 64.3 kJ mol^{-1}, that is comparable with other values reported in literature.[21,53]

3.4. Conclusions

In this Chapter the study and the characterization of two novel asymmetrical azobenzene derivatives was presented. A molecular design was done in order to plan and create moieties with one reactive suitable site for polymer functionalization. The molecules were set to have electron-donor groups that permit isomerization when irradiated by visible light irradiation and a sufficiently stable *Z*-isomer with a thermal relaxation at temperatures above 303K. A wide-ranging study on the *E–Z–E* isomerization mechanism of the azo-derivatives was performed. The definite substitutional pattern was found to change the specific photochemistry of the molecules. A hindered isomerization was discovered in case of AZO1 molecule, subsequently analyzed by the TD-DFT calculations.

On the other hand, by methylating AZO1 to AZO2, the photochemistry of AZO2 was found to follow the bibliography trends. AZO2 isomerization occurs under visible light irradiation, giving a stable *Z*-isomer at room temperature, with thermal relaxation rate constants increasing at higher temperature, as expected. The interaction between solvent and chromophore plays a role in determining the rate of this process and therefore should be considered in future applications. The rate of photo-switching was experimentally determined to be k_i(AZO1)= 1.5×10-4 s^{-1} and k_i(AZO2)= 3.08×10-3 s^{-1} using DMF as solvent.

By means of TD-DFT calculations the molecules were studied and compared. The calculated bands (TD-PBE0) relate well to the experimental ones, presenting a minor systematic redshift. The conventional assignment of distinctly separated n→ π* and π→ π* transitions was found to be not rigorously valid in the case of E-AZO1 since an admixture of both transitions in

the first two bands was found. The spectral features of E-AZO2 are different in that n→π* transitions do not admix with the π→ π* type excitations.

The dynamic photochemical and thermal processes involved in the isomerisation of AZO1 and AZO2 was studied by means of multi-configurational self-consistent field theory with a posteriori perturbational corrections (NEVPT2 approach). The rotation mechanism of the planes that make up the □(C-N=N-C) dihedral angle was found to be the most favourable for the E-Z isomer change. The photo-chemical process originates with the electronic promotion of S0□S2 and an energetic barrier in the S_2 surface was found along the reaction coordinate valued at +36.0 and +27.4 kJ mol-1 for AZO1 and AZO2 respectively. This difference in thermal barriers for the S_2 state explains why AZO1 is kinetically more inert to isomerisation with respect to AZO2.

While the topology of the hydrogen bonds in the ortho position may be relevant in the photo-switching of certain azo derivatives, this feature is entirely reliant on the nature of the most favourable reaction coordinate. In light of previous results,[46] this altogether shows that subtle interplays between substituent groups and the aryl rings prevent pose difficulties in the modular design of tuneable azo compounds since their interconversion shows up as system specific. The photo-switching in AZO1 is inhibited due to a stronger π bond order hindering rotation around the N-N bond axis. Further studies will be required to attempt to draw systematic functional group trends within the same mechanistic scenario.

To conclude, in this work a molecular design approach was used to plan and produce two novel moieties, suitable candidates for applications that aim to take advantage of visible light irradiation. Combined with TD-DFT calculation a comprehensive study of their properties was achieved giving also more information about the important role of the substituents that must be selected during the planning phase of these molecules. These findings can provide new insights regarding substituted azobenzene isomerization as well as the possibility to reveal new applications for a well-known organic molecule. These molecules are good candidate that will be used to modify the selected copolymer (EVOH) in order to produce simuli responsive membranes.

3.5. References

1. Baba, K. *et al.* Kinetic study of thermal Z to e isomerization reactions of azobenzene and 4-dimethvlaniino-4′-nitroazobenzene in Ionic Liquids [1-R-3- methyliniidazolium bis(trifluoromethylsulfonyl)imide with R = Butyl, Pentyl, and Hexyl]. *Chemistry (Weinheim an der Bergstrasse, Germany)* **12**, 5328–5333 (2006).
2. Garcia-Amorós, J. *et al.* Kinetico-Mechanistic Study of the Thermal Cis-to-Trans Isomerization of 4,4′-Dialkoxyazoderivatives in Nematic Liquid Crystals. *J. Phys. Chem. B* **114**, 1287–1293 (2010).
3. Bandara, H. M. D. *et al.* Photoisomerization in different classes of azobenzene. *Chem. Soc. Rev.* **41**, 1809–1825 (2012).
4. Spiridon, M. C. *et al.* 2-Oxazoline based photo-responsive azo-polymers. Synthesis, characterization and isomerization kinetics. *European Polymer Journal* **49**, 452–463 (2013).
5. Adriana Jerca, F. *et al.* Simultaneous two and three photon resonant enhancement of third-order NLO susceptibility in an azo-dye functionalized polymer film. *Physical Chemistry Chemical Physics* **15**, 7060–7063 (2013).
6. Tamai, N. *et al.* Ultrafast Dynamics of Photochromic Systems. *Chem. Rev.* **100**, 1875–1890 (2000).
7. *Photochromism: molecules and systems*. (Elsevier ; Distributors for the U.S. and Canada, Elsevier Science Pub. Co, 1990).
8. El'tsov, A. V. *et al. Organic photochromes*. (1990).
9. Bang, C.-U. *et al.* Azobenzene Liquid-Crystalline Polymer for Optical Switching of Grating Waveguide Couplers with a Flat Surface. *Macromolecular Rapid Communications* **28**, 1040–1044 (2007).
10. Gibbons, W. M. *et al.* Surface-mediated alignment of nematic liquid crystals with polarized laser light. *Nature* **351**, 49–50 (1991).
11. Camacho-Lopez, M. *et al.* Fast liquid-crystal elastomer swims into the dark. *Nature Mater* **3**, 307–310 (2004).
12. Yamada, M. *et al.* Photomobile Polymer Materials: Towards Light-Driven Plastic Motors. *Angewandte Chemie International Edition* **47**, 4986–4988 (2008).

13. Ruoyuan Yin *et al.* Can sunlight drive the photoinduced bending of polymer films? *J. Mater. Chem.* **19**, 3141–3143 (2009).
14. Deng, W. *et al.* Light-responsive wires from side-on liquid crystalline azo polymers. *Liquid Crystals* **36**, 1023–1029 (2009).
15. Tylkowski, B. *et al.* Photo-Triggered Microcapsules. *Macromol. Symp.* **360**, 192–198 (2016).
16. Tylkowski, B. *et al.* Light-Induced Switching of the Wettability of Novel Asymmetrical Poly(vinyl alcohol)-co-ethylene Membranes Blended with Azobenzene Polymers. *Langmuir* **26**, 14821–14829 (2010).
17. Trojanowska, A. *et al.* Smart microcapsules for precise delivery systems. *Funct. Mater. Lett.* **11**, 1850041 (2018).
18. Del Pezzo, R. *et al.* Ortho-substituted azobenzene: shedding light on new benefits. *Pure and Applied Chemistry* **0**, (2018).
19. Pirone, D. *et al.* Molecular Design of Microcapsule Shells for Visible Light-Triggered Release. *Polymers* **11**, 904 (2019).
20. Nicolescu, F. A. *et al.* New Organic–Inorganic Hybrids with Azo-dye Content. *Designed Monomers and Polymers* **13**, 437–444 (2010).
27. Whitten, D. G. *et al.* Solvent and substituent on the thermal isomerization of substituted azobenzenes. Flash spectroscopic study. *J. Am. Chem. Soc.* **93**, 2004–2008 (1971).
22. Merino, E. & Ribagorda, M. Control over molecular motion using the cis–trans photoisomerization of the azo group. *Beilstein J Org Chem* **8**, 1071–1090 (2012).
23. Marcandalli, B., Liddo, L. P.-D., Fede, C. D. & Bellobono, I. R. Solvent and substituent effects on thermal cis–trans-isomerization of some 4-diethylaminoazobenzenes. *J. Chem. Soc., Perkin Trans. 2* 589–593 (1984) doi:10.1039/P29840000589.
24. Jerca, V. V. *et al.* Advances in understanding the photoresponsive behavior of azobenzenes substituted with strong electron withdrawing groups. *Optical Materials* **48**, 160–164 (2015).
25. Dong, M. *et al.* Red-Shifting Azobenzene Photoswitches for in Vivo Use. *Acc. Chem. Res.* **48**, 2662–2670 (2015).
26. te Velde, G. *et al.* Chemistry with ADF. *J. Comput. Chem.* **22**, 931–967 (2001).

27. Adamo, C. *et al.* Toward reliable density functional methods without adjustable parameters: The PBE0 model. *J. Chem. Phys.* **110**, 6158–6170 (1999).
28. Adamo, C. *et al.* Toward chemical accuracy in the computation of NMR shieldings: the PBE0 model. *Chemical Physics Letters* **298**, 113–119 (1998).
29. Ernzerhof, M. *et al.* Assessment of the Perdew–Burke–Ernzerhof exchange-correlation functional. *J. Chem. Phys.* **110**, 5029–5036 (1999).
30. Klamt, A. *et al.* COSMO: a new approach to dielectric screening in solvents with explicit expressions for the screening energy and its gradient. *J. Chem. Soc., Perkin Trans. 2* **0**, 799–805 (1993).
31. Casida, M. E. *et al.* Time-Dependent Density Functional Response Theory for Molecules. in *Recent Advances in Density Functional Methods* vol. Volume 1 155–192 (WORLD SCIENTIFIC, 1995).
32. Roos, B. O. *et al.* The Complete Active Space Self-Consistent Field Method and its Applications in Electronic Structure Calculations. in *Advances in Chemical Physics* 399–445 (John Wiley & Sons, Ltd, 2007).
33. Neese, F. *et al.* Software update: the ORCA program system, version 4.0. *Wiley Interdisciplinary Reviews: Computational Molecular Science* **8**, e1327 (2018).
34. Neese, F. *et al.* The ORCA program system. *WIREs Computational Molecular Science* **2**, 73–78 (2012).
35. Angeli, C. *et al.* A quasidegenerate formulation of the second order n-electron valence state perturbation theory approach. *J. Chem. Phys.* **121**, 4043–4049 (2004).
36. Angeli, C. *et al.* Introduction of n-electron valence states for multireference perturbation theory. *J. Chem. Phys.* **114**, 10252–10264 (2001).
37. Nakano, H. *et al.* Quasidegenerate perturbation theory with multiconfigurational self-consistent-field reference functions. *J. Chem. Phys.* **99**, 7983–7992 (1993).
38. Schäfer, A. *et al.* Fully optimized contracted Gaussian basis sets for atoms Li to Kr. *J. Chem. Phys.* **97**, 2571–2577 (1992).

39. Neese, F. *et al.* An improvement of the resolution of the identity approximation for the formation of the Coulomb matrix. *Journal of Computational Chemistry* **24**, 1740–1747 (2003).
40. Glendening, E. D. *et al.* NBO 6.0: Natural bond orbital analysis program. *Journal of Computational Chemistry* **34**, 1429–1437 (2013).
41. Reed, A. E. *et al.* Chemical bonding in hypervalent molecules. The dominance of ionic bonding and negative hyperconjugation over d-orbital participation. *J. Am. Chem. Soc.* **112**, 1434–1445 (1990).
42. Asano, T. *et al.* Thermal Z-E isomerization of azobenzenes. The pressure, solvent, and substituent effects. *J. Org. Chem.* **49**, 4387–4391 (1984).
24. Wazzan, N. A. *et al.* Cis-Trans isomerisation of azobenzenes studied by laser-coupled NMR spectroscopy and DFT calculations. *Photochem. Photobiol. Sci.* **9**, 968–974 (2010).
44. Shepard, R. *et al.* The Multiconfiguration Self-Consistent Field Method. in *Advances in Chemical Physics* 63–200 (John Wiley & Sons, Ltd, 2007). doi:10.1002/9780470142943.ch2.
45. Angeli, C. *et al.* N-electron valence state perturbation theory: a fast implementation of the strongly contracted variant. *Chemical Physics Letters* **350**, 297–305 (2001).
46. H. M. Dhammika Bandara *et al.* Proof for the Concerted Inversion Mechanism in the trans→cis Isomerization of Azobenzene Using Hydrogen Bonding To Induce Isomer Locking. *J. Org. Chem.* **75**, 4817–4827 (2010).
47. Casellas, J. *et al.* Excited-State Decay in the Photoisomerisation of Azobenzene: A New Balance between Mechanisms. *ChemPhysChem* **17**, 3068–3079 (2016).
48. Gagliardi, L. *et al.* A theoretical study of the lowest electronic states of azobenzene: the role of torsion coordinate in the cis–trans photoisomerization. *Theor Chem Acc* **111**, 363–372 (2004).
49. Persico, M. *et al. Photochemistry: A Modern Theoretical Perspective*. (Springer International Publishing, 2018). doi:10.1007/978-3-319-89972-5.

25. Magennis, S. W. *et al.* Two-Photon-Induced Photoisomerization of an Azo Dye. *Chem. Mater.* **17**, 2059–2062 (2005).

51. Beltrame, P. L. *et al.* Thermal cis-trans isomerization of azo dyes in poly(methyl methacrylate) matrix: A kinetic study. *Journal of Applied Polymer Science* **49**, 2235–2239 (1993).

28. Beharry, A. A. *et al.* Azobenzene Photoswitching without Ultraviolet Light. *J. Am. Chem. Soc.* **133**, 19684–19687 (2011).

29. Matczyszyn, K. *et al.* Influence of the environment on kinetics and electronic structure of asymmetric azobenzene derivatives — experiment and quantum-chemical calculations. *Journal of Molecular Structure* **565–566**, 53–57 (2001).

3.6. Supporting Information section

1. Twisting mechanism

A potential energy scan was performed for both AZO1 and AZO2 compounds for the twisting of the ∡CNN angle starting from the trans equilibrium geometry and ending in the linear *sp* hybridized transition state. Since both aromatic rings have different substituents a twisting of both sites was performed. These results are displayed on Figure S 1. Clearly the S_2 pathway has a considerable thermal barrier (close to 20 kcal mol^{-1}) in the case of AZO1. This is much lower in the case of AZO2 where the value drops by almost half. The magnitude of this barrier is likely related to the steric repulsion caused by the in plane lone pair of nitrogen which must adapt to the linearization i.e.

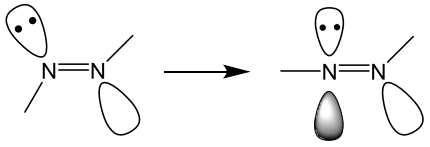

(Scheme 1)

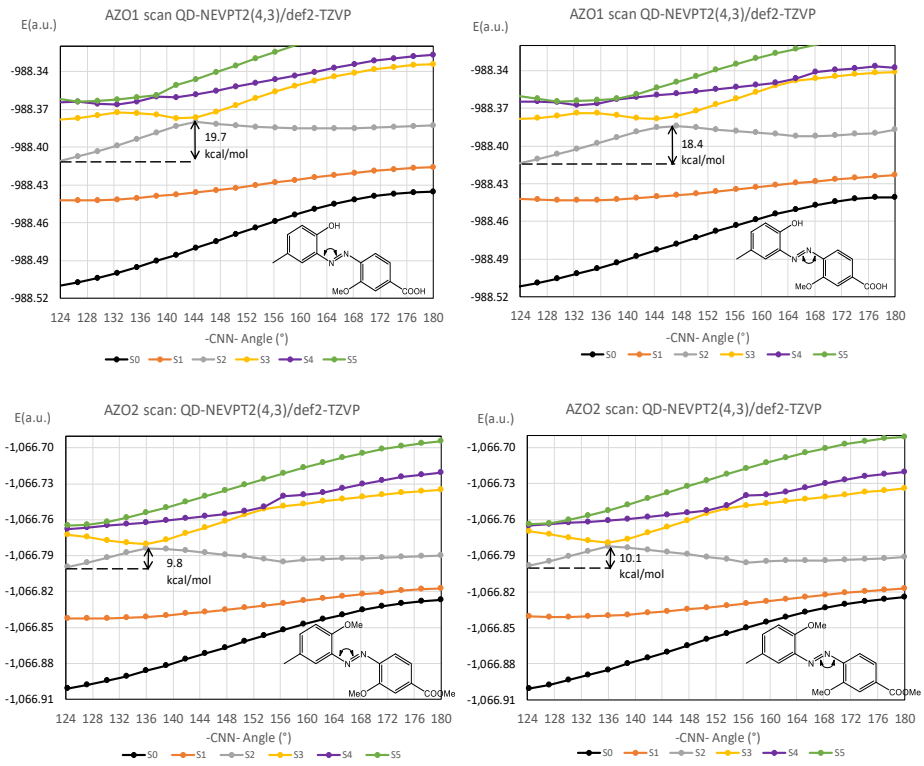

Figure S 1 – QD-NEVPT2//CASSCF(4,3)/def2-TZVP Potential energy surface scans of AZO1 (top) and AZO2(bottom) relative to the ∠(NNC) angle twisting to the linear position.

If one compares the NEVPT2 Mulliken reduced populations of the 2p orbitals in nitrogen it may be seen that q(AZO1)=3.6 and q(AZO2)=3.5 while the 2s populations remain steady at 1.5 in both compounds (at their respective equilibrium position).

For this reason the higher charge in AZO1 is likely the reason why the thermal barrier is higher for this compound since a larger repulsion has to be overcome.

The thermal back-isomerization starting from the Z isomer is evaluated to be $\Delta E^{\ddagger}$=28.4 kcal mol^{-1} for AZO1 and 32.6 kcal mol^{-1} for AZO2. These are comparably larger than the values reported in the main text for the rotation mechanism (17.9 and 14.0 kcal mol^{-1}).

2. Avoided crossings

As support for Figures 3.7-3.8 a tighter grid of potential energy points was carried out near the crossing regions between S_2 and S_3. While it is clear that AZO1 has an avoided crossing with a 2.7 kcal mol^{-1} energy gap, AZO2 has a state crossing which cannot be clearly resolved at this level of theory as the points differ by an order of magnitude less than the accuracy of the method itself 0.2 kcal mol^{-1} (Figure S 2). This may be a very weakly avoided crossing but it cannot be confirmed with certainty.

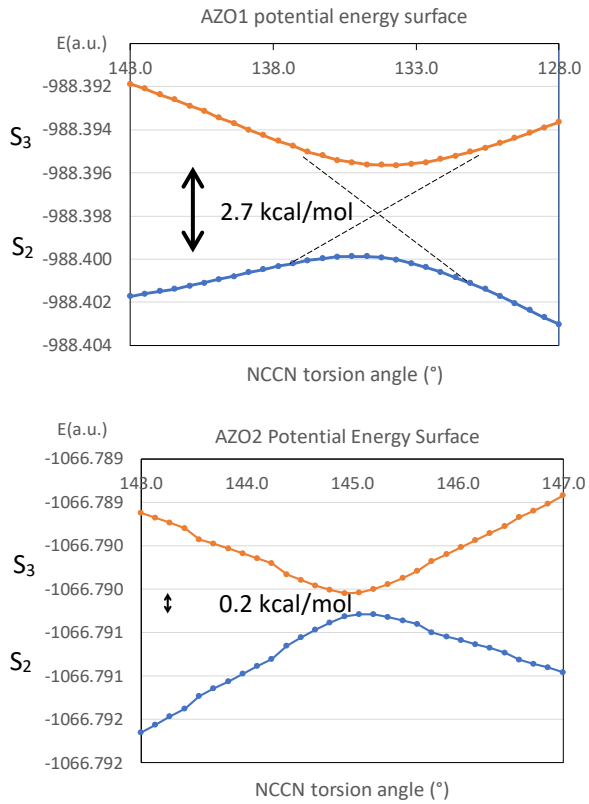

Figure S 2– Tight grid scan of AZO1 (top) and AZO2 (bottom) evidencing the two (avoided) crossings of S_2 and S_3.

Chapter 4. Advances in the design of self-supported stimuli-responsive membrane and coatings: smart controlled release systems

4.1 Introduction

Smart polymer membranes and surfaces, also recognized under different names including stimuli-responsive surfaces and adaptive or intelligent membranes, refer to those interfaces capable of undergoing reversible switchable transitions.[1,2] The reversible transitions observed in these interfaces are associated to environmental changes such as pH, temperature, conductivity or electromagnetic irradiation. Surfaces with *a priori* antagonistic behaviours that can be changed in an accurate and predictable fashion have increasingly received attention due to the novel requirements to advanced materials. In particular, such interfaces may find potential application in the fabrication of micro- and nanofluidic devices, self-cleaning, antifog surfaces along with sensor devices and systems that can control gas separation and evaporation.[3,4] In addition, stimulus-responsive surfaces have been employed to "mimic," at least to some extent, biologically occurring processes. More precise examples include the modulation of biological activity, protein immobilization or the control over cell adhesion, and migration processes. [1]

Stimulus-responsive membranes are created by the immobilization of stimuli-responsive polymers in a flat or curve conformation. As already explained in Chapter 1, stimuli-responsive polymers exhibit fast and large changes on their conformation, charge, or solubility among others as a function of environmental variations such as temperature,[5,6] ionic strength,[7] pH,[8] electric field,[4,9,10] light,[11–16] or solvent exposure.[2,17,18]

A large variety of synthetic strategies have been developed for the fabrication of smart polymer membranes. Examples of these procedures include the use of physisorption of copolymers either on an inorganic support or produced by surface segregation/surface rearrangement at polymer surfaces or by using grafting approaches.[19] As a function of the type of polymer selected, membranes with variable surface responsiveness can be fabricated. Herein we will focus the attention on membranes produced by using photo responsive polymers to give an idea of how and which properties can be modulated when a photo-switcher is bounded or included into the selected polymer.

Azobenzenes[20] and spiropyrans[21] are among the most extended molecules incorporated onto polymers to induce light responsiveness. Photo-responsive polymers react to light in different ways following photoisomerization, photoreaction, reversible ionic dissociation, or the addition–fragmentation processes. These, in turn, have associated different chain movements such as twisting, rotation, or oscillations. As a result, macroscopic properties can be modulated depending on the exposure or lack thereof to light. As an example of this behaviour, Athanassiou et al.[22] investigated the wettability of photochromic spiropyran-doped polymeric surfaces. In the study, the team witnessed that irradiation *via* UV lasers augmented the hydrophilic properties, as conversion to polar merocyanine isomers from nonpolar spiropyran molecules took place. It was also found that the process is completely reversible with irradiation provided from a green laser.

Azobenzenes are strong compounds and receptive to inclusion in different types of materials. This brilliant property of azobenzenes makes them useful in the preparation of different photoresponsive membranes. For this purpose. an azo molecule or chromophore can be directly blended into a polymer matrix or grafted (covalently attached) to a polymer. Moreover, the study of these molecules, included in polymers that can form bulky systems like membranes, can help to better understand their photoresponse, thus, they can be further used for the development of photoresponsive devices having precise applications in various fields. However, although the blending method is suitable, it shows instabilities in the photoresponse of the membranes, which can be attributed to the mobility of the azobenzenes in the polymer matrix and the tendency of the dipolar azobenzene molecules to form aggregates. Therefore, grafting these moieties onto a polymeric main chain or a substrate (even inorganic) can be the most suitable method for the preparation of photoresponsive membranes with azobenzenes. In a recent study, azobenzene was grafted over the pore walls of a novel family of periodic mesoporous organosilicas. In this study, three novel bis-silylated azobenzenes, were used to synthesize three novel azobenzene-bridged periodic mesoporous organosilica materials. This resulted in the successful formation of mesoporous materials that are promising for reversible gas

adsorption under the influence of light; therefore, they can be used for the preparation of light-responsive membranes for gas-separation applications. [23] Similarly, metal organic frameworks (MOFs) were used as hosts for light-responsive azobenzene molecules.[24,25] Azobenzene was loaded as a side group in these MOFs. Therefore, the flux and separation factor of a gas mixture can be controlled by regulating the configurational state of the light-responsive azobenzene molecules, as shown in Figure 4.1.

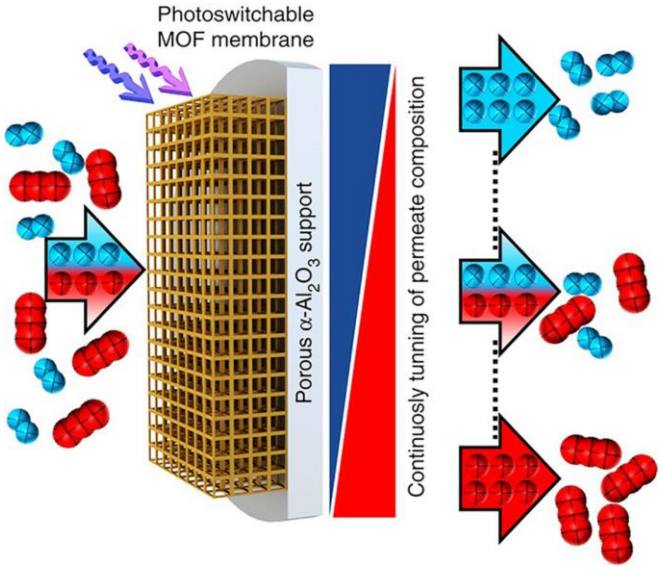

Figure 4.28 - Switchable membrane separation. Schematic illustration of tuneable, remote controllable molecular selectivity by a photoswitchable MOF membrane. The molecular feed mixture (left-hand side), where the molecules are depicted in red and blue, is separated by the nonporous membrane. The molecular separation factor, giving the composition of the permeation flux (right-hand side), can be continuously tuned by light irradiation.[24]

In this chapter the modification of a selected specific copolymer, with the novel asymmetric azobenzene moiety produced during this work, will be described. The production method of self-supported dense membranes and of the dense coatings, onto the pre-existing commercial membrane, made out from this innovative polymer will be discussed. Finally, the study of the stimuli-responsive properties of the new system, with the use of visible light irradiation and temperature, as triggers, will be presented.

In this chapter we report the synthesis of a new stimuli-responsive polymer obtained by chemical modification of commercially available copolymer with 3-

methoxy-4-((2-methoxy-5-methylphenyl)diazenyl)benzoyl chloride (AZO4), a novel asymmetrical ortho-substituted azobenzene derivative.

The light sensitive membranes produced out of this modified copolymer, would provide release of perfume in absence of external mechanical forces. However, the incorporation of a light sensitive moiety as a pending group into the polymeric mainchain requires a smart design of the modification strategy to balance the sensitivity to light with the possibility of formation and stability of the system. The presence of the ortho-substituted azobenzene molecule as a side chain group should help the membrane to release the perfume when exposed to visible light. The light-sensitive monomer to be incorporated into the polymeric chain, was synthesized with a four-steps procedure that yields AZO4, an azobenzene derivative functionalized with ortho-donor groups which leads to a red-shift of the absorption wavelength of the monomer and therefore, of the resulting polymer. The synthesis of light sensitive monomer was reported in Chapter 2.

The final aim of this work is to produce a coating adaptable to the pre-existing system in order to control the evaporation rate of the perfume raw materials from the device. The main innovation that this work is bringing is represented by the mechanism driving the evaporation of the volatile species present in the device reservoir. The direct modification of the commercial copolymer is expected to produce a stimuli-responsive system with properties that are directly tuned by the grafted moieties; this system, as already discussed in the previous chapters, can modify its configurations by the use of two different triggers (e.g. light and temperature). More specifically, the morphology and the internal structure (e.g. interchain volume) of the membrane will depend on the isomerization process of the moieties linked to the polymer backbone. To achieve this objective, it is important that the membranes produced in this work are a dense layer, in order to avoid porosity that can affect the release of the PRMs.

Besides, we aimed also at tuning the general profile of the perfume, by balancing the rate of evaporation of the perfume top notes (with higher volatility) and the bottom ones (with lower volatility), taking advantage of the interactions that these different perfume compounds could have with the

azobenzene pending groups (depending on their polarity), giving to the consumer an improved product experience.

4.2. Experimental part

4.2.1. Materials

4.2.2. Methods and characterizations:

4.2.2.1 P&G membranes:

4.2.2.2. Scanning electron microscopy (SEM)

A scanning electron microscope (SEM) scans a focused electron beam over a surface to create an image. The electrons in the beam interact with the sample, producing various signals that can be used to obtain information about the surface topography and composition.

The main SEM components include (Figure 4.2.):

- **Source of electrons**: Electrons are produced at the source by thermo-ionic heating. These electrons are then accelerated to a voltage between 1-40 kV and condensed into a narrow beam which is used for imaging and analysis. There are 3 commonly used types of electrons sources: Tungsten filament; Solid state crystal (Cerium hexaboride or Lanthanum hexaboride); Field emission gun (FEG).
- **Lenses**: A series of condenser lenses focus the electron beam as it moves from the source down the column. The narrower the beam the smaller the spot it will have when contacting the surface, thus the term ‘spot size’.
- **Detectors**: When the electron beam interacts with a sample in a scanning electron microscope (SEM), multiple events happen. In general, different detectors are needed to distinguish secondary electrons, backscattered electrons, or characteristic X-rays. Depending upon the accelerating voltage and sample density, the signals come from different penetration depths.

- **Sample Chamber**: Samples are mounted and placed into a chamber that is evacuated. The sample chamber can include a translation stage, tilt and rotation devices, feed-throughs to the outside, temperature stages, optical cameras, and a variety of other devices to assist in imaging the sample.
- **Scanning Coil**: After the beam is focused, scanning coils are used to deflect the beam in the X and Y axes so that it scans in a raster fashion over the surface of the sample. Electrons are produced at the top of the column, accelerated down and passed through a combination of lenses and apertures to produce a focused beam of electrons which hits the surface of the sample. The sample is mounted on a stage in the chamber area and, unless the microscope is designed to operate at low vacuums, both the column and the chamber are evacuated by a combination of pumps. The level of the vacuum will depend on the design of the microscope.

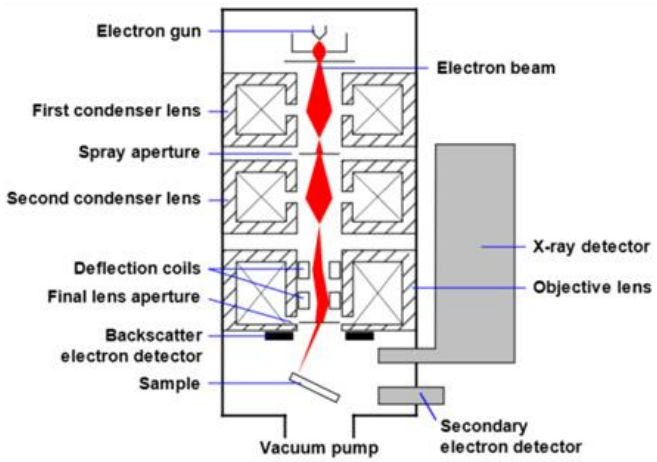

Figure 4.29. - Schematic of a Scanning Electron Microscope

The position of the electron beam on the sample is controlled by scan coils situated above the objective lens. These coils allow the beam to be scanned over the surface of the sample. This beam rastering or scanning, as the name of the microscope suggests, enables information about a defined area on the sample to be collected. As a result of the electron-sample interaction, a number

of signals are produced. These signals are then detected by appropriate detectors. The scanning electron microscope (SEM) produces images by scanning the sample with a high-energy beam of electrons. As the electrons interact with the sample, they produce secondary electrons, backscattered electrons, and characteristic X-rays (Figure 4.3.). These signals are collected by one or more detectors to form images which are then displayed on the computer screen. When the electron beam hits the surface of the sample, it penetrates the sample to a depth of a few microns, depending on the accelerating voltage and the density of the sample.

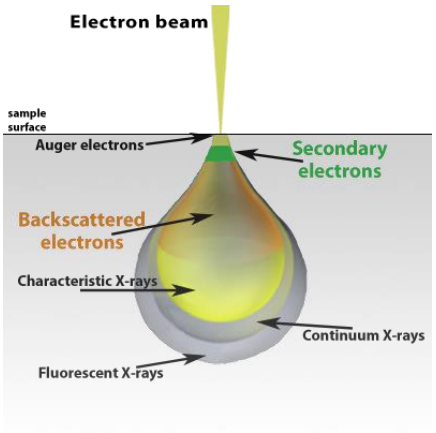

Figure 4.30. - Schematic of an electron beam interaction

There are many types of information that can be obtained from SEM microscopy analyzing the data from the different type of electrons collected by the different sensors:

Backscattered electrons (BSD) vary in their amount and direction due to the composition and topography of the specimen. Materials with elements composed of a higher atomic number (Z) yield more backscattered electrons than lower Z elements. Compositional and topographic images can be acquired in the same location to provide insight to correlate material properties to topography, grain size or morphology.

Energy Dispersive Spectroscopy (EDS): In scanning electron microscopy, an x-ray is emitted when the electron beam displaces an inner shell electron that is replaced by an outer shell electron. Because each element

has a unique energy difference between outer and inner electron shells, the x-rays that are detected yield an elemental identification. EDS data can be obtained at a point, along with a line or mapped over an area.

The surface morphology of the obtained membranes and coatings were investigated in this work by environmental scanning electron microscopy (ESEM). ESEM analyses were carried out in low vacuum mode, using an accelerating voltage ranging between 15 and 20 kV by means of an ESEM FEI Quanta 600 apparatus. To study the cross-section of each sample, the fractures were done by cracking the samples after cooling them in liquid nitrogen. In the resulting specimens a brittle fracture was obtained. The membrane thickness was measured during the analysis by xT microscope control connected with an ESEM FEI Quanta 600 apparatus. The average thickness of the membrane (10 measurements) was calculated from cross-section ESEM micrographs with Image-ProPlus 5 software (Media Cybernetics Inc.). No coating was needed for all the samples analyzed due to the low vacuum conditions. In these experiments, the membrane morphology was analyzed at three different times:

1. No irradiated membrane;
2. Same membrane exposed to white light irradiation for 30 min at 25 °C;
3. Same sample after a thermal treatment at 60°C for 30 min in a dark environment (closed oven chamber).

In this way, the changes in the membranes external surface morphology before and after white-light irradiation and temperature were investigated.

4.2.2.3. Atomic force microscopy (AFM)

AFM is a high-resolution scanning probe microscopy which helps to measure local properties such as roughness of the surface, magnetism or morphology height, with a probe. The are few basic principles that control **AFM:**

- **Surface Sensing**: An AFM uses a cantilever with a very sharp tip to scan over a sample surface. As the tip approaches the surface, the close-range, attractive force between the surface and the tip causes the cantilever to deflect towards the surface. However, as the cantilever is

brought even closer to the surface, such that the tip makes contact with it, increasingly repulsive force takes over and causes the cantilever to deflect away from the surface.

- **Detection Method**: A laser beam is used to detect cantilever deflections towards or away from the surface. By reflecting an incident beam off the flat top of the cantilever, any cantilever deflection will cause slight changes in the direction of the reflected beam. A position-sensitive photo diode (PSPD) can be used to track these changes. Thus, if an AFM tip passes over a raised surface feature, the resulting cantilever deflection (and the subsequent change in direction of reflected beam) is recorded by the PSPD.
- **Imaging**: An AFM images the topography of a sample surface by scanning the cantilever over a region of interest. The raised and lowered features on the sample surface influence the deflection of the cantilever, which is monitored by the PSPD. By using a feedback loop to control the height of the tip above the surface, thus maintaining constant laser position, the AFM can generate an accurate topographic map of the surface features.

The analyzed sample was a membrane of (1x1) cm^2 produced from the polymer modified with azomoieties. The AFM images were recorded with an Agilent 5500 Environmental Atomic Force Microscope (Agilent Technology) equipped with an extender electronics module, which enables phase imaging in Tapping Mode. All the images were recorded in tapping mode using Multi 75 (Budget Sensors) silicon cantilevers (length = 225 μm, width = 28 μm, and thickness = 3 μm) with a force constant of 3 N/m and a resonance frequency of 190 kHz. The scan rate was typically 0.7−2 Hz. All images were measured at room temperature. The microscope was placed on an active vibration isolation chamber (Agilent Technology) to eliminate external vibration noise. The temperature of the chamber was 25°C. Membrane topography was analyzed at three different times:

1. Unirradiated membrane;
2. Same membrane exposed to white light irradiation for 30 min at 25 °C;

3. Same sample after a thermal treatment at 60°C for 30 min in a dark environment (closed hoven chamber).

The changes in the membranes topography before and after white-light irradiation and temperature were investigated to test the effect of the triggers on the modified polymer. Results were quantified by means of several parameters, which calculus are summarized below:

- **Average roughness (R_a)**: Gives the deviation in height. Different profiles can give the same R_a.

$$R_a(N,M) = \frac{1}{N}\sum_{x=1}^{N}\left(z(x,y) - \bar{z}(N,M)\right) \quad \text{(2D)} \qquad \text{Eq. 4.1}$$

$$R_a(N,M) = \frac{1}{NM}\sum_{x=1}^{N}\sum_{y=1}^{M}\left(z(x,y) - \bar{z}(N,M)\right) \quad \text{(3D)} \qquad \text{Eq. 4.2}$$

- **Root Mean Square (RMS) roughness (R_q)**: Represents the standard deviation of surface heights.

$$R_a(N,M) = \sqrt{\frac{1}{N}\sum_{x=1}^{N}\left(z(x,y) - \bar{z}(N,M)\right)^2} \text{ (2D)} \qquad \text{Eq. 4.3}$$

$$R_a(N,M) = \sqrt{\frac{1}{NM}\sum_{x=1}^{N}\sum_{y=1}^{M}\left(z(x,y) - \bar{z}(N,M)\right)^2} \quad \text{(3D)} \qquad \text{Eq. 4.4}$$

- **Skewness (R_{Sk})**: Skewness is the third moment of profile amplitude probability density function and is used to measure the profile symmetry about mean line. When the height distribution is symmetrical R_{Sk} is zero. If the height distribution is asymmetrical, and the surface has more peaks than valleys the Skewness moment is positive and if the surface is more planar and valleys are predominant the Skewness is negative.

$$R_{Sk} = \frac{1}{NR_q^3}\sum_{i=1}^{N}[z_i - \bar{z}]^3 \qquad \text{Eq. 4.5.}$$

- **Kurtosis (R_{Ku})**: Kurtosis moment is the fourth moment of profile amplitude probability function and corresponds to a measure of surface

sharpness. When R_{Ku} is 3 indicates a Gaussian amplitude distribution, and the surface is called Mesokurtic, but if Kurtosis is smaller than 3 the surface is flat and called Platykurtic. If the Kurtosis is higher than 3, the surface has more peaks than valleys.

$$R_{Ku} = \frac{1}{NR_q^4}\sum_{i=1}^{N}[z_i - \bar{z}]^4 \qquad \text{Eq. 4.6}$$

4.2.2.4. Differential scanning calorimetry (DSC)

Differential Scanning Calorimetry, or DSC, is a thermal analysis that studies the change of materials heat capacity (C_p) with temperature. DSC is the most applied technique to study the thermal events of polymers like melting temperature, glass transition, crystalline phase transition temperature and energy, precipitation energy and temperature and specific heat or heat capacity. Moreover, by use this technique the heat of fusion, latent heat of melting, reaction energy and temperature can be determined. It is based on the heat flow difference between a substance and a reference, during a controlled temperature program. DSC analysis measures the amount of energy absorbed or released by a sample when it is heated or cooled, providing quantitative and qualitative data on endothermic (heat absorption) and exothermic (heat evolution) processes. The Figure 4.4. shows a schematic illustration of the apparatus.

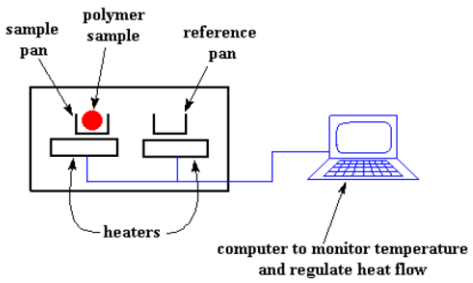

Figure 4.4. - Scheme of DSC equipment.

It consists of two pans, the sample one where the operator puts the polymer and the reference pan that will be left empty. Each pan is on top of a heater and using a software, the heat/cool cycle can be set. When a sample

undergoes a physical transformation such as a phase transition, more or less heat will need to flow to it than to the reference to maintain both at the same temp. Whether more of less heat must flow to the sample depends on whether the process is exothermic or endothermic.[26] Generally, the temperature program for a DSC analysis is designed such that the sample holder temperature increases linearly as a function of time. Only a few mg of material are required to run the analysis. DSC is the most often used thermal analysis method, primarily because of its speed, simplicity, and availability. It is mostly used for quantitative analysis.

For DSC system, it is possible to write the equation (Eq. 4.7.):

$$dHdt = C_p dT + f(T,t) \qquad \text{Eq. 4.7}$$

Where H is the enthalpy in J mol^{-1}, C_p is the specific heat capacity expressed in $JKmol^{-1}$ and *f*(T, t) is the kinetic response of the sample in $Jmol^{-1}$. The result of a DSC experiment is a curve of heat flux versus temperature or time (Figure 4.5). This curve can be used to calculate enthalpies of transitions, by integrating the peak corresponding to a given transition.

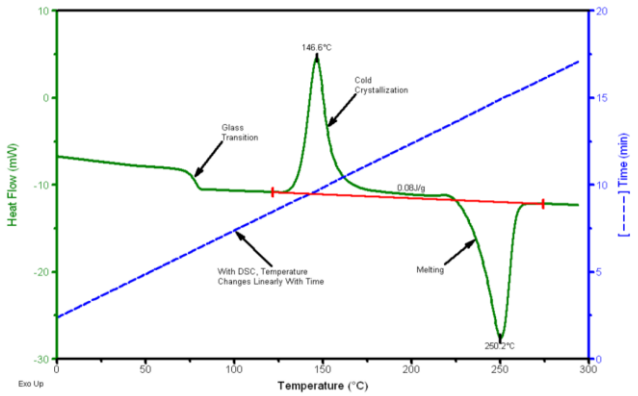

Figure 4.5. - Typical DSC curve (example of PET)

Area under the peak is directly proportional to heat absorbed or evolved by the reaction. Height of the peak is directly proportional to rate of the reaction.[27]

Calorimetric studies were performed in aluminium standard 40 µL crucibles without pin (ME-26763) with a Mettler DSC822e thermal analyser at the heating rate of 10˚C/min using about 5 mg of sample, nitrogen as a purge gas (100 mL/min) and liquid nitrogen for the cooling system. The equipment was previously calibrated with indium (156.6˚C) and zinc (418.6˚C) pearls.

4.2.3 Modification of the copolymer by means of novel asymmetric ortho-substituted azobenzene moieties.

4.3. Results and discussions

4.3.1. Polymer preparation and characterization

4.3.2. Membrane preparation

4.3.4. Study of the compatibility of the membranes.

4.5. Bibliography

1. Mendes, P. M. *et al.* Stimuli-responsive surfaces for bio-applications. *Chem. Soc. Rev.* **37**, 2512–2529 (2008).
2. Motornov, M. *et al.* Reversible Tuning of Wetting Behavior of Polymer Surface with Responsive Polymer Brushes. *Langmuir* **19**, 8077–8085 (2003).
3. Alexander, C. *et al.* Responsive Polymers at the Biology/Materials Science Interface. *Advanced Materials* **18**, 3321–3328 (2006).
4. Gras, S. L. *et al.* Intelligent control of surface hydrophobicity. *Chemphyschem* **8**, 2036–2050 (2007).
5. Crevoisier, G. *et al.* Switchable Tackiness and Wettability of a Liquid Crystalline Polymer. *Science* **285**, 1246–1249 (1999).

6. Sun, T. *et al.* Reversible Switching between Superhydrophilicity and Superhydrophobicity. *Angewandte Chemie International Edition* **43**, 357–360 (2004).
7. Kontturi, K. *et al.* Modeling of the Salt and pH Effects on the Permeability of Grafted Porous Membranes. *Macromolecules* **29**, 5740–5746 (1996).
8. Wilson, M. D. *et al.* The anthranilate amide of 'polyethylene carboxylic acid' shows an exceptionally large change with pH in its wettability by water. *J. Am. Chem. Soc.* **110**, 8718–8719 (1988).
9. Lahann, J. *et al.* A Reversibly Switching Surface. *Science* **299**, 371–374 (2003).
10. Katz, E., *et al.* Electromechanics of a Redox-Active Rotaxane in a Monolayer Assembly on an Electrode. *J. Am. Chem. Soc.* **126**, 15520–15532 (2004).
11. Ichimura, K., *et al.* Light-Driven Motion of Liquids on a Photoresponsive Surface. *Science* **288**, 1624–1626 (2000).
12. Feng, C. L. *et al.* Reversible light-induced wettability of fluorine-containing azobenzene-derived Langmuir–Blodgett films. *Surface and Interface Analysis* **32**, 121–124 (2001).
13. Radüge, C. *et al.* Controlling wettability by light: illuminating the molecular mechanism. *Eur. Phys. J. E* **10**, 103–114 (2003).
14. Cooper, C. G. F. *et al.* Non-Covalent Assembly of a Photoswitchable Surface. *J. Am. Chem. Soc.* **126**, 1032–1033 (2004).
15. Berná, J. *et al.* Macroscopic transport by synthetic molecular machines. *Nature Mater* **4**, 704–710 (2005).
16. Jiang, W. *et al.* Photo-switched wettability on an electrostatic self-assembly azobenzene monolayer. *Chem. Commun.* 3550–3552 (2005) doi:10.1039/B504479K.
17. Zhao, B. *et al.* Nanopattern Formation from Tethered PS-b-PMMA Brushes upon Treatment with Selective Solvents. *J. Am. Chem. Soc.* **122**, 2407–2408 (2000).
18. Julthongpiput, D. *et al.* Shaped Amphiphilic Brushes with Switchable Micellar Surface Structures. *J. Am. Chem. Soc.* **125**, 15912–15921 (2003).

19. Wischerhoff, E. *et al.* Smart Polymer Surfaces: Concepts and Applications in Biosciences. in *Bioactive Surfaces* (eds. Börner, H. G. & Lutz, J.-F.) 1–33 (Springer Berlin Heidelberg, 2011).
20. Behrendt, R. *et al.* Photomodulation of the Conformation of Cyclic Peptides with Azobenzene Moieties in the Peptide Backbone. *Angewandte Chemie International Edition* **38**, 2771–2774 (1999).
21. Bunker, B. C. *et al.* Direct Observation of Photo Switching in Tethered Spiropyrans Using the Interfacial Force Microscope. *Nano Lett.* **3**, 1723–1727 (2003).
22. Athanassiou, A. *et al.* Photocontrolled Variations in the Wetting Capability of Photochromic Polymers Enhanced by Surface Nanostructuring. *Langmuir* **22**, 2329–2333 (2006).
23. Abboud, M. *et al.* Novel family of periodic mesoporous organosilicas containing azobenzene within the pore walls. *Microporous and Mesoporous Materials* **249**, 157–164 (2017).
24. Wang, Z. *et al.* Tunable molecular separation by nanoporous membranes. *Nat Commun* **7**, 1–7 (2016).
25. Knebel, A. *et al.* Azobenzene Guest Molecules as Light-Switchable CO2 Valves in an Ultrathin UiO-67 Membrane. *Chem. Mater.* **29**, 3111–3117 (2017).
26. Kv, K. *et al.* Research and Reviews: Journal of Pharmaceutical Analysis. **3**, 12 (2014).
27. Pijper, D. *et al.* Light-Controlled Supramolecular Helicity of a Liquid Crystalline Phase Using a Helical Polymer Functionalized with a Single Chiroptical Molecular Switch. *J. Am. Chem. Soc.* **130**, 4541–4552 (2008).
28. Taylor, J. *et al.* Identification of kafirin film casting solvents. *Food Chemistry* **3**, 401–408 (2005).
29. Tsuda, M. *et al.* Schotten-baumann esterification of poly(vinyl alcohol). II. *Makromol. Chem.* **72**, 183–190 (1964).
30. Arranz, F. *et al.* Partial esterification of poly(vinyl alcohol) with acid chlorides. *Die Angewandte Makromolekulare Chemie* **92**, 121–132 (1980).
31. Fernández, M. D. *et al.* Cyclic ureas as solvents for esterification of poly(vinyl alcohol) and vinyl acetate-vinyl alcohol copolymers with acid chlorides. *Journal of Applied Polymer Science* **107**, 2509–2519 (2008).

32. Mormann, W. *et al.* Acylation of (partially) silylated poly(vinyl alcohol)s with acyl chlorides. Vinyl chloride/vinyl ester copolymers by polymer analogous reaction. *Macromolecular Chemistry and Physics* **197**, 3463–3471 (1996).
33. Virtanen, S. *et al.* Modified nanofibrillated cellulose–polyvinyl alcohol films with improved mechanical performance. *RSC Advances* **4**, 11343–11350 (2014).
34. Stenstad, P. *et al.* Chemical surface modifications of microfibrillated cellulose. *Cellulose* **15**, 35–45 (2008).
35. Qua, E. *et al.* Preparation and Characterization of Poly(vinyl alcohol) Nanocomposites Made from Cellulose Nanofibers. *Journal of Applied Polymer Science* **113**, 2238–2247 (2009).
36. Tylkowski, B. *et al.* Light-Induced Switching of the Wettability of Novel Asymmetrical Poly(vinyl alcohol)-co-ethylene Membranes Blended with Azobenzene Polymers. *Langmuir* **26**, 14821–14829 (2010).
37. Giménez, V. *et al.* Modification of poly(vinyl alcohol) with acid chlorides and crosslinking with difunctional hardeners. *Journal of Polymer Science Part A: Polymer Chemistry* **34**, 925–934 (1996).
38. Champetier, G. *et al.* Introduction à la chimie macromoléculaire: par Georges Champetier, Lucien Monnerie. (Masson et Cie, 1969).

Chapter 5. Smart controlled release membranes.

5.1 Introduction

Air fresheners are consumer products that typically emit fragrances. Their use is generally addressed to house environments, commercial interiors such as restrooms, foyers other smaller indoor areas and cars. Some of the different types of air fresheners include electric fan air fresheners, gravity drip hygiene odor control cleaning systems, passive non-mechanical evaporating aroma diffusers, metered aerosol time-operated mist dispensers, sprays, candles, oils, gels, beads, and plug-ins.

Air freshening is not only limited to modern day sprays, air freshening also can involve the use of organic and everyday house hold items. Although air fresheners are primarily used for odor elimination, some people use air fresheners for the pleasant odors they emit. Fragrances have been used to mask odors since antiquity. A variety of compounds have been used over the past two millennia for their abilities to create pleasant aromas or eliminate unpleasant odors.

The first modern air freshener was introduced in 1948.[1] Its function was based on a military technology for dispensing insecticides and adapted into a pressurized spray using a chlorofluorocarbon (CFC) propellant. The product delivered a fine mist of aroma compounds that would remain suspended in the air for an extended period. This type of product became the industry standard and air freshener sales experienced tremendous growth. In the 1950s, many companies began to add chemicals that counteract odors to their fragrance formulas. These chemicals, intended to neutralize or destroy odors, included unsaturated esters, pre-polymers, and long-chain aldehydes.[2–5]

In the 1980s, the air freshener market shifted away from aerosols, due to concerns over the destruction of the ozone layer by chlorofluorocarbons (CFCs). Many other air freshener delivery methods have become popular since then, including under the seat wafer air fresheners, scented candles, reed diffusers, potpourri, and heat release products.

Delivery of the air freshener mechanisms falls into two broad categories: continuous action and instant action. Continuous action products include scented candles and devices which use a candle flame or some other heat source to heat and vaporize a fragrance formulation, incense burners; wall

plug-ins which either use piezoelectric technology to aerosolize fragrance or heat to vaporize it; fragrance impregnated gels which release fragrance as the gel evaporates sometimes with the help of an electric fan; wick and reed diffusers which release fragrance by evaporation from fragrance-soaked wicks or wooden reeds; and fragrance impregnated materials like floor wax, paper, plastics, wood which release fragrance by off gassing; and lastly nebulization systems which convert liquid fragrances into a vapor in a cold process without the use of heat.

Instant action systems are mainly aerosol sprays, or atomizers. The aerosol spray uses a propellant and fragrance packaged under pressure in a sealed metal or glass container with a valve which is opened by pressing down a button which contains a spray nozzle – the actuator.

Air fresheners introduce fragrance into the air of interior spaces either as droplets which transition to vapor, or as the molecules of fragrance ingredients directly evaporating from a source. Fragrance diffuses into the air to mask other odors or to introduce a specific odor. In addition to the adsorbents, oxidizers, surfactants, and disinfectants, ingredients in air fresheners can include fragrances, aerosol propellants, preservatives, and solvents. Thus, the perfume inside these devices, is a mixture of fragrant essential oils or aroma compounds, fixatives and solvents, used to give the living-spaces an agreeable scent.[6]

The most practical way to start describing a perfume is according to the elements of the fragrance notes of the scent or the "family" it belongs to, all of which affect the overall impression of a perfume from first application to the last lingering hint of scent.[7,8] A perfume generally has three sets of notes, making the scent accord. The notes unfold over time, with the immediate impression of the top note leading to the deeper middle notes, and the base notes gradually appearing as the final stage. These notes are created carefully with knowledge of the evaporation process of the perfume:

- **Top notes:** Also called the *head notes*. The scents that are perceived immediately of a perfume. Top notes consist of small, light molecules that evaporate quickly.

- **Middle notes**: Also referred to as *heart notes*. The scent of a perfume that emerges just prior to the dissipation of the top note. The middle note compounds form the "heart" or main body of a perfume and act to mask the often-unpleasant initial impression of base notes, which become more pleasant with time.
- **Base notes**: The scent of a perfume that appears close to the departure of the middle notes. The base and middle notes together are the main theme of a perfume. Base notes bring depth and solidity to a perfume. Compounds of this class of scents are typically rich and "deep" and are usually not perceived until 30 minutes after application.

The scents in the top and middle notes are influenced by the base notes; conversely, the scents of the base notes will be altered by the types of fragrance materials used as middle notes. (Figure 5.1.).

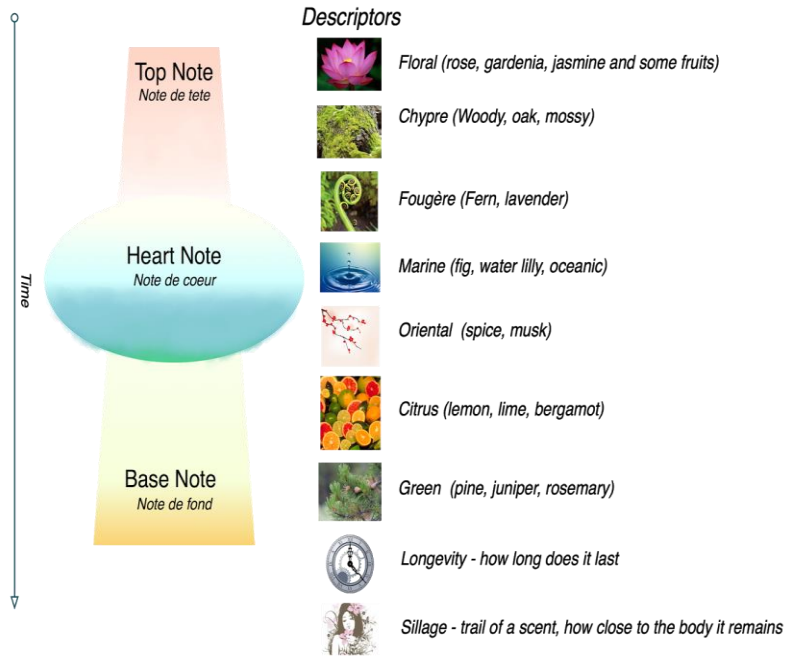

Figure 5.31. - Perfume notes chart.

5.2. Experimental part

5.2.1. Materials:

5.2.3. Gravimetric test method for perfume release

5.3. Results and discussions:

5.3.1 Gravimetric test results overview:

5.4. Conclusions

5.5. Bibliography

Conclusions

General Objectives

General Conclusions:

Appendix A – List of abbreviations

^{13}C NMR	Carbon Nuclear Magnetic Resonance Spectroscopy
^{1}H NMR	Proton Nuclear Magnetic Resonance Spectroscopy
α_Z	content of the *Z*-isomer at the PSS
A_∞	absorbance at PSS time
A_t	absorbance at time t
A	Steric factor
A_0	absorbance at time 0
AFM	Atomic force microscopy
A_{PSS}	Absorbance at PSS
ATR	attenuated total reflection
AZO1	4-((2-hydroxy-5-methylphenyl)diazenyl)-3-methoxybenzoic acid
AZO2	methyl 3-methoxy-4-((2-methoxy-5-methylphenyl)diazinyl) benzoate
AZO3	3-methoxy-4-((2-methoxy-5-methylphenyl)diazenyl)benzoic acid
AZO4	3-methoxy-4-((2-methoxy-5-methylphenyl)diazenyl)benzoyl chloride
BA	Benzyl acetate
BSD	Backscattered electrons
C18TMACl	octadecyltrimethylammonium chloride
CD-RW	rewritable recording media
CFC	chlorofluorocarbon
CH2Cl2	Chloroform
CH_3I	methyl iodide
COSMO	COnductor like Screening MOdel
C_p	heat capacity
d1	retention time between consecutive pulses
d-DMSO	deuterated dimethylsulfoxide
DMAP	4-Dimethylaminopyridine

DMF	N,N-dimethylformamide
DMSO	Dimethyl sulfoxide
DSC	Differential Scanning Calorimetry
E_a	activation energy
EAA	Ethyl aceto-acetate
EDS	Energy Dispersive Spectroscopy
EDX	Energy Dispersive X-ray Analysis
ESEM	environmental scanning electron microscope
EVOH	poly(vinyl alcohol-co-ethylene)
EVOH	elastin-like polypeptides
EVOH_45	modififed EVOH at 45% with azobezene moieties
FD&C	food, drug and cosmetics
FEG	Field emission gun
f_{osc}	oscillator strengths
FT-IR	Fourier-Transform Infrared-Spectroscopy
GSH	glutathione
h	Planck constant
H_{02}	squared energy gap
HCl	hydrochloric acid
HCST	higher critical solution temperature
HOMO	Highest Occupied Molecular Orbital
I	intensity of light passing through a sample cell
I_o	intensity of light passing through a reference cell
k	thermal rate costant
k_i	rate constant of *E*–*Z* photoisomerization
KOH	potassium hydroxide
k_r	rate constant of the *Z*–*E* relaxation
L	d-Limonene
LbL	layer-by-layer
LCST	lower critical solution temperature
LUMO	Lowest Unoccupied Molecular Orbital

MHA	(16-mercapto) hexadecanoic acid
MOFs	metal organic frameworks
NaH	sodium hydride
$NaNO_2$	sodium nitrite
NaOH	sodium hydroxide
NBO	Natural Bond Orbital
NLMO	Natural Localized Molecular Orbital
NMP	N-methylpyrrolidone
NMR	Nuclear Magnetic Resonance
OEGMA	oligo(ethylene glycol) methacrylate
OPD	optical path difference
P&G	Procter and Gamble Company
P2VP	Poly(2-vinylpyridine)
P4VP	Poly(4-vinylpyridine)
PAAc	Poly(acrylic acid)
p-Cresol	4-methylphenol
PDEAEMA	Poly(N,N-diethyl aminoethyl methacrylate)
PDMAEMA	Poly(nN,N-dimethyl aminoethyl methacrylate)
PE	polyethylene
PEAAc	Poly(2-ethyl acrylic acid)
PES	potential energy surface
PMAAc	Poly(methacrylic acid)
PNIPAAm	poly(N-alkyl-substituted acrylamides)
PNIPAM	poly(N-isopropylacrylamide)
PPAAc	Poly(2-propyl acrylic acid)
ppm	parts-per-million
ppm	parts per milion
PRM	Perfume raw material
PSPD	position-sensitive photo diode
PSS	photostationary state
Py	Pyridine

QD-NEVPT2	multi-configurational wavefunction methodology
QD-NEVPT2	Quasi-Degenerate N-Electron Valence Perturbation Theory
R	universal gas constant
R_a	Average roughness
rf	radio frequency
RH %	relative humidity index
RKu	Kurtosis
R_q	Root Mean Square (RMS) roughness
R_{Sk}	Skewness
SEM	scanning electron microscope
$SOCl_2$	thionyl chloride
T	temperature in Kelvin
TD-DFT	Time-dependent density-functional theory
THF	Tetrahydrofuran
TLC	Thin Layer Chromatography
TMS	tetramethylsilane
TS	Transition state
TZP	polarization function
UCST	upper critical solution temperature
UV	Ultra violet
UV-Vis	Ultra violet-visible light
UV-Vis	UV-Visible spectroscopy
α	collection of constants incorporating nuclear velocity
β-CD	β-cyclodextrin
ΔE	energy difference
$\Delta H^{\neq}$	enthalpy of activation
$\Delta S^{\neq}$	entropy of activation
λ	Wavelenght
λ_{max}	maximum absorption band
$\tau_{1/2}$	half-life of Z-isomer in the dark

Appendix B – List of Figures and Tables

Appendix C - Congresses and contributions

Authors: D. Pirone , V. Marturano , R. Del Pezzo , S. Fernandez Prieto , T. Underiner , M. Giamberini , Bartosz Tylkowski
Title: **Molecular Design of Microcapsule Shells for Visible Light-Triggered Release**, Polymers, 11(5), 904 (2019) doi: 10.3390/polym11050904

Authors: D. Pirone, R. del Pezzo, T. Underiner, S. Fernandez Prieto, A. Trojanowska, M. Giamberini, B. Tylkowski
Title: Photo-triggered microcapsules, in book Microencapsulation, DeGruyter Publisher, Berlin/Boston, in press. DOI: 10.1515/9783110642070-001

Authors: R.del Pezzo, A. Trojanowska, D.Pirone, N.A.G. Bandeira, K.A. Boganowicz, M. Giamberini, B. Tylkowski,
Title: Light sensitive microcapsules based on un-modified azobenzene moieties, in book Microencapsulation, DeGruyter Publisher, Berlin/Boston, in press. DOI: 10.1515/9783110642070-002

Authors: D. Pirone, N. A.G. Bandeira, B. Tylkowski, E. Boswell, R. Labeque, R. Garcia-Valls, M. Giamberini
Title: Contrasting photo-switching rates in Azobenzene derivatives: how the nature of the substituent plays a role, Polymers Special Issue , submitted

Authors: D. Pirone, M. Giamberini, R. Garcia-Valls.
Title: Asymmetric azobenzene photo-switchers and their potentials
Congress: POLYCHAR27 - 27th annual world Forum on Advanced Materials
Format (poster or oral): Oral presentation
Date: 14-17 October 2019 **Place**: Naples, Italy

Authors: D. Pirone, M. Giamberini, R. Garcia-Valls
Title: Asymmetric azobenzene photo-switchers and their potentials
Congress: International symposium on encapsulation technology
Format (poster or oral): Oral presentation
Date: 22-24 October 2018.**Place**: Tarragona, Spain

Authors: D. Pirone, M. Giamberini, R. Garcia-Valls.
Title: Visible Light and thermo-trigging of new asymmetric azobenzene compounds
Congress: Georgia Tech 93rd ACS colloid & surface science symposium

Format (poster or oral): Poster
Date: 16-19 June 2019.**Place**: Atlanta, Georgia

Authors: M. Ammendola, J. Ma, D. Pirone, R. del Pezzo, G. Colace
Title: SMARTMEM: Bridging the emerging technology platform around smart-membranes and consumer goods products
Congress: 2019 MCAA General Assembly & Conference
Format (poster or oral): Poster
Date: 24-25 February 2019 **Place**: Vienna, Austria

Authors: D. Pirone, M. Giamberini, R. Garcia-Valls
Title: SMARTMEM ESR2 project: Visible Light and thermo-trigging of new asymmetric azobenzene compounds
Congress: 2019 MCAA General Assembly & Conference
Format (poster or oral): Poster
Date: 24-25 February 2019 **Place**: Vienna, Austria

Authors: D. Pirone, M. Giamberini, R. Garcia-Valls.
Title: Visible light and thermo-trigging of new asymmetric azobenzene compounds
Congress: 15th Doctoral day 2018
Format (poster or oral): Poster
Date: 23 May 2018 **Place**: Tarragona, Spain

UNIVERSITAT
ROVIRA i VIRGILI